AD-A025 399

BROADBAND DIGITAL MODEM

HARRIS CORPORATION

PREPARED FOR
ROME AIR DEVELOPMENT CENTER

MAY 1976

WIDEBAND DIGITAL MODEM

Harris Corporation

Approved for public release;
distribution unlimited.

Laboratory Directors' Fund No. 01717412

Rome Air Development Center
Air Force Systems Command
Griffiss Air Force Base, New York 13441

PREPARED:

_____
Project Engineer

APPROVED:

_____
Technical Director
Communications and Control Division

FOR THE COMMANDER:

_____
JOHN   HUES
Acting Chief, Plans Office

This program was funded under the Laboratory Directors' Fund.

Do not return this copy.   Retain or destroy.

REPORT DOCUMENTATION PAGE		READ INSTRUCTIONS BEFORE COMPLETING FORM
1. REPORT NUMBER RADC-TR-76-117	2. GOVT ACCESSION NO.	3. RECIPIENT'S CATALOG NUMBER
4. TITLE (and Subtitle) BROADBAND DIGITAL MODEM		5. TYPE OF REPORT & PERIOD COVERED Final Technical Report 13 May 74 - 13 Nov 75
		6. PERFORMING ORG. REPORT NUMBER N/A
7. AUTHOR(s) Thomas R. Losson Daniel D. McRae		8. CONTRACT OR GRANT NUMBER(s) F30602-74-C-0263
9. PERFORMING ORGANIZATION NAME AND ADDRESS Harris Corporation/Electronic Systems Division P O Box 37 Melbourne FL 32901		10. PROGRAM ELEMENT, PROJECT, TASK AREA & WORK UNIT NUMBERS 61101F 01717412
11. CONTROLLING OFFICE NAME AND ADDRESS Rome Air Development Center (DCLD) Griffiss AFB NY 13441		12. REPORT DATE May 1976
		13. NUMBER OF PAGES 157
14. MONITORING AGENCY NAME & ADDRESS(if different from Controlling Office) Same		15. SECURITY CLASS. (of this report) UNCLASSIFIED
		15a. DECLASSIFICATION DOWNGRADING SCHEDULE N/A

16. DISTRIBUTION STATEMENT (of this Report)

Approved for public release; distribution unlimited.

17. DISTRIBUTION STATEMENT (of the abstract entered in Block 30, if different from Report)

Same

18. SUPPLEMENTARY NOTES

RADC Project Engineer: Brian M. Hendrickson (DCLD)

This program was funded under the Laboratory Directors' Fund.

19. KEY WORDS (Continue on reverse side if necessary and identify by block number)

Digital Modulation	Multiple Symbol Detection
Bandwidth Efficiency	Line-of-Sight Microwave
Coherent FSK	

20. ABSTRACT (Continue on reverse side if necessary and identify by block number)

The objective of this program was to develop a practical modem technique providing the means to trunk a large volume of digitized voice channels within the present FDM-FM bandwidth allocations. Specifically, a bandwidth efficiency of 2 bits per hertz of RF bandwidth and a bit error of 10^{-7} or less at an E_b/N_o of 20 dB were desired. These characteristics, provided in conjunction with hard-limiting radio sets, allow efficient conversion of analog FDM-FM line-of-sight microwave systems to digital operation by replacement of the modulation elements.

(Cont'd)

DD FORM 1 JAN 73 1473 EDITION OF 1 NOV 65 IS OBSOLETE

It was determined that 4-ary FSK was the best signal design, given the performance objectives and the constant-envelope constraint. A continuous-phase, coherent detection, multisymbol observation modem was constructed and successfully tested. The performance objective of a 10^{-7} bit error rate at an E_b/N_o of 20dB was bettered by approximately 0.5 dB in laboratory tests.

EVALUATION

The projected conversion of the Defense Communication System (DCS) from a predominantly analog system to a predominantly digital system has created the need for more efficient utilization of frequency spectrum. This is a direct result of the more demanding spectral requirements imposed by digital signals.

A first step in obtaining efficient utilization of spectrum over digital microwave channels has become a reality in the Broadband Digital Modem Program. Bandwidth efficiencies which heretofore were no better than one bit/sec of data per Hz of RF Bandwidth have been doubled via this program to two bits/sec/Hz.

Hardware in breadboard form was successfully tested over the RADC Microwave System. All design objectives were not only met but improved upon.

Additional work will continue in this area to obtain even higher Bandwidth efficiencies most notably with cross-polarization, more efficient modulation technique design, and development of linear power amplifiers. A follow-on experimental model of the Broadband Digital Modem will also be developed in the FY76-77 time frame.

BRIAN M. HENDRICKSON
Project Engineer

III

CONTENTS

CONTENTS (Continued)

ILLUSTRATIONS

ILLUSTRATIONS (Continued)

ILLUSTRATIONS (Continued)

TABLES

Section I

INTRODUCTION

1.1   OBJECTIVE

The objective of this program was to develop a practical modem technique providing the means to trunk a large volume of digitized voice channels within the present FDM-FM bandwidth allocations. Specifically, a bandwidth efficiency of 2 bits per hertz of RF bandwidth and a bit error of 10^{-7} or less at an E_b/N_o of 20 dB were desired. These characteristics, provided in conjunction with hard-limiting radio sets, allow efficient conversion of analog FDM-FM line-of-sight microwave systems to digital operation by replacement of the modulation elements.

1.2   APPROACH

The program consisted of three major phases. During the first phase, an analytical study of constant-envelope modulation techniques was performed to locate candidates providing the desired performance. In the second phase, the selected techniques were evaluated in terms of implementation complexity and operational characteristics. The best approach was selected and a breadboard model constructed. The breadboard performance characteristics were evaluated in the laboratory and on actual microwave links in the final phase.

1.3   RESULTS

It was determined that 4-ary FSK was the best signal design, given the performance objectives and the constant-envelope constraint. A continuous-phase, coherent detection, multisymbol observation modem was constructed and successfully tested. The performance objective of a 10^{-7} bit error rate at an E_b/N_o of 20 dB was bettered by approximately 0.5 dB in laboratory tests.

7

A major accomplishment of this program was the development of a demodulation technique for FSK providing near optimum performance (based on the signal structure) with modest hardware complexity. The performance and complexity of the modem are comparable to more conventional designs, with the added advantages of operation with hard-limiting amplifiers and reduced RF filtering requirements.

1.4   REPORT ORGANIZATION

The results of the analytical effort are presented in Section II. The implementation considerations and trade-offs are described in Section III. Section IV discusses the design and construction of the breadboard unit. In Section V, the test program and results are presented. The conclusions and recommendations are in Section VI.

Section II

THEORETICAL RESULTS

2.1 STATEMENT OF THE PROBLEM

Current trends indicate a continued evolution toward an all-digital military communications network. Existing analog voice/data communications over the 4-kHz channel will be replaced by Pulse Code Modulation (PCM) and Time Division Multiplexing (TDM). In the existing FDM-FM system, each 4-kHz baseband channel requires a transmitted RF bandwidth of approximately 32 kHz. The planned digital system requires 64 kb/s per 4-kHz baseband channel. Conventional digital modulation techniques such as QPSK provide a bandwidth efficiency of approximately 1 bit per hertz of RF bandwidth. Thus, each baseband channel occupies 64 kHz of RF bandwidth and the system channel capacity is reduced by a factor of 2 if the RF bandwidth is not increased. In many instances, additional bandwidth allocations are not available.

The existing analog FDM-FM line-of-sight microwave system represents a substantial investment in fixed plant. Although portions of this system are somewhat dated and have a limited life expectancy, many sections are relatively new, and, if digital conversion rather than total replacement were possible, a substantial investment savings could result. The existing radios utilize hard-limiting power amplifiers almost exclusively, and this practically limits the choice of modulation to constant-envelope techniques.

The objective of this program was to develop a practical modem technique providing a bandwidth efficiency of 2 bits per hertz of RF bandwidth with hard-limiting radio sets. The RF bandwidth is defined as that portion of the radiated signal spectrum wherein 99% of the signal power is contained. The performance objective was a bit error rate (BER) of 10^{-7} or less, at an E_b/N_o of 20 dB. It was further desired that the modem interface at an IF of 70 MHz and that application of the modem not require RF filters or linearization of the power amplifier to achieve the desired performance.

2.2   GENERAL APPROACH

The analytical task focused on locating constant-envelope signals which simultaneously provided the desired BER and spectral requirements. The class of signals investigated is of the form

$$S_i(t) \;=\; A\cos\left(\omega_c t + \varphi_i(t)\right)$$

where

$$
\begin{aligned}
A &= \text{constant envelope} \\
\omega_c &= \text{carrier frequency} \\
\varphi(t) &= \text{information-carrying angle modulation}
\end{aligned}
$$

This signal is completely defined by a plot of the phase (relative to the carrier phase) versus time. This plot will be referred to as the phase trajectory plot. Some examples of phase trajectory plots for familiar signals are illustrated in Figure 1. The distinction between accumulated and nonaccumulated phase trajectories is shown in Figure 2. Two techniques for jointly optimizing BER and spectral occupancy were utilized. It was concluded that continuous-phase 4-ary FSK was the best choice for the signal structure.

2.3   ANALYTICAL APPROACH

In the analytical approach, expressions were developed for BER and spectral occupancy and an attempt was made to mathematically optimize the two expressions. The expressions used for spectral occupancy are developed in Appendix A. A union bound approximation was utilized for BER.

$$P_s \;<\; \frac{1}{M} \sum_{\substack{i=1}}^{M} \sum_{\substack{j=1 \\ j\neq i}}^{M} \; Q\!\left(\sqrt{E_s/N_o\,(1-P_{ij})}\right) \tag{1}$$

Binary

Split-Phase FSK:
    (Nonaccumulated Phase)
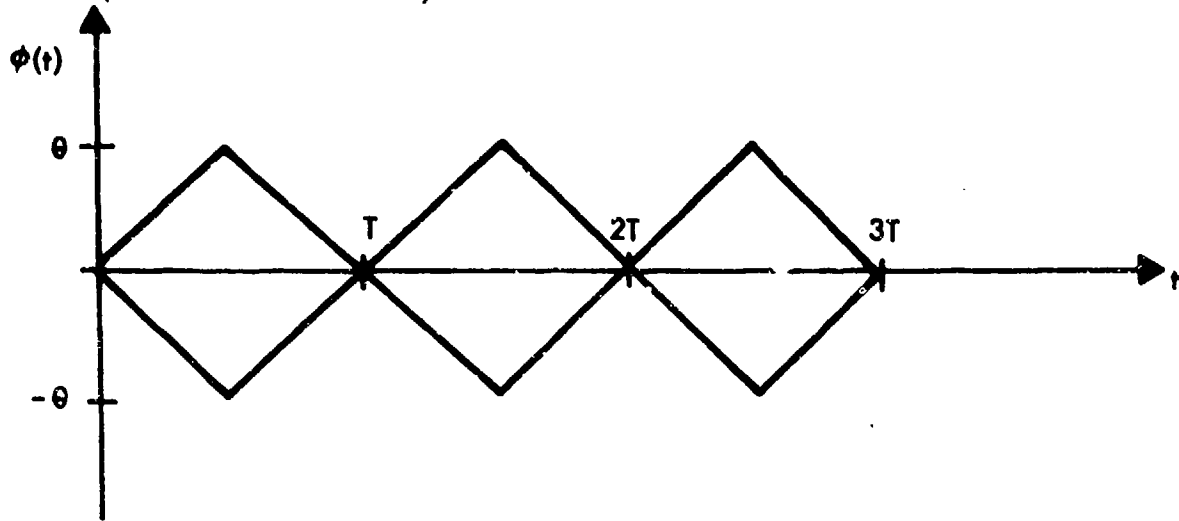
Binary

Continuous-Phase FSK:
    (Accumulated Phase)
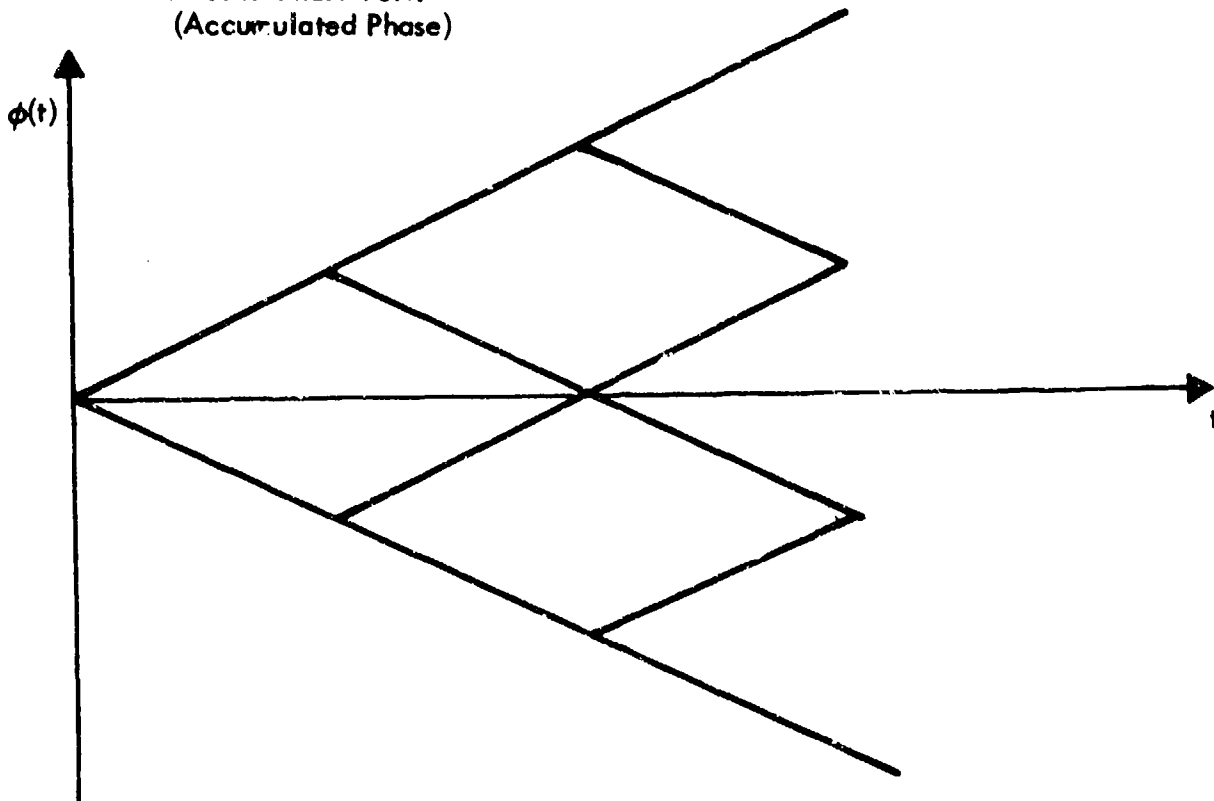
Figure 1.   Phase Trajectory Plots

11

Figure 2. Distinction Between Accumulated and Nonaccumulated Phase Trajectories

12

where

P_s = symbol error probability

P_{ij} = correlation coefficient between the ith and j^{th} signals

E_s = energy per symbol

N_o = one-sided noise density

$$\phi(X) = \frac{1}{\sqrt{2\pi}} \int_X^\infty e^{-y^2/2} \, dy$$

For constant-envelope signalling

$$P_{ij} = \mp \int_0^T \cos\left[\phi_2(t) - \phi_i(t)\right] dt \tag{2}$$

where

$\phi_2(t)$ = the phase trajectory for the ith symbol

Combining (1) and (2) and overbounding

$$\phi(X) < 1/2 \, e^{-X^2/2} \tag{3}$$

yields

$$P_s < \frac{e^{-E_s/2N_o}}{2M} \sum_{i=1}^{M} \sum_{\substack{j=1 \\ i \neq 2}} e^{E_s/2N_oT \int_0^T \cos\left[\phi_2(t) - \phi_2(t)\right] dt} \tag{4}$$

Equation (4) is the union bound on symbol error rate for constant-envelope signals. Using Equation (4) and the expression derived in Appendix A for spectral occupancy, a calculus of variations approach was used to locate a phase trajectory which minimized spectral occupancy subject to a performance constraint.

In general, this approach did not yield useful results. It was concluded that finding an analytical solution for optimum trajectories was not possible within the time scale of the study. As an alternative, the performance of specific trajectories was analyzed as described in the following paragraphs.

13

2.4   COMPUTER SEARCH

Since the signal design effort for finding good modulation techniques by analytical means was not successful, a computer search technique was implemented. This effort used the computer program for spectral occupancy described in Appendix B, and was developed during the study. It is capable of computing the spectral occupancy of very general types of angle modulation. The classes of signals considered are those angle-modulated signals for which the only mechanism of intersymbol influence inherent in the modulation is that the phase of the sinusoid at the beginning of a signal is dependent on the data history. Other than this starting phase, the shape of the phase function during a symbol time is dependent only on the symbol being transmitted; the shape can be completely arbitrary.

The computer program evaluates, on the analytical basis presented in Appendix A, the percent power within any bandwidth for any M-ary angle-modulation signal. In the computer program, the shape of the M-ary phase functions $\left[\phi_k(t), k = 1, M\right]$ is approximated by up to 32 phase steps over the symbol time. M can range from 2 to 16. It was found that the 32-step approximation to the phase functions gives essentially the same 99-percent spectral occupancy bandwidth as continuous phase functions.

2.4.1   Nonaccumulative Phase Trajectories

2.4.1.1   M-ary PSK - No Pulse Shaping

M-ary PSK is one of the most common types of constant-envelope signalling. It has the advantage of being relatively simple to generate and to demodulate. Since the scheme is one of the more common modulation techniques, its performance relative to the goals of the study should be known.

Unfiltered M-ary PSK, for all M, with the phases equispaced 0 to 2π, has the well known $(\sin x/x)^2$ spectral density. The 99-percent spectral occupancy is roughly 20 times the symbol rate for all M. Since the bit   is ($\log_2 M$) times symbol rate, the spectral occupancy of course changes with M. The   percent spectral occupancy for

14

binary is 20 times bit rate and for 4-ary (quadraphase) is 10 times bit rate. M-ary PSK was used as a check case for the spectral occupancy program and gave the results of Figure 3, which are based upon the $(\sin(x)/x)^2$ spectrum. Thus the program was correct for this test case.

The spectral occupancy of the unfiltered 0 to 2π equispaced phase PSK signalling schemes is excessive in relation to the study goals. For a 99-percent spectral occupancy of 0.5 times bit rate, for example, Figure 3 indicates M would have to be very large, as determined by:

$$99\% \text{ BW} = 20 \times \text{symbol rate}$$

$$= \frac{20}{\log_2 M} \times \text{bit rate}$$

$$0.5 = \frac{20}{\log_2 M}$$

$$M = 2^{40} \quad \text{for } 99\% \text{ BW} = 0.5 \times \text{bit rate}$$

An M this large is obviously impractical. The behavior of spectral occupancy was examined as the phase deviation was reduced, as in Figure 4. The M phases are equispaced by θ, but for a total spread in phase less than 2π. It can be shown that the spectrum contains a continuous part having $(\sin x/x)^2$ form and a spectral line at the center frequency.

If the phase relative to carrier is θ_i for the ith signal, then it can be shown that the fraction of total power placed in the carrier is

$$P_c = \left| \frac{1}{M} \sum_{i=1}^{M} e^{j\theta_i} \right|^2 \tag{5}$$

15
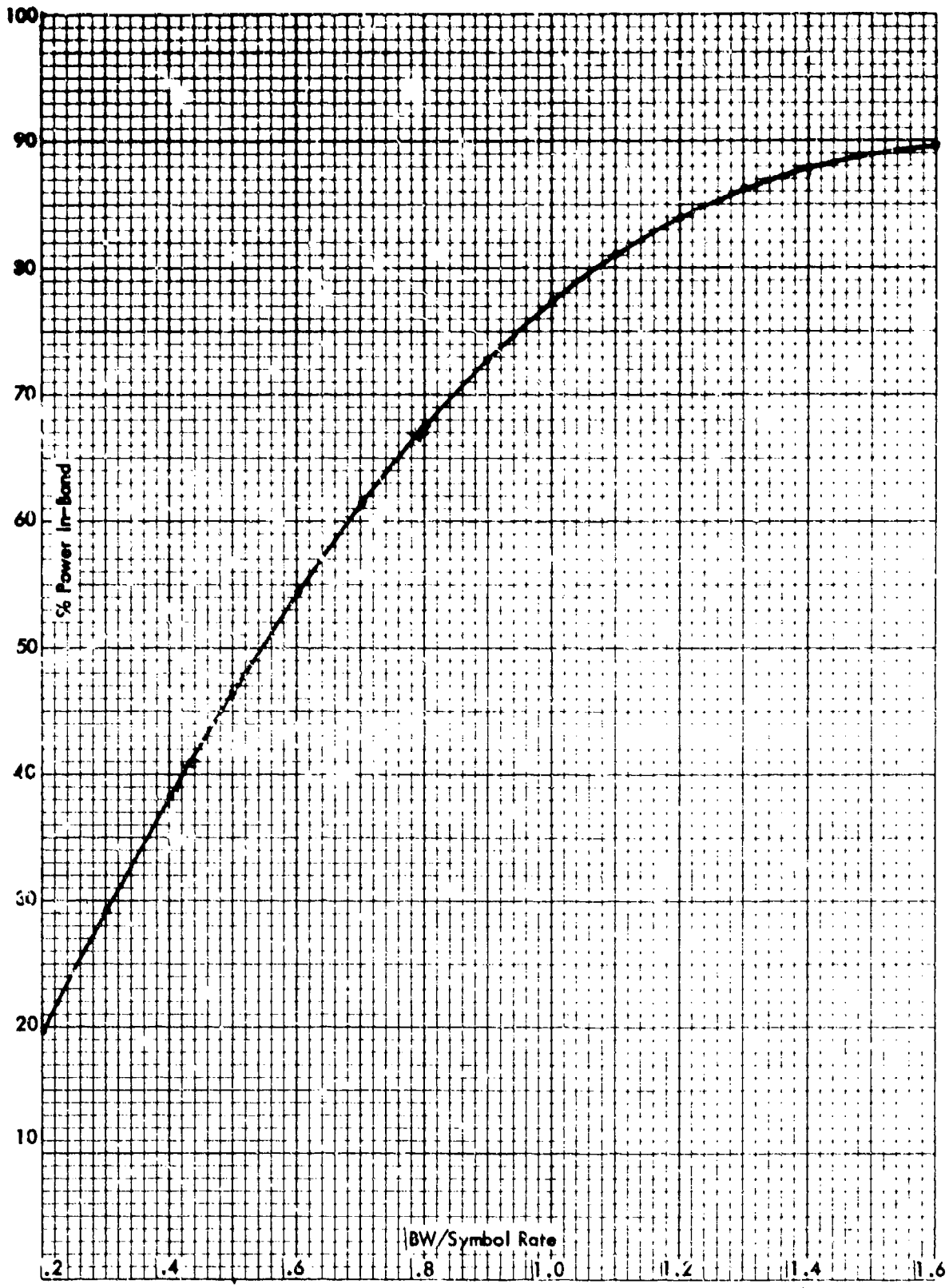
Figure 3. Percentage of In-Band Power vs Bandwidth/Symbol Rate for PSK Modulation$\left(\left(\frac{\sin x}{x}\right)\right)$ Spectrum

4-ary Case Shown
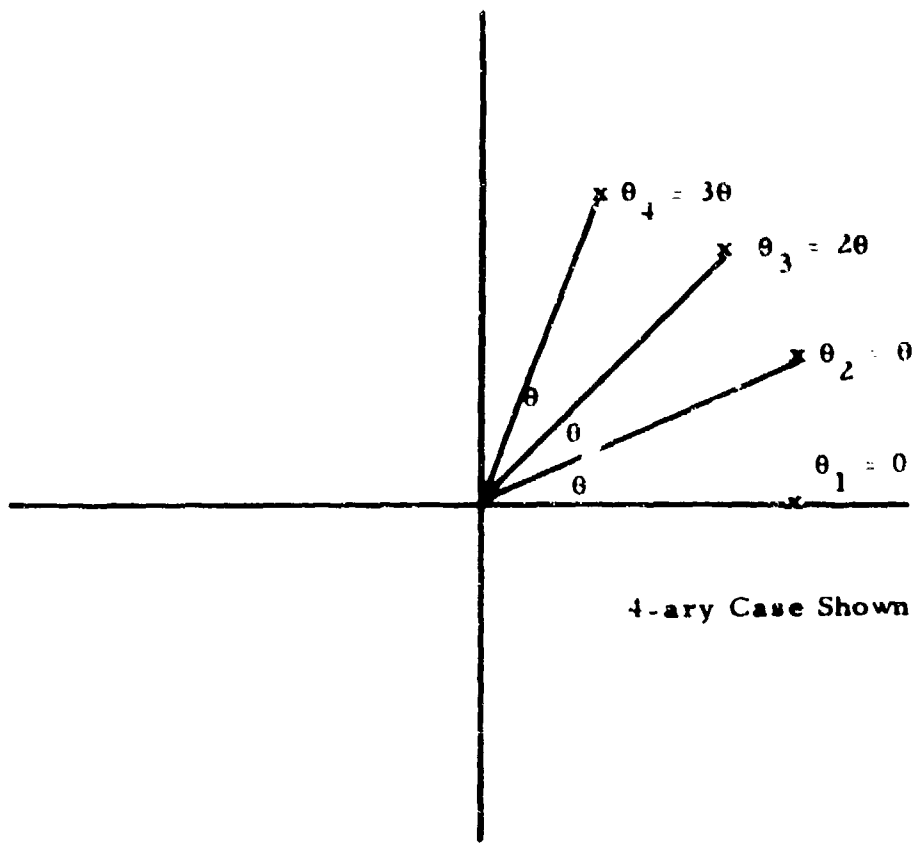
Figure 4.   Reduced Phase Deviation M-ary PSK

17

The remaining fraction of power, $(1-P_c)$, is in the $(\sin x/x)^2$ continuous portion of the spectrum. By the strict definition of spectral occupancy as the bandwidth within which a given fraction of total power is contained, the spectral occupancy of this type of M-ary PSK is computed in the following way. The total power in a bandwidth B is given by

$$P_B = P_c + \text{Power in B of } (\sin x/x)^2$$

or

$$P_B = P_c + (1-P_c)\, P_s \qquad (6)$$

where P_s is the percent power contained in B of a $(\sin x/x)^2$ spectrum as given in Figure 3.

Note that the carrier power is counted toward fulfilling the spectral occupancy goal. The spectral line at the carrier contains no data information. The continuous spectrum is the data-carrying portion. The presence of large discrete spectral lines can lead to a misleading spectral occupancy figure for the signalling scheme. The 99-percent spectral occupancy may bear no relation at all to the required bandwidth for signalling with the modulation scheme. For example, one could design a PSK scheme which has 99-percent of the total radiated power in the carrier, which has a strict definition spectral occupancy of zero bandwidth. Obviously, any attempts to operate the signalling scheme through a bandwidth anywhere near as narrow as the 99-percent spectral occupancy are doomed to failure. All this is pointed out to highlight the fact that one should be appropriately skeptical of the specification of spectral occupancy alone as an indication of the required bandwidth for communication with a signalling scheme.

Figure 5 shows the performance attainable with the reduced phase deviation M-ary PSK schemes for various 99-percent spectral occupancies around one-half bit rate. The curves plot the dB loss relative to coherent antipodal binary PSK of a coherent receiver versus the 99-percent spectral occupancy. An implicit parameter at a given point

18
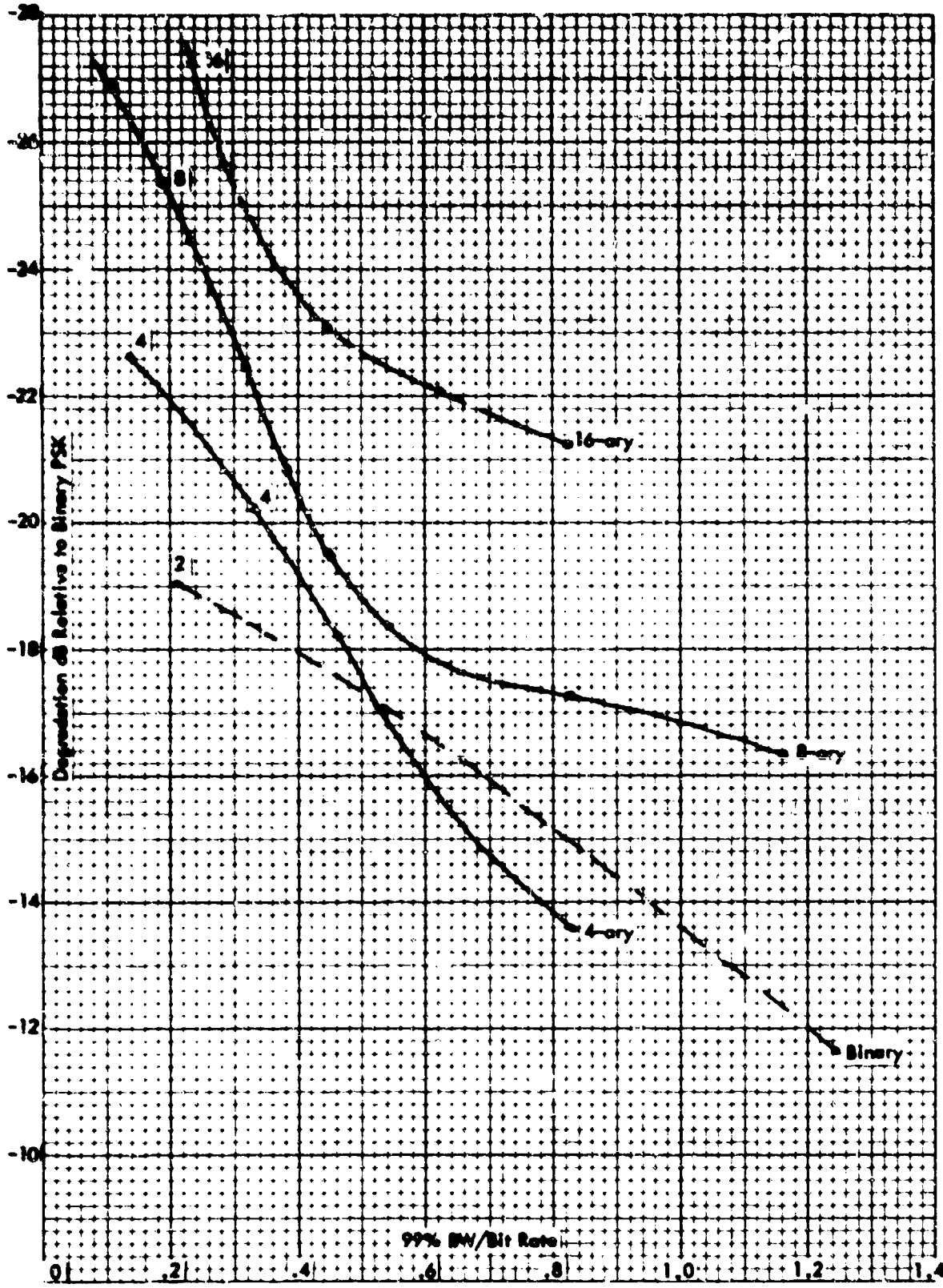
Figure 5. Relative Degradation vs 99% Bandwidth for Unshaped M-ary PSK

19

on the curves is the θ spacing between phases. As θ is reduced the spectral occupancy is reduced, and the performance is simultaneously degraded. As an example of how Figure 5 was obtained, consider the binary case. First, let the θ spacing necessary to yield 99-percent spectral occupancy equals one-half bit rate be found. From Equation (6), we have

$$P_B = .99 = P_c + (1-P_c) P_s \tag{7}$$

P_s, the fraction of the continuous $(\sin x/x)^2$ power in a one-half bit rate band, is given in Figure 3 as .465. Therefore,

$$.99 = P_c + (1-P_c) (.465)$$

or

$$P_c = .982 \tag{8}$$

Equation (8) indicates that 98.2 percent of the total transmitted power must be put into carrier to attain 99-percent spectral occupancy of one-half bit rate. Combining Equations (5) and (8) allows one to solve for the θ spacing to attain this; i.e.,

$$.982 = \left| \frac{1}{2} (e^{i\theta/2} + e^{-i\theta/2} \right|^2$$

$$.982 = (\cos \frac{\theta}{2})^2 = \frac{1}{2} (1 + \cos \theta)$$

$$\cos \theta = .964$$

or

$$\theta = 15.3°$$

The performance is computed by noting that the normalized correlation between the two signals is

$$\rho = \cos \theta = .964$$

The probability of error for a coherent receiver is given by

$$P(\epsilon) = Q\sqrt{\frac{E_b(1-\rho)}{N_o}}$$

$$P(\epsilon) = Q\sqrt{\frac{2E_b}{N_o}}\,(.018) \qquad (9)$$

$$Q(x) \triangleq \frac{1}{\sqrt{2\pi}} \int_x^\infty e^{-y^2/2}\, dy$$

Comparing Equation (9) to the well-known error rate for PSK,

$$(PSK)\ P(\epsilon) = Q\sqrt{\frac{2E_b}{N_o}}$$

shows that there is a degradation of a factor of 0.018 in power, which corresponds to 17.4 dB. Thus, a 99-percent spectral occupancy of one-half bit rate binary PSK is plotted in Figure 5 with 17.4-dB degradation relative to antipodal binary PSK. The other points and curves were obtained in a similar manner.

Because of the excessive amount of wasted carrier power, which serves no purpose except to maintain a constant envelope on the transmitted signal, unfiltered M-ary PSK was discarded as being undesirable in light of the signal design study goals.

2.4.1.2   M-ary PSK — Raised Cosine Pulse Shaping

The effect of pulse shaping on M-ary PSK pulses was considered next. The pulse shaping brought under study was raised cosine, as shown in Figure 6. The peak phase difference between adjacent symbols was set equal to θ. The computer program was used to determine the spectral occupancy.

The performance of a coherent demod for these schemes was estimated in the following way. For a coherent demod, the correlation ρ between two signals determines the probability of making an error in additive white Gaussian noise. The probability of error, $P(\epsilon)$, is given by

$$P(\epsilon) = Q\left(\sqrt{\frac{E_s}{N_o}(1-\rho)}\right) \tag{10}$$

For two constant envelope symbols, the correlation is given by

$$P = \frac{1}{T}\int_o^T \cos(\varphi_1(t) - \varphi_2(t)) \, dt \tag{11}$$

For the raised cosine shaping as shown in Figure 6, the phase difference, $\varphi_1(t) - \varphi_2(t)$, is given by:

$$\varphi_\phi(t) \triangleq \varphi_1(t) - \varphi_2(t) = \frac{\theta}{2}\left[1 - \cos\left(\frac{2\pi t}{T}\right)\right]$$

$$\varphi_\phi(t) = \theta \sin^2\left(\frac{\pi t}{T}\right) \tag{12}$$

Equation (11) thus becomes

$$P = \frac{1}{T}\int_o^T \cos\left(\theta \sin^2 \frac{\pi t}{T}\right) \, dt \tag{13}$$

22
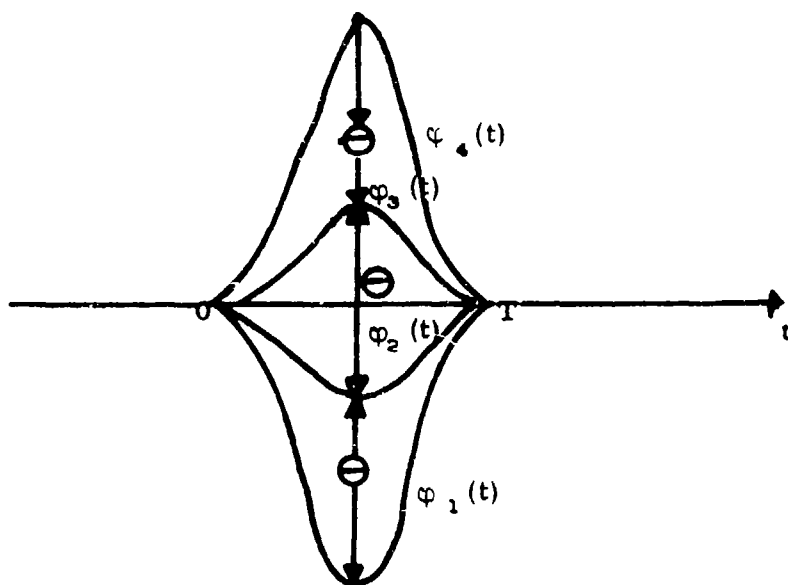
Figure 6.   4-ary Case of Raised Cosine PSK
             Pulse Shaping

Figure 7 shows the degradation in dB relative to antipodal PSK for various 99-percent spectral occupancy bandwidths. Comparing Figures 5 and 7, note that the binary case best performance for either shaped or unshaped pulses at a 99-percent spectral occupancy of 0.5 times bit rate is approximately 18 dB worse than unfiltered binary PSK. The raised cosine shaping also requires roughly 1 dB more power for the same error rate at this spectral occupancy. From this it can be seen that phase continuity is not necessarily all that indispensable a quality when it is desired to maximize the performance for a given spectral occupancy.

2.4.1.3 Combination of Phase and Frequency Modulation

Figure 8 shows the result of using the computer program to evaluate a 7-ary signalling scheme with the phase trajectories shown in the figure. From the phase trajectories shown, it can been seen that this scheme has three frequencies: a center frequency and two symmetrical frequencies about the center frequency. The parameter θ (controlled by the deviation about the center frequency) was varied to obtain the desired 99-percent bandwidth. At 2 bits/Hz this scheme is roughly 15.5 dB worse than binary PSK, therefore there can be no hope of its meeting the design goals.

2.4.1.4 Summary of Noncumulative Phase Schemes

The schemes we have considered above are schemes for which the phase does not cumulate with respect to the carrier. For 2 bits/Hz 99-percent spectral occupancy, the phase of the transmitted signal never deviates very widely from the carrier phase. For this reason, there is a large spectral line at the carrier in all these schemes. The schemes examined represent signals which contain at least 94 percent of the total power in the carrier. These spectral lines carry no information, therefore that portion of power is wasted. This dooms these noncumulative schemes to poor performance relative to our design goals, even were the continuous part of the spectrum to carry information as efficiently as antipodal binary PSK. On top of this disadvantage, the idea of obtaining narrow "spectral occupancy" on the basis of simply putting a large carrier component in,
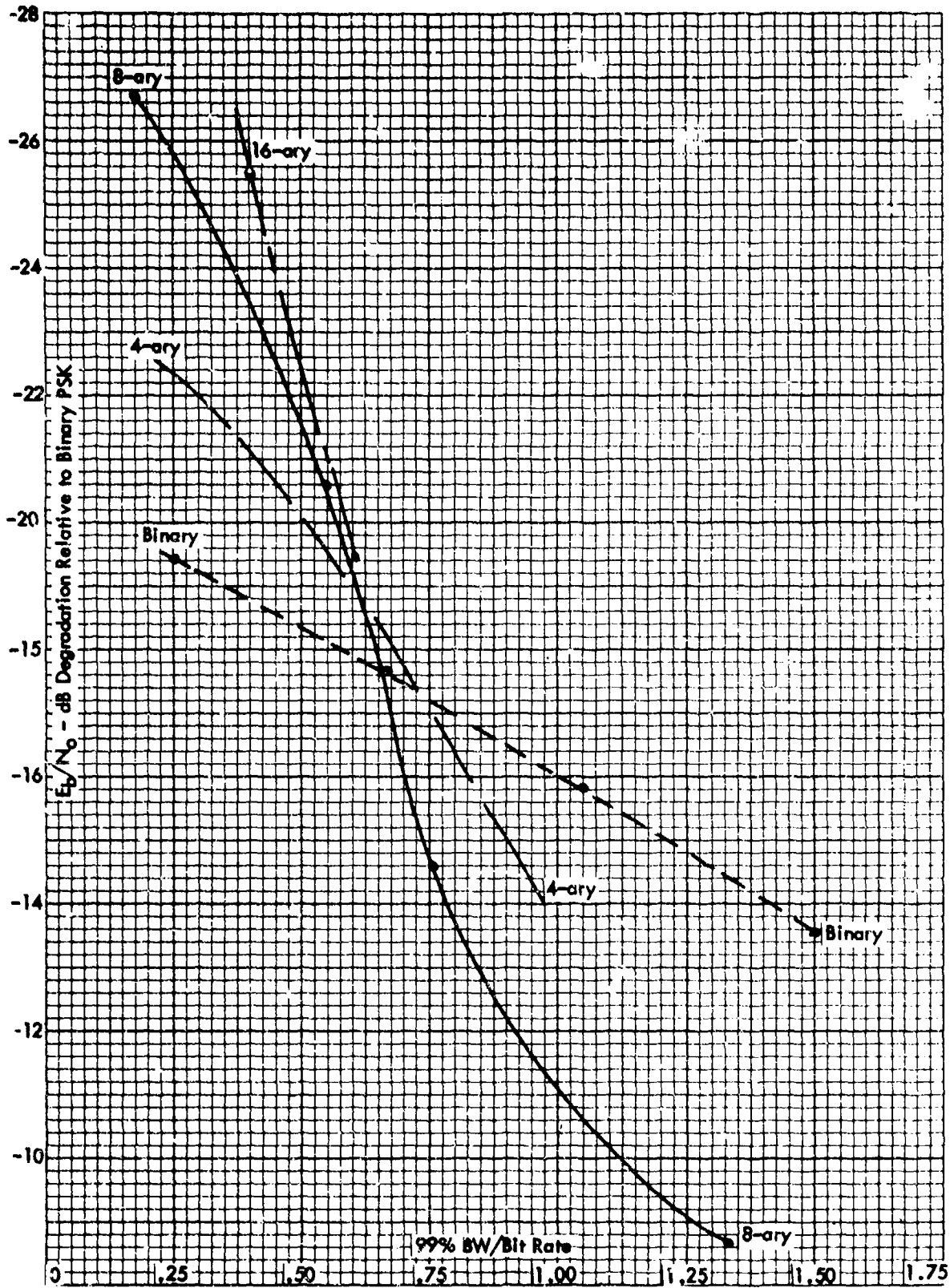
Figure 7.   Relative Degradation vs 99% Bandwidth for Raise Cosine Phase Trajectories
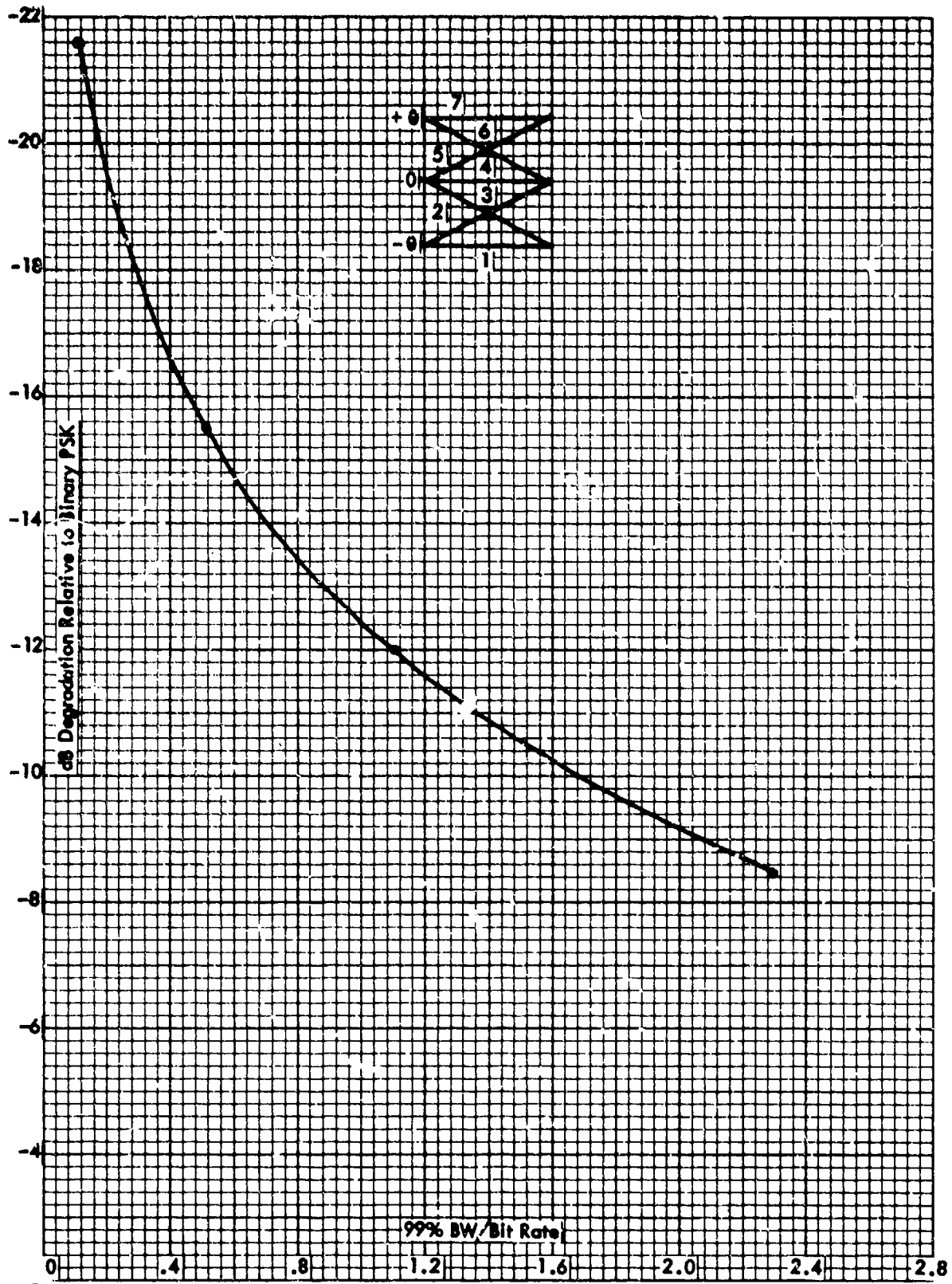
Figure 8. Relative Degradation vs 99% Bandwidth 4-ary Phase Trajectories

is extremely artificial. The data-carrying continuous spectrum is still very wide and would require channel bandwidth out of all proportion to the "spectral occupancy." For these reasons, the ability to find any noncumulative phase-modulation schemes which met the design goals of 99-percent bandwidth equals one-half bit rate and 10^{-7} error rate at 20 dB E_b/N_o was discounted.

2.4.2   Cumulative Phase Trajectories

At this point in the signal design effort, the only hope of obtaining the design goals lay in the angle-modulation schemes wherein phase is allowed to accumulate relative to center frequency, such as in M-ary FSK. For these schemes, there are no spectral lines (and hence essentially no wasted power) for the small deviations required for 99-percent bandwidth equals one-half bit rate. Consequently, several schemes of the cumulated-phase variety were investigated to see if improvement in performance or spectral occupancy could be made on 8-ary FSK, which was the best known scheme found here prior to this study.

Figure 9 shows the performance of M-ary FSK schemes with a one-symbol coherent receiver versus the 99-percent bandwidth of the signal. 8-ary FSK is only 8.8 dB worse than PSK, with 4-ary FSK about 9.7 dB worse at 2 bits/Hz. With both these signalling schemes a multisymbol observation receiver can do 3.0 dB better, yielding degradations of only 5.8 dB for 8-ary FSK and 6.7 dB for 4-ary FSK. The signalling schemes are very powerful in terms of their performance for 2 bits/Hz spectral occupancy. In an attempt to improve upon their performance, the possibility of allowing the phase trajectories to contain jumps (as in Figure 10) was investigated. The analysis started with the basic 8-ary FSK trajectories (linear with ending-phase separation equals 45 degrees) and made stepwise approximations with N steps (N = a parameter on the curves). Intuitively, the jumps in phase would allow a greater distance to be obtained between signals and thus yield better performance. As shown in Figure 10, the 32-step approximation to the phase trajectories resulted in very little increase in the 99-percent bandwidth of the signal; however, the phase jump is at most a little over 4 degrees for N = 32 on the outermost

27
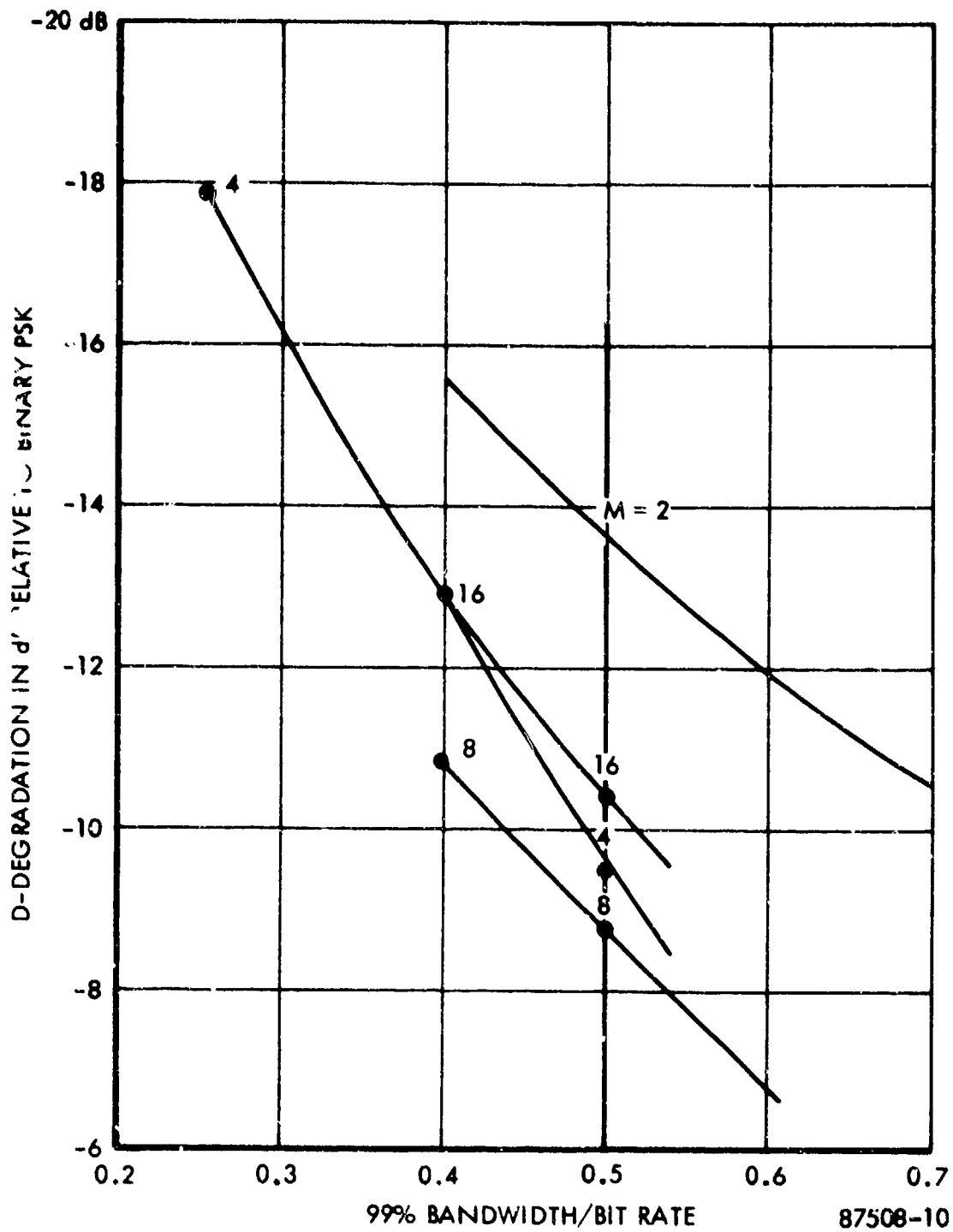
Figure 9.   Degrudation of M-ary FSK Relative to Binary PSK When Demodulated
by a One-Symbol Coherent Receiver

28
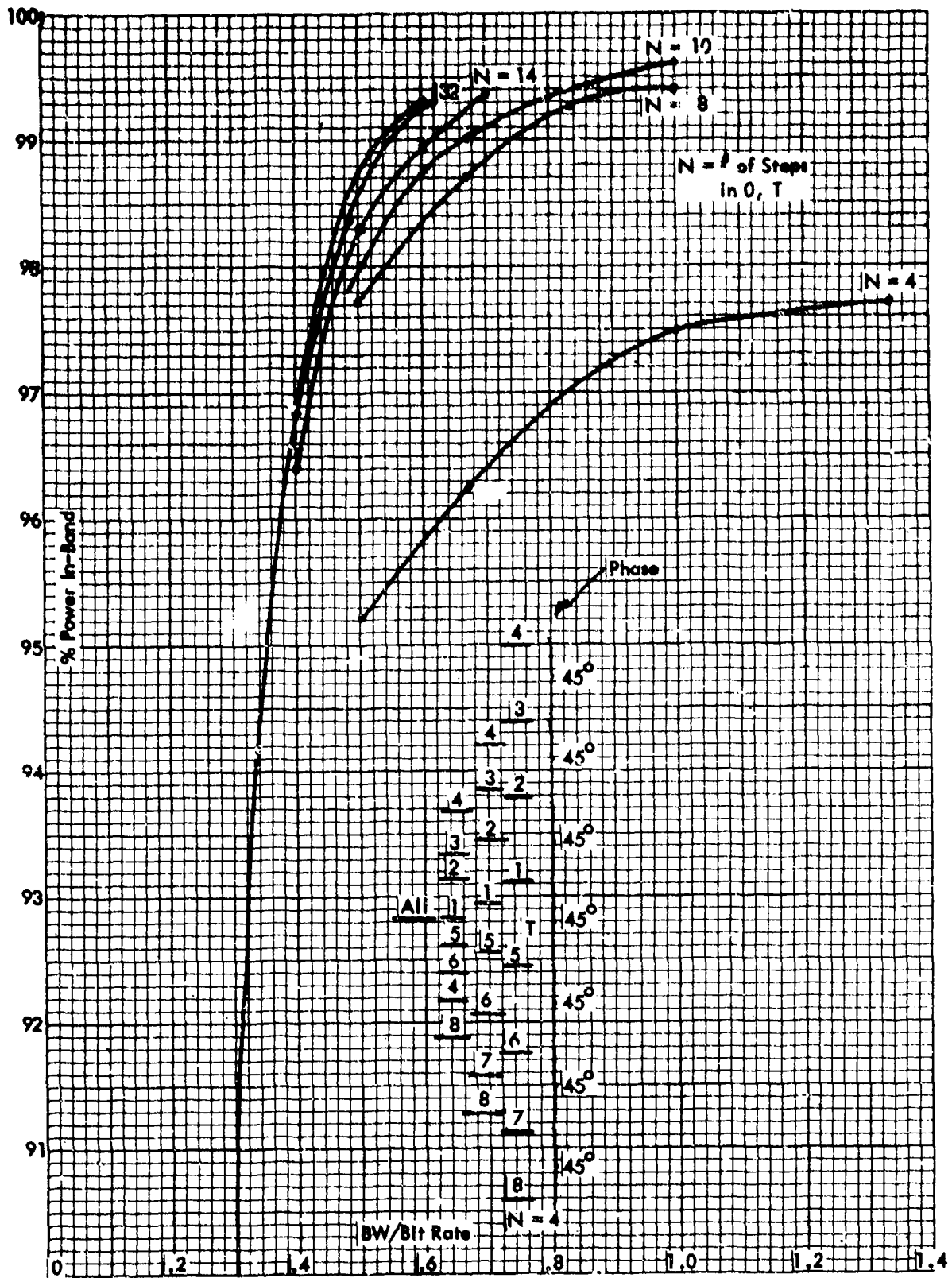
Figure 10. Percentage of In-Band Power vs Bandwidth-Bit Rate Ratio, Allowing Phase Jumps

trajectories. Therefore, little advantage in distance is obtained over the original linear FSK trajectories. Thus, although a slight step in phase was allowable without unduly affecting spectral occupancy (at 99-percent bandwidth point), the step was so small that negligible performance improvement would result.

Next, an attempt was made to obtain a performance improvement by employing phase trajectories for 8-ary FSK, as shown in Figure 10. Here, a step of M° in phase between adjacent symbols was allowed, followed by a frequency ramp in phase to a total of $m^\circ + n^\circ$ phase difference between adjacent symbols at the end of a symbol time. The parameters m and n were chosen to make the performance with a coherent receiver the same as in 8-ary FSK with 99-percent bandwidth equals 0.53 times bit rate. As shown in Figure 11, the 99-percent bandwidth was improved slightly from 0.53 to 0.5 times bit rate for $m = 5^\circ$ and $n = 37^\circ$. This slight improvement is remarkable only in that it is the only scheme found which outperforms 8-ary FSK.

An attempt was also made to improve the performance of 8-ary FSK by smoothing the transition from one phase to another in a symbol time, as shown below.
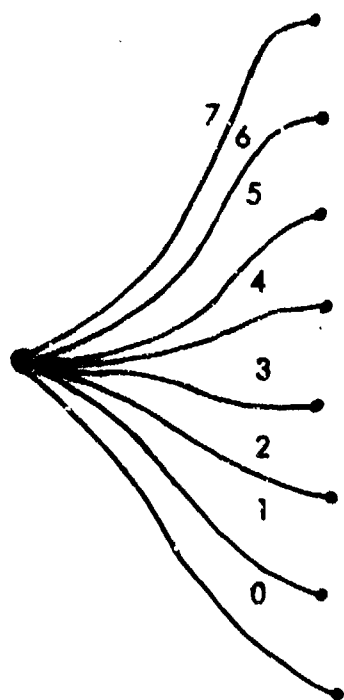
$\frac{1}{2}$ cycle sinusoid phase transitions
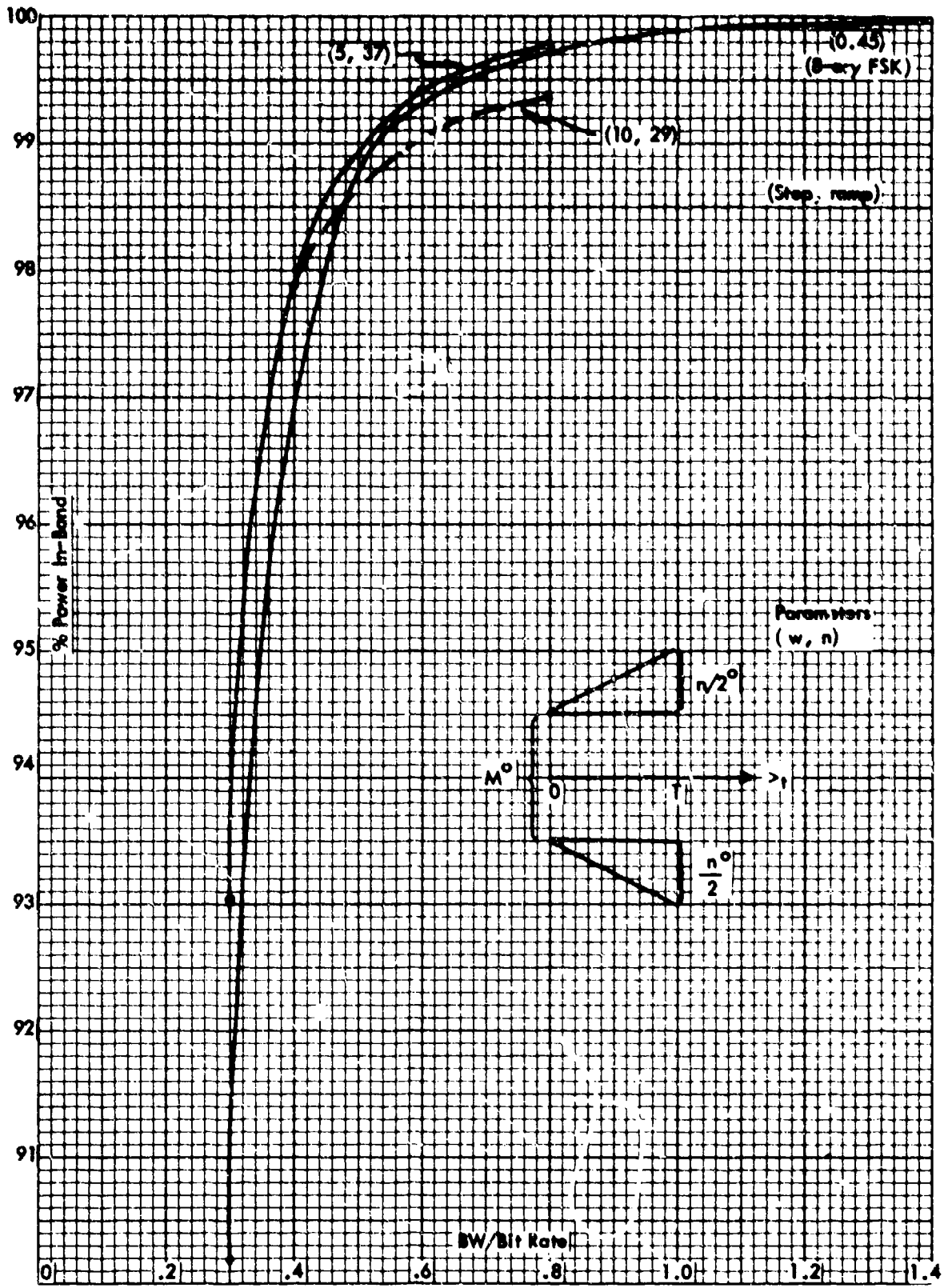
Figure 11. Percentage of In-Band Power vs Bandwidth-Bit Rate Ratio with a Phase Jump of M°

The transitions vary sinusoidally from the initial phase at start of a symbol, to one of eight equispaced phases at the end of a symbol time. The ending phases were spaced such that the performance obtained with a coherent demod is the same as 8-ary FSK with 99-percent bandwidth equals one-half bit rate. The 99-percent spectral occupancy was found to be 0.95 times bit rate. Thus its spectral occupancy was almost doubled relative to 8-ary FSK.

From the data, it can be concluded that no significant improvement can be had over 8-ary FSK in spectral occupancy or performance in a phase-modulation (constant envelope) scheme wherein the shape of the phase trajectory within a symbol time is determined solely by the symbol to be transmitted in that symbol time. The only remaining hope for improvement is some form of partial response scheme wherein the shape of the phase trajectory in a symbol time can depend upon not only the present symbol but also upon the symbols that have previously been transmitted. Generalized partial response is discussed below, with the aid of the following illustration.
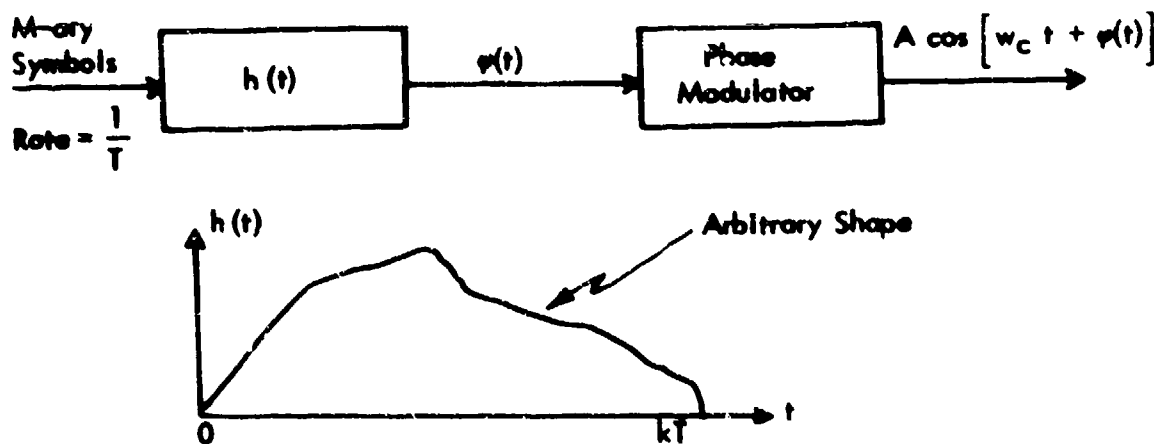
$\varphi(t)$ during a symbol time is determined by the most recent k symbols.

In general, the phase trajectory during a symbol time is given by

$$\varphi(t) = \sum_{i=1}^{k} a_i \, h \, (t + iT) \qquad\qquad a_i = M\text{-ary symbol}$$

and can therefore be one of M^k different functions. A coherent Viterbi Demod would have correlators for each of the M^k different signals.

The development of a computer program for this type of generalized partial-response signalling was begun. Difficulties were encountered in producing an analytical result for spectral occupancy of this type of signalling. A program to compute the spectrum from an FFT routine was started, but was not completed.

An RADC-funded study, "Line-of-Sight Technical Investigation," investigated binary partial-response schemes. In particular, schemes for h (t) being trapezoidal, triangular, and raised cosine in shape were investigated. It was found that the triangular shape produced the best 99-percent spectral occupancy. The length of h (t) (triangle) was set at 7 bits. A 95 -percent bandwidth equals 0.55 times bit rate and performance within 5.16 dB of binary PSK for an optimum demodulator was obtained. For this 99-percent bandwidth, both 8-ary and 4-ary FSK are within 5 dB of binary PSK with optimum demods. The binary partial-response scheme was thus worse than either of the FSK schemes located. It is not clear at this point if there is any implementation advantage with the optimum demods for this binary partial-response scheme over the FSK schemes. It is doubtful that one would be able to improve on the binary partial-response scheme reported in this study. The only reason to even consider partial-response schemes, then, is the possibility that a higher M alphabet than two (M = 4, 8, 16) might result in better performance than could be obtained with the FSK schemes. Going to higher M, though, complicates the demod in requiring correlators for M^k signals in a symbol time. It was concluded that even if some performance gain could be had with larger M partial response, the increased complexity in the demod would probably be significant.

2.5   SUMMARY OF RESULTS

The theoretical results obtained are listed in Table 1. The listed signals include all those examined for which the only mechanism of intersymbol influence is through the fact that the phase of the sinusoid at the beginning of a symbol is dependent on the data history. The shape of the phase trajectory during a symbol time is dependent only on the current bit. This class of signals includes, for example, all M-ary phase-modulation schemes. These PSK types correspond to no phase accumulation relative to the carrier phase. Also included are all types of M-ary FSK modulation wherein the phase does accumulate.

The PSK schemes (Table 1, entries 1 thru 15) all fall miserably short of the 20-dB E_b/N_o goal, even with raised cosine pulse-shaping. These schemes also have the disadvantage of creating a large carrier component in the transmitted signal. As a matter of fact, greater than 90 percent of the total transmitted power is in the carrier for many of these schemes. The small 99-percent spectral occupancy is obtained through this mechanism of simply putting most of the power in the carrier component, rather than reducing the bandwidth of the data-carrying continuous spectrum. This indicates that the schemes probably cannot be filtered to a bandwidth approaching the 99-percent spectral occupancy bandwidth without unduly distorting the data-carrying portion of the spectrum. These PSK schemes also have the disadvantage that even with coherent demods the performance is worse than the simpler schemes involving limiter-discriminator or noncoherent demods for 8-ary continuous-phase FSK (see Table 1, entries 23, 24, and 25).

Based on the results listed in Table 1, it was concluded that M-ary FSK represented the signal structure most likely to meet the design goals.

TABLE 1. CONSTANT ENVELOPE MODULATION SCHEMES EXAMINED

	Modulation Technique	Demodulation Technique	99% BW/Bit Rate	dB E_b/N_o, for $P_e = 10^{-7}$
1.	Binary PSK	Coherent 1-symbol (optimum)	0.5	28.6
2.	"	"	0.25	30.1
3.	4-ary PSK	"	0.5	28.9
4.	"	"	0.25	32.6
5.	8-ary PSK	"	0.5	30.1
6.	"	"	0.25	35.3
7.	16-ary PSK	"	0.5	33.9
8.	"	"	0.25	37.9
9.	Binary PSK Raised Cosine Pulses	"	0.5	29.6
10.	"	"	0.25	30.7
11.	4-ary PSK Raised Cosine Pulses	"	0.5	31.4
12.	"	"	0.25	33.7
13.	8-ary PSK Raised Cosine Pulses	"	0.5	32.8
14.	"	Coherent 1-symbol (optimum)	0.25	37.1

(continued)

TABLE 1. (CONTINUED)

	Modulation Technique	Demodulation Technique	99% BW/Bit Rate	E_b/N_o for $P_e = 10^{-7}$ dB
15.	16-ary PSK Raised Cosine Pulses	Coherent 1-symbol (optimum)	0.5	33.6
16.	7-ary Phase Trajectories (Combination of Phase and Frequency Modulation)	"	0.5	26.8
17.	"	"	0.25	29.9
18.	8-ary Continuous Phase FSK	Coherent 1-symbol	0.5	19.7
19.	"	"	0.25	25.3
20.	"	Coherent Viterbi Demod (Optimum)	0.5	16.7
21.	4-ary Continuous Phase FSK	Coherent 1-symbol	0.5	20.8
22.	4-ary Continous Phase FSK	Coherent Viterbi Demod (Optimum)	0.5	17.8
23.	8-ary Continuous Phase FSK	Limiter/Discriminator	0.5	27.

(continued)

36

TABLE 1. (CONTINUED)

	Modulation Technique	Demodulation Technique	99% BW/Bit Rate	E_b/N_o for $P_e = 10^{-7}$ dB
24.	8-ary Continuous Phase FSK	Noncoherent 1-symbol	0.5	26
25.	"	Noncoherent 3-symbol	0.5	20.8
26.	8-ary FSK w/phase jumps at beginning of symbols	Coherent 1-symbol	0.5	19.7
27.	8-ary PSK (Raised Cosine Pulses)	Coherent 1-symbol (Optimum)	1.33	19.7
28.	8-ary Split-Phase FSK	Coherent 1-symbol (Optimum)	1.33	19.7
29.	8-ary FSK Half-Cycle Sine Pulses	Coherent 1-symbol	0.95	19.7

Section III

IMPLEMENTATION CONSIDERATIONS

It was determined that signalling with 4-ary continuous-phase FSK with modulation index h = 1/8 satisfies the bandwidth constraint (99 percent of the power in a bandwidth of one-half bit rate) and has the theo oal potential of satisfying the performance design goal (BER of 10^{-7} with E_b/N_o of 20 dB). Techniques for modulating and demodulating such signals are considered in this section, with the ultimate goal of selecting the best techniques for implementation. The primary considerations for such selection are estimates of performance and implementation complexity for each technique.

3.1 MODULATION

First, consider modulation techniques for accomplishing continuous-phase 4-ary FSK with modulation index 1/8. Two data bits must be used each symbol-time to select a waveform having one of four possible frequencies for transmission. To maintain phase continuity, it is necessary that all of the four waveforms have the same phase at the symbol transition times. This requires that each pair of frequencies differs by exactly an integer number of cycles per symbol-time; hence, at this point the modulation index is unity rather than 1/8. The required modulation index of 1/8 is obtained by frequency-dividing the resultant waveforms either before or after mixing, so that the resultant center frequency is 70 MHz. One straightforward approach to getting the continuous-phase, mod, index 1 signal is to phase-lock one or more VCO's at multiples of the symbol rate and count down the VCO output, as shown in Figure 12, to obtain the four waveforms to be selected by the data bits. Symbol transition times then occur at zero-phase points for all waveforms.

Another approach which requires lower frequency rates for the digital operation, and appears more desirable to implement, is shown in Figure 13. In this approach, the data bits are used to select four possible pairs of input frequencies to a mixer such that the mixer output (sum frequencies) is one of four frequencies differing by the symbol rate. The same symbol-rate frequency is used to obtain the frequency differences between

Preceding page blank
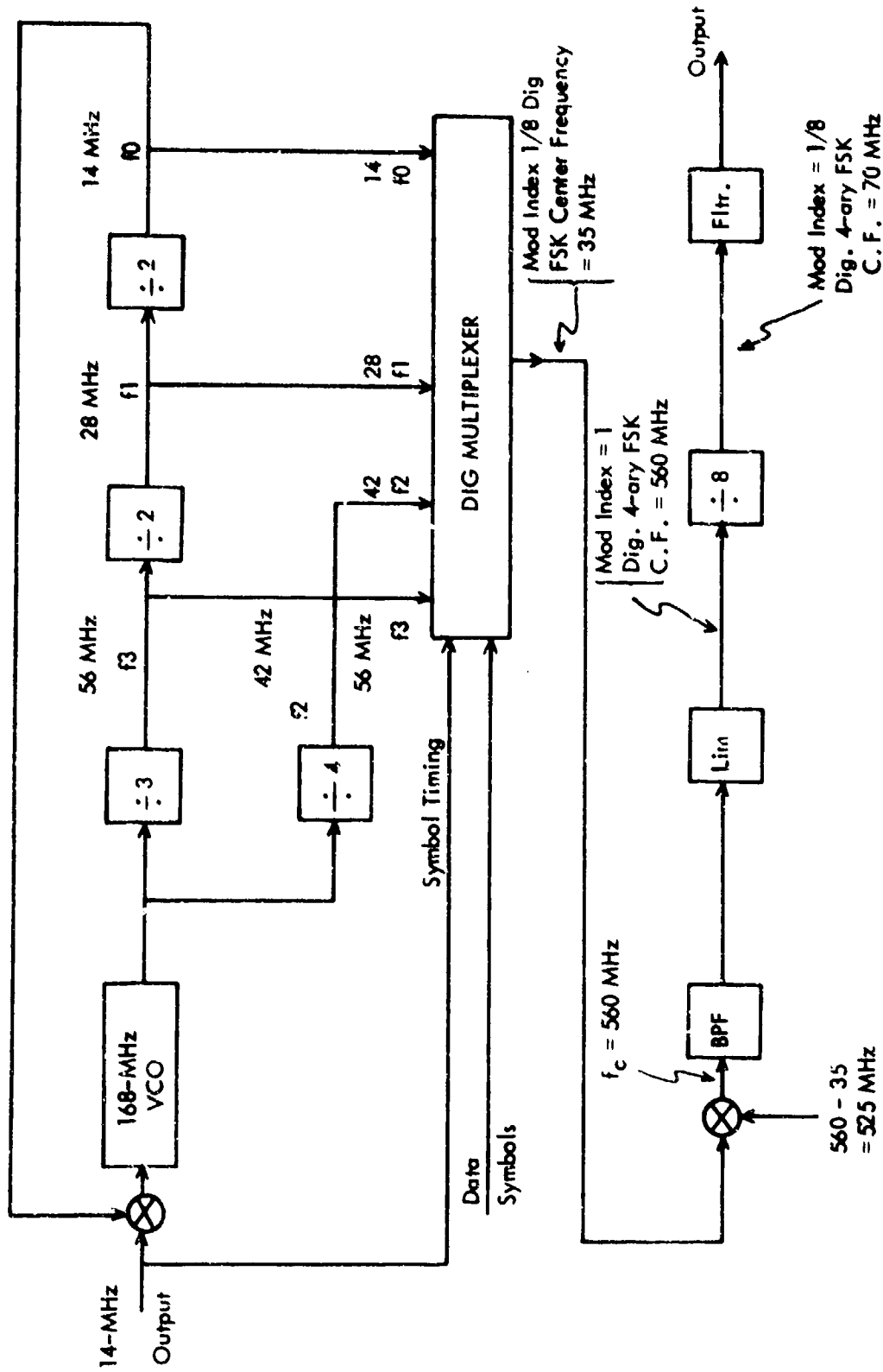
Figure 12. VCO Phase-Locking to Obtain Continuous-Phase, Mod, Index 1 Signal
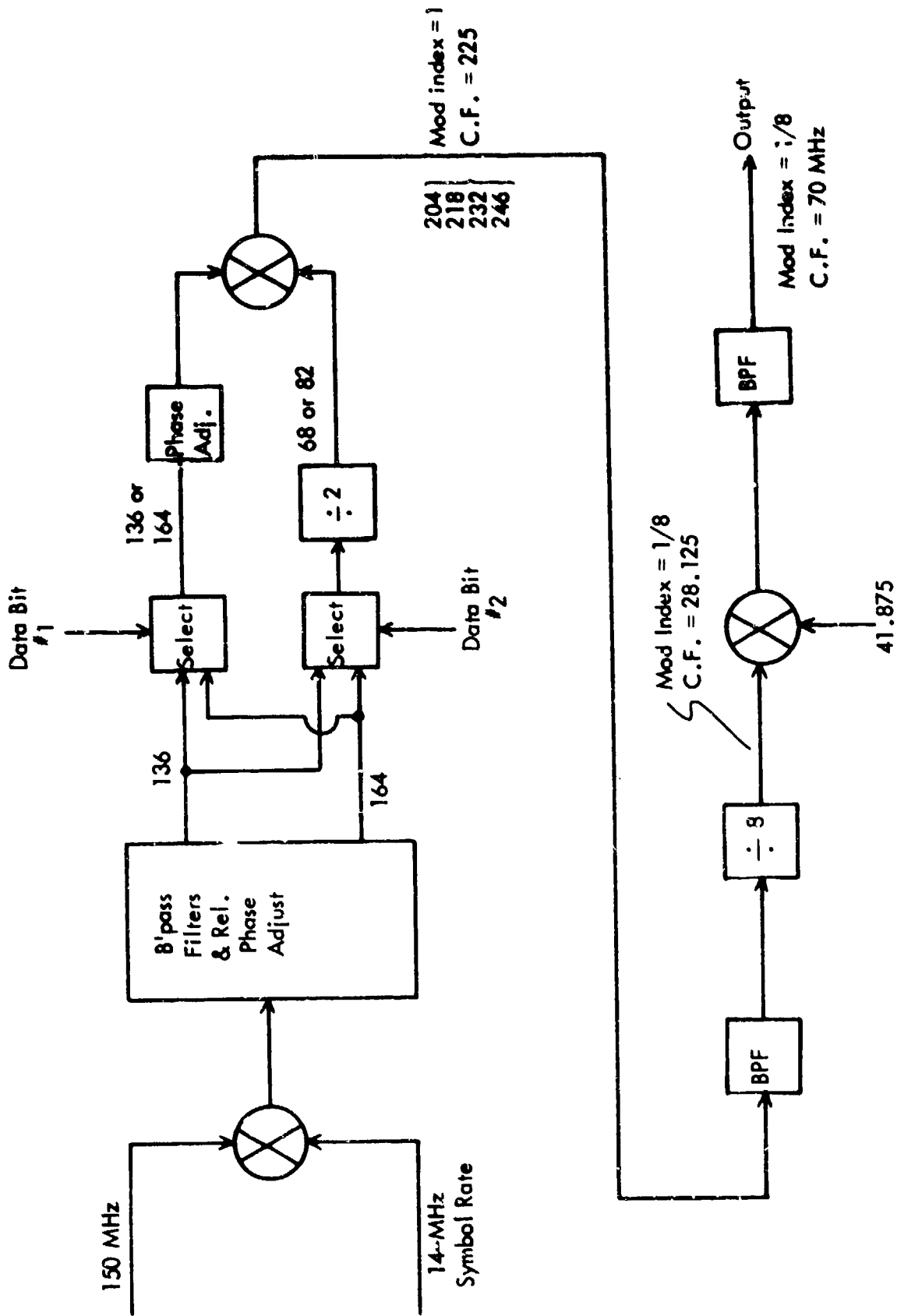
Figure 13. Alternate Approach to Deriving Continuous-Phase, Mod, Index 1 Signal

41

waveforms, as well as the transition times. Hence, if the transition times occur at the zero-phase points of the symbol-rate frequency, and relative shifts through the mixing circuits are matched, all waveforms will have the same phase (though not necessarily zero phase) at these transition times.

3.2   DEMODULATION

Consider first several "optimum" demodulation techniques to provide performance reference points and perhaps furnish guidance to implementation approaches for sub-optimum demodulation. In this category, single-symbol and multisymbol receivers for both coherent and noncoherent demodulation of 4-ary continuous-phase waveforms with modulation index 1/8 are considered. For such signalling, the signal waveform $s(t)$ during the nth symbol time is

$$s(t) = A \cos \left(\omega_c t + a_n \left(\frac{\pi}{4T_s} \right) t + \phi_n \right)$$

ω_c = center frequency

ϕ_n = Phase at beginning of nth symbol time

a_n = 1/2, -1/2, 3/2, or - 3/2 (depending upon which of the four symbols is transmitted in the nth symbol time).

3.2.1   Coherent Demodulation

Consider the performance of a coherent demodulator for 4-ary FSK. The signal is described by the phase trajectory plot of Figure 14. The coherent demodulator has knowledge of ϕ_n at the beginning of a symbol and correlates with each of four references,

$\cos \left\{ \left[\omega_c + a_n \left(\frac{\pi}{4T_s} \right) \right] t + \phi_n \right\}$, over the interval 0, T_s. For the small mod index used here for spectral compactness, the high S/N ratio performance is dominated by the probability of an error between two adjacent frequencies. The correlation between two sinusoids that are in phase at $t = 0$, and θ radians out-of-phase at T_s, is well known and given by

$$\rho = \frac{\sin \theta}{\theta} \underset{=}{\Delta} \text{sinc} (\theta) \tag{14}$$

42

$\phi(t)$

$\frac{6\pi}{8}$

$\frac{5\pi}{8}$

$\frac{4\pi}{8}$

$\frac{3\pi}{8}$

$\frac{2\pi}{8}$

$\frac{\pi}{8}$

0

$\frac{-\pi}{8}$

$\frac{-2\pi}{8}$

$\frac{-3\pi}{8}$

$\frac{-4\pi}{8}$

-5π

$\frac{-6\pi}{8}$

Etc . . .

t

0   T_S $2T_S$
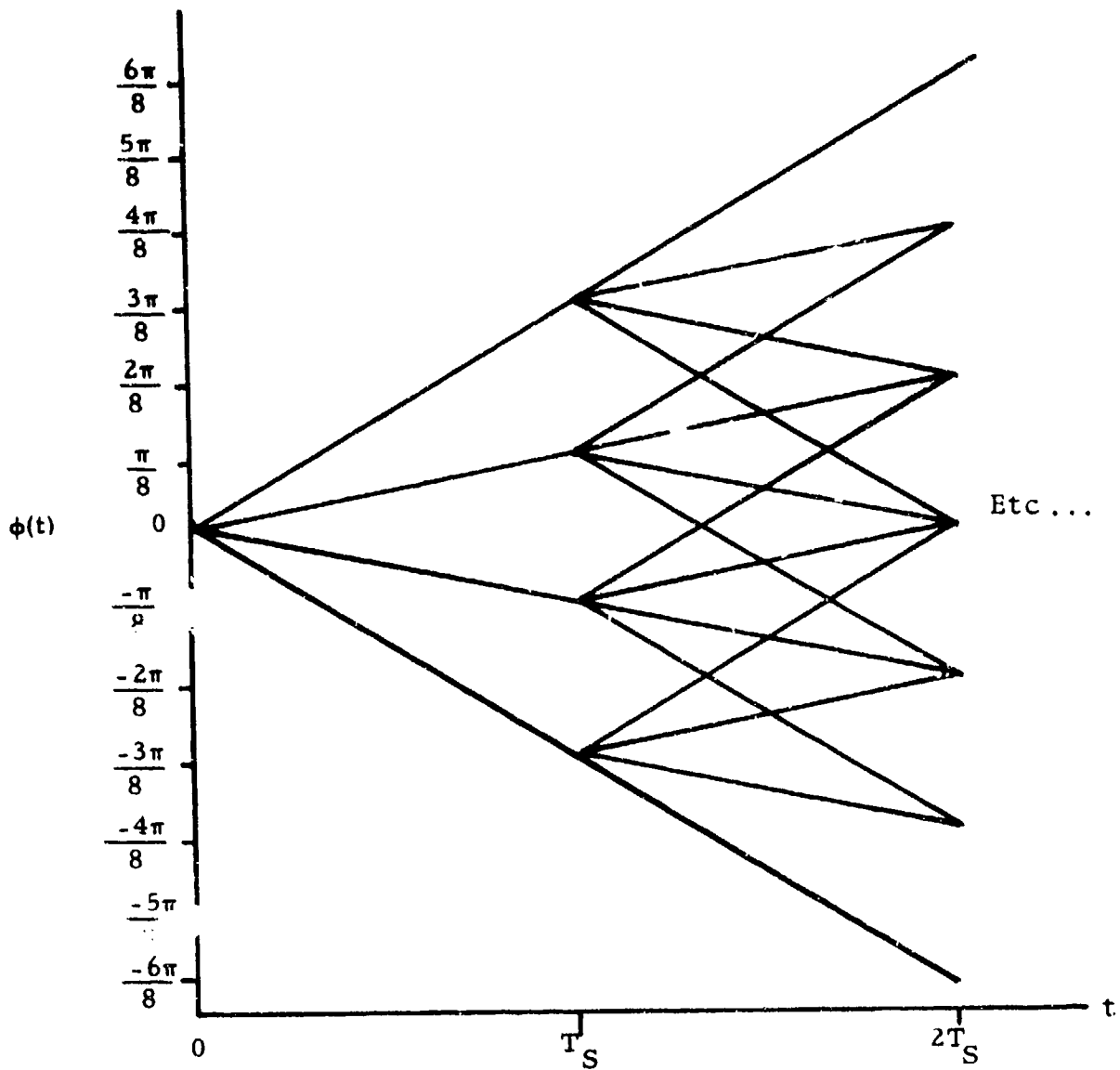
Figure 14.   Phase Trajectories for 4-ary FSK
With Mod Index = 1/8

43

The probability of making an error between the two sinusoids with a coherent receiver
is given by

$$P(e) = Q\left(\sqrt{\frac{E_s(1-\rho)}{N_o}}\right) \tag{15}$$

where $\quad E_s \quad = \quad$ Energy in a symbol

$\quad N_o \quad = \quad$ One-sided Gaussian white noise spectral density

and

$$Q(X) = \int_x^\infty \frac{e^{-\frac{y^2}{2}}}{\sqrt{2\pi}} \, dy$$

In a 4-ary FSK scheme, 2 bits are used to select one of the four frequencies to be trans-
mitted. The average energy per bit, E_b, is then half the energy-per-symbol, E_s:

$$E_s \quad = \quad 2E_b$$

From Equations (14) and (15), the error rate for an M-ary FSK mod index 1/8 coherent
single symbol observation receiver is given by

$$Q\left(\sqrt{\frac{2E_b}{N_o}} \, (1 - \text{sinc}\, \frac{\pi}{4})\right) \tag{16}$$

at high E_b/N_o. At the error rates of interest ($< 10^{-5}$), Equation (16) provides an accurate
prediction of performance for single-symbol demodulation and predicts an error rate of
10^{-7} at E_b/N_o of 21.3 dB. Even this ideal prediction is above the design goal of 20 dB.
But, note in Figure 14 that the continuous-phase property of the FSK signal leads to the
introduction of intersymbol influence among the transmitted signals in successive symbol
times. The one-symbol-time coherent demod, with the performance derived above,

ignores this property. A demod that recognizes and exploits this continuous-phase property might (and, in fact, does) perform better than the one-symbol-time demod.

The demod is one which observes the signal over n symbol times and makes a decision on the first symbol time by choosing the first symbol from the maximum likelihood signal sequence. The demod must select the allowable sequence having the largest correlation with the received waveform over the observation interval. The allowable sequences are defined as those having a phase trajectory that is a path through an n-symbol tree such as in Figure 14. The initial starting phase is presumed known at the coherent receiver. The performance of the multiple observation interval coherent receiver will be calculated, with the assumption that the signal-to-noise ratio is sufficiently high so that the error rate is dominated by the minimum distance error path (s) from the transmitted path. Distance over a time interval T between the ith and j^{th} signals, $s_i(t)$ and $s_j(t)$, is defined as

$$d_{ij}^2 = \int_0^T \left[s_i(t) - s_j(t) \right]^2 dt \qquad (17)$$

The probability that the ith signal has higher correlation with the received signal in additive white Gaussian noise than the jth signal was transmitted is given by the well-known relation

$$P_{ij} = Q\left(\frac{d_{ij}}{2N_o} \right) \qquad (18)$$

Referring to Figure 14, for the small mod indices of interest, it can be shown that over an n-symbol observation interval the minimum distance error paths for coherent correlation are those that start at $t = 0$ in phase, are $\pi/4$ radians out-of-phase at $t = T_s$, and are back in phase at $t = 2T_s$ through nT_s (see Figure 15).

This distance is given by

$$d^2 = 4E_s (1 - \sin \pi/4) \qquad (19)$$

45
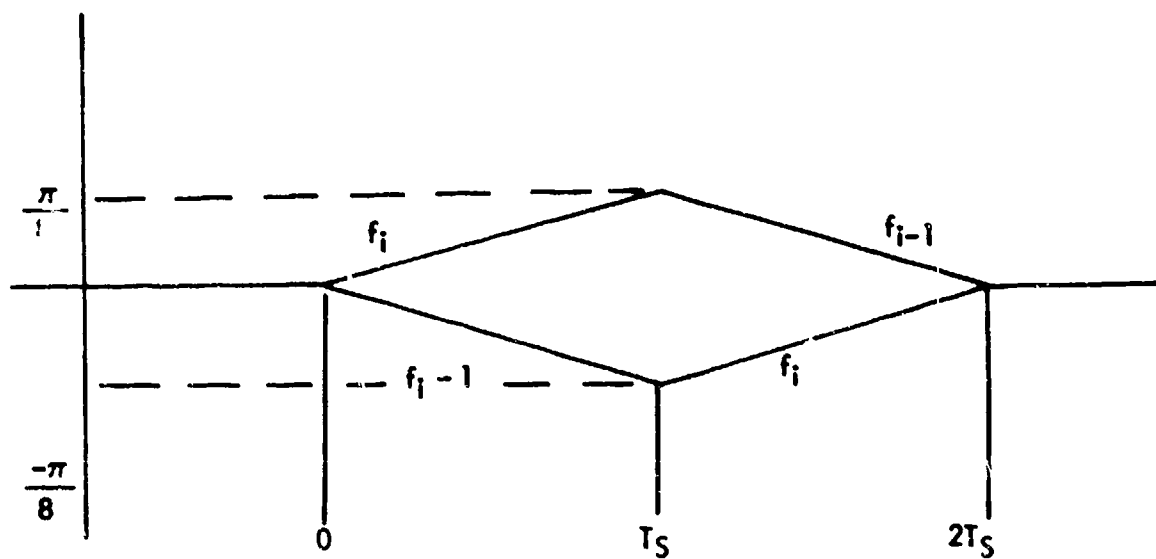
Figure 15. Example of Minimum Distance Error Paths

where

$$E_s = \text{energy in one symbol} = 2E_b.$$

$$E_b = \text{Average energy/bit}$$

For small mode indices, all other signal sequences are at distances corresponding to several dB larger E_b. The error rate given the ith sequence transmitted in the n-symbol times is therefore dominated by the path at the distance given by Equation (19). If all sequences over the n-symbol times are equally likely, then the probability of erroneously deciding the initial symbol is given by

$$Q\left(\sqrt{\frac{4E_b}{N_0}} \ (1 - \text{sinc } \pi/4)\right) \tag{20}$$

Comparing Equations (16) for one-symbol coherent and (20) for $n \geq 2$ - symbol coherent demodulation, it can be concluded that multiple-symbol observation yields a 3 dB performance improvement. The multisymbol coherent reception results theoretically in an error rate of 10^{-7} for E_b/N_0 of 18.3 dB.

The coherent references required during each symbol time for a one-symbol observation receiver are the four possible frequencies, each with one of eight different phases modulo 2π. The separation of the eight phases is $\pi/4$ for the h=1/8 system. These coherent references can be obtained in the following way for the h = 1/8 system. Considering Figure 16, the signal is first input to a device which multiplies frequency by 8. This leads to a mod index = 1, 4-ary FSK signal at eight times carrier frequency. As shown in Anderson and Salz[3], the mod-index-one signal has spectral lines at the four discrete frequencies corresponding to those transmitted. These four frequencies are selected by the bandpass filters (BPF) and phase-lock loops (PLL) are locked to each.

---

[3]Anderson, R.R. and J. Salz, "Spectra of Digital FM." BSTJ, July-August, pp. 1165 - 1189.

47
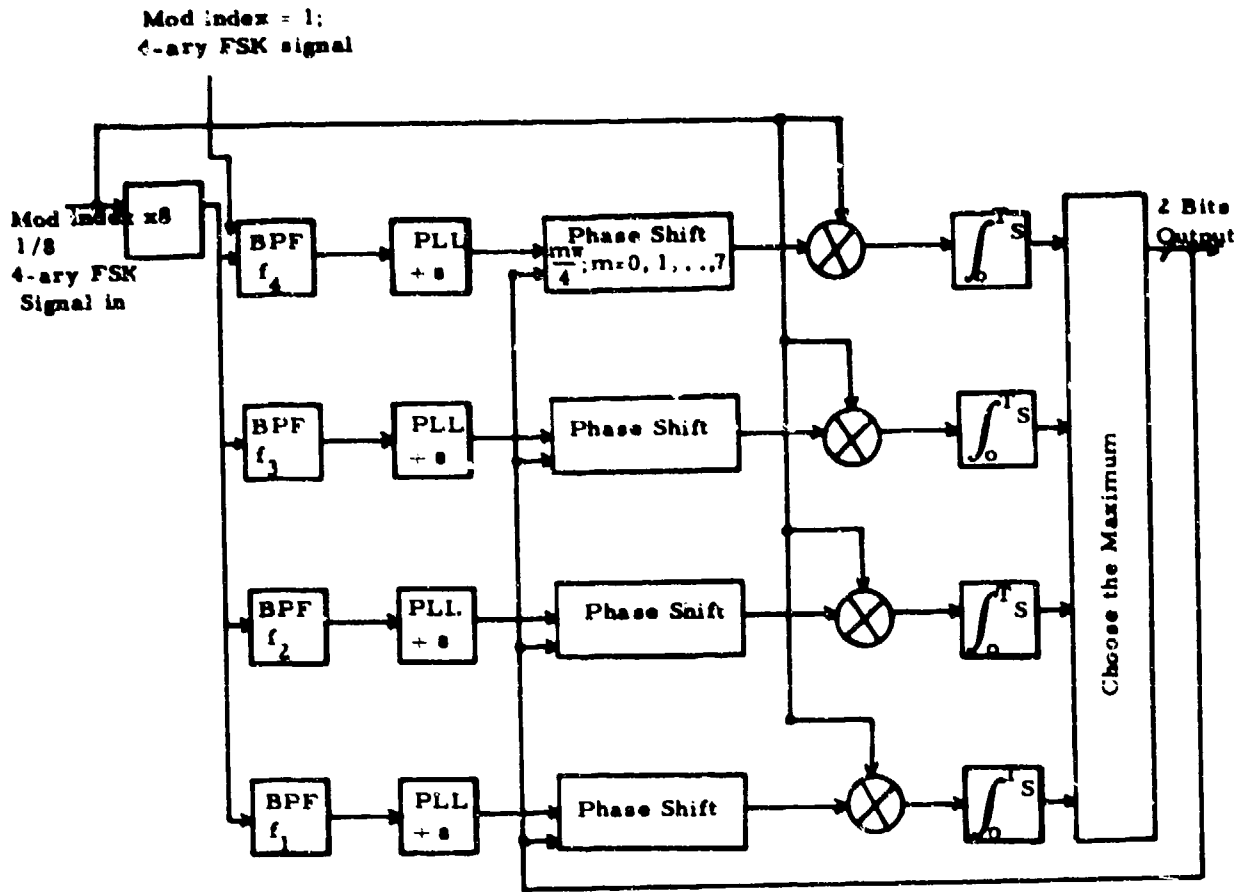
Figure 16. One Symbol Coherent Receiver
Structure for h=1 1/8 4-ary FSK

48

The PLL outputs are divided by eight, resulting in references at the original four frequencies coherent to within some multiple of $\pi/4$ radians, to the transmitted four frequencies. These references are fed to phase shifters which correct the phases by the proper amount to make all four frequencies in phase at the beginning of a symbol time. This phase must be the same phase as the received signal, which is assumed known. There is the practical problem, then, of establishing the ohase of the received signal. Assuming this has been done, the phase shifters are initially set accordingly. The coherent references are then correlated against the incoming symbol, and the symbol with largest correlation is decided. A phase trajectory plot such as in Figure 14 then defines the phase to which the coherently decided symbol would advance the signal. The decoded symbol is therefore fed back to the phase shifters to modify the reference phases to form the coherent references for the following symbol time.

The demod structure of Figure 16 is complicated; in addition, there are several practical decisions that need to be made in determining the feasibility of implementation. For example, the maximum correlation must be determined, the corresponding symbol must then be fed back to the phase shifters and the new coherent references established thereby, in a time short relative to a symbol time. At the rates relevant to this study, the symbol time is less than 100 nanoseconds; therefore this problem is a severe one. It is also possible that there is an error propagation problem, in that whenever an error is made erroneous references are used until a decision is made that puts the phase of the references back in step with the received signal. To avoid such an error-propagation problem would require eight times as many correlators, or a total of 32 (one for each of eight possible phases for each of four possible frequencies). An intriguing possibility that eliminates the necessity for the phase shifters involves simply coherently demodulating the mod-index-one signal that comes out of the times-eight nonlinearity of Figure 16. The PLL outputs of Figure 16, without the divide-by-eight, are the coherent references required to do so. The performance loss for such a suboptimum demodulator can be approximately predicted as follows:

The error probability for either the optimum coherent receiver or the suboptimum receiver is given by Equation (15). But for the suboptimum receiver suggested above,

49

the correlation coefficient ρ is the correlation coefficient for two adjacent frequencies with mod-index-one ($\rho = 0$) rather than $1/8$ ($\rho = .9$), and the effective N_o for the suboptimum receiver is 64 times that for the optimum receiver, since the rms phase noise is eight times as great after the times-eight multiplication. Hence,

$$(1-\rho)\,opt. = 1 - .9 = .1$$

$$(1-\rho)\,sub.\,opt. = 1 - 0 = 1$$

and it can be seen from Equation (15) that 10 dB has been gained due to the change in ρ and approximately 19 dB (i.e., $10\,\log_{10}64$) has been lost because of the increased phase noise due to the frequency multiplication of the signal. The net predicted loss is therefore 8 dB. Performance predictions for the suboptimum system were also made utilizing a computer simulation program. The net loss from this simulation was 6 dB.

It was also noted that times-four frequency multiplication produces mod index of $1/2$, which also corresponds to $\rho = 0$ (gain of 10 dB). The effective N_o for times-four frequency multiplication, however, is 16 times that for the optimum received (loss of $10\,\log_{10}16 = 12$ dB). Hence, coherently demodulating after times-four frequency multiplication of the signal results in a predicted net loss of 2 dB relative to the optimum receiver. The computer simulation program predicts approximately the same performance for this receiver as for the optimum receiver. Therefore, this appears to be a simpler and hence a more desirable one-symbol coherent receiver structure than the optimum correlation receiver. However, as noted above, one-symbol demodulator performance does not meet the design goal requirement, whereas multiple-symbol coherent performance does.

But the multiple-symbol coherent demodulator is even more complex to implement. As indicated earlier, the minimum-distance error-path for the low modulation index of interest is two symbol times long (see Figure 15). For the low error rates of interest here, the two-symbol coherent demodulator will achieve performance very close to that of an n-symbol coherent demodulator for $n > 2$. But even a two-symbol coherent demodulator would require 128 two-symbol correlator references, since there are 16 possible combinations of four frequencies and eight starting phases for each combination.

This could be reduced to 32 by utilizing the principle of the maximum-likelihood decod-ing techniques noted by Viterbi[1] for convolution codes. From Figure 14, it is seen that when two signal paths reach the same phase modulo 2π, identical input symbols to the modulator thereafter produce identical signals out of the modulator during successive symbol intervals. This is the same type of structure exhibited by convolution codes, and the same maximum-likelihood demodulation techniques used for convolution codes can be used here. Nevertheless, this technique still requires 32 correlators and considerable logic to keep track of competing signal paths and cumulative correlation measures for each path, as well as decision-making logic to choose the most likely path, and hence, most likely symbol decision, each symbol-time. The speed requirements for the logic circuitry would also be high for the symbol rates of interest here.

3.2.2 Noncoherent Demodulation

The structure of a one-symbol noncoherent receiver for 4-ary FSK is shown in Figure 17. This receiver is equivalent to the optimum noncoherent receiver. It con-sists of four matched filters (one for each of the four symbols), each followed by an envel-ope detector whose outputs are sampled at the symbol rate and at the proper time, and the largest output selected. (The required timing circuitry is not shown.) The corresponding matched symbol is then the demodulator output decision. (Practical approximations to matched filters for FSK symbols are narrow-band filters tuned to the symbol frequency.)

The symbol error probability for such a receiver, for the high signal-to-noise ratios of interest here, is given by

$$P_e = Q\left(\sqrt{\frac{E_s}{N_o}}\,(1 - |\rho|\,)\right) = Q\left(\sqrt{\frac{2E_b}{N_o}}\,(1 - |\rho|\,)\right)$$

---

[1]Viterbi, A.J., "Error Bounds for Convolutional Codes and an Asymptotically Optimum Decoding Algorithm," IEEE Trans. on Information Theory, April 1967, page 260.

51
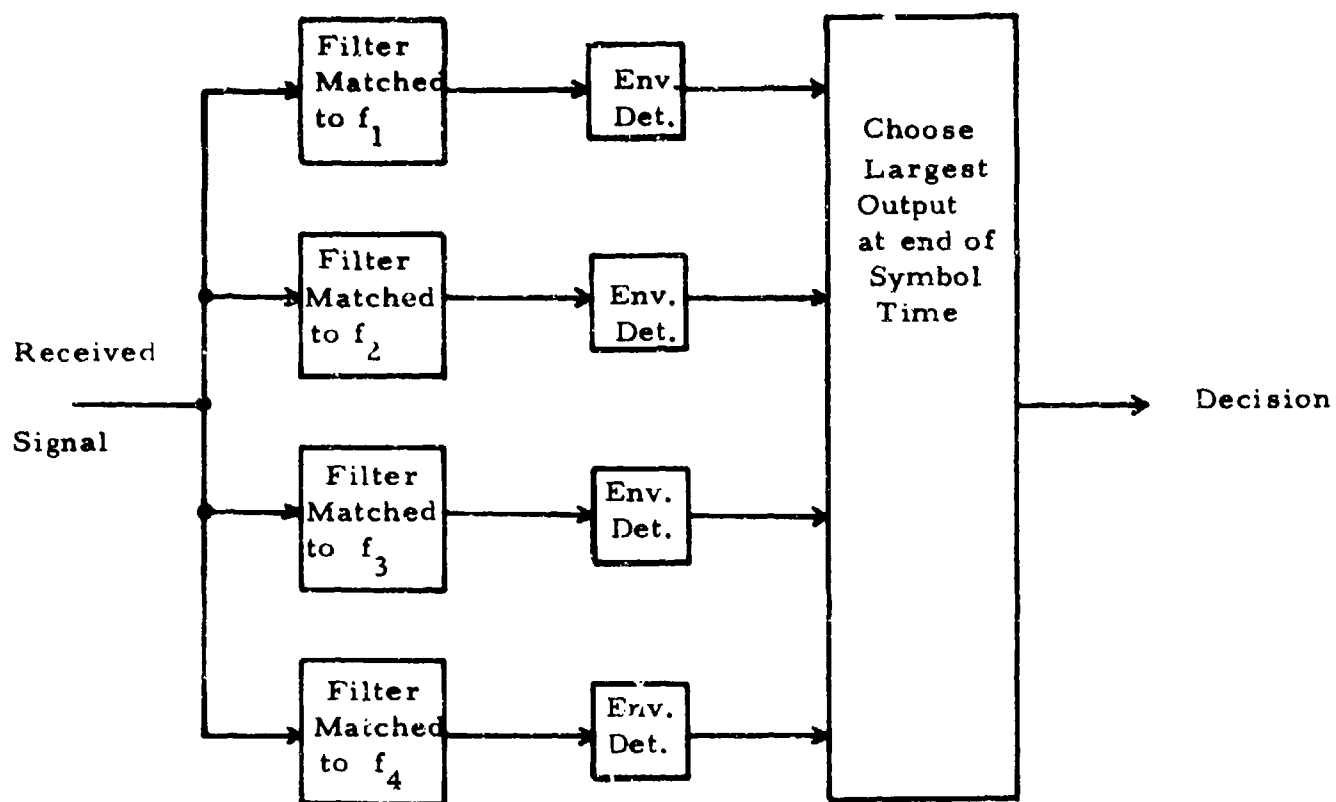
Figure 17.   One-Symbol Noncoherent Receiver for 4-ary FSK

where

$$\rho = \frac{1}{T_s} \int_0^T e^i \left[\phi_1(t) - \phi_2(t) \right] dt$$

$\phi_1(t)$ and $\phi_2(t)$ are the phase trajectories for adjacent symbols. That is, for the 4-ary continuous-phase FSK signals of interest here, $\phi_1(t) - \phi_2(t) = (\frac{\pi}{4T_s}) t$

$$\therefore \rho = \frac{1}{T_s} \int_0^{T_s} e^{i(\frac{\pi}{4T_s}) t} = \frac{4}{i\pi} \left[e^{i\frac{\pi}{4}} - 1 \right] = e^{i\frac{\pi}{8}} \left(\text{sinc} \frac{\pi}{8} \right)$$

or $|\rho| = \text{sinc} \frac{\pi}{8} = .975$

$$\therefore P_e = Q\left(\sqrt{\frac{2E_b}{N_0}} (.025) \right) = 10^{-7} \text{ for } \frac{E_b}{N_0} = 27.4 \text{ dB}$$

This performance is not very close to the design goal. But if more than one symbol is observed in making each symbol decision, the continuous-phase property of FSK may also be used in a noncoherent receiver to improve its performance.

In Figure 18 is shown a receiver which observes the 4-ary received signal over three symbol times and matches noncoherently to each of the $4^3 = 64$ possible transmitted signals in that three-symbol interval. At the sampling time, once per symbol, the output of each of the 64 envelope detectors is sampled and the largest detector output is selected. The middle symbol in the filter corresponding to the largest output becomes the output decision over that symbol time. For high signal-to-noise ratios, this receiver can be shown to be equivalent to the optimum receiver for continuous-phase binary FSK with a 3-bit observation interval.[2]

---

[2]Osborne, W.P. and Luntz, M.B., "Coherent and Noncoherent Detection of CPFSK," IEEE, Transactions on Communication Technology, Vol. COM-22, No. 8, pp. 1023 - 1036, August 1974
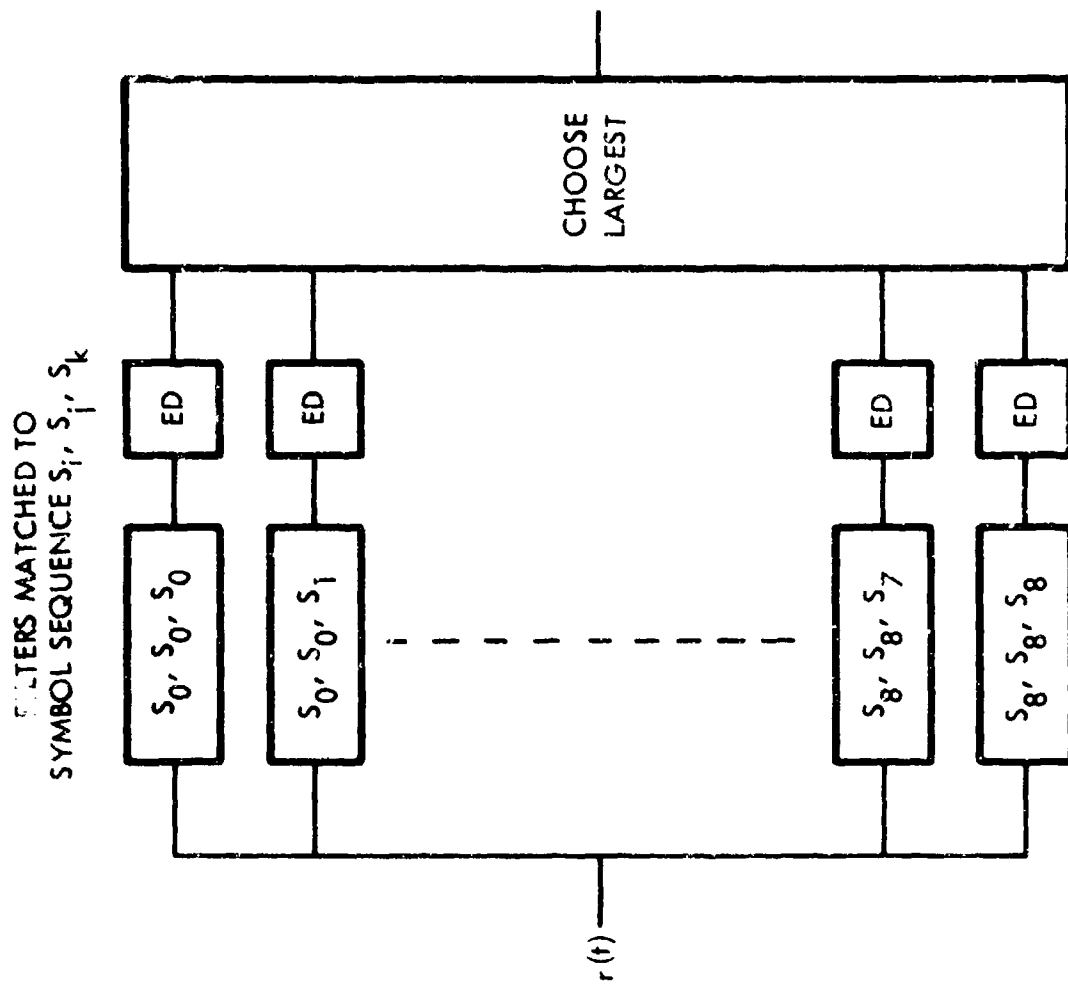
Figure 18. Three-Symbol Noncoherent Receiver

87508-5

54

The performance of this receiver cannot be rigorously computed, but a union bound on the receiver performance is not particularly difficult to find. The probability of error is limited by the probability of error for the worst-case data sequence. That is, the overall error probability, P_e, is

$$P_e' \leq P_r \ (\epsilon | S_i \cdot S_k \cdot S_l) \Big| \max i, k, l,$$

the error probability for the worst-case three-symbol sequence S_i, S_k, S_l. By considering each possible error individually, the union bound on probability of error

$$P_e < \sum_{\substack{IKL \\ K \neq k}} P_r \left(R_{IKL} > R_{ikl} \mid S_i \ S_k \ S_l \right) \tag{21}$$

may be written. That is, the probability of error will be less than the sum of probabilities that an error filter output, R_{IKL}, exceeds the correct filter output, R_{ikl}, given the input sequence S_i, S_k, S_l. At high signal-to-noise ratio, the sum of Equation (21) is dominated by the largest pairwise error probability, $P \left(R_{IKL} > R_{ikl} \mid S_i, S_k, S_l \right)$. Thus, the probability of error for the three-symbol receiver of Figure 18 may be found by considering the binary error performance for the worst-case pair of three-symbol-duration filters. For the FSK signal with peak-to-peak deviation of 3/8 the symbol rate, the worst-case pair is one which contains an adjacent symbol error for each of the three transmitted symbols. Additionally, for the worst-case pattern the errors in the first and third symbols will be in the opposite direction from the center symbol error. That is, if the transmitted symbol sequence were S_2, S_3, S_3, then the most probable error sequences are S_1, S_4, S_2 and S_3, S_2, S_4. At high signal-to-noise ratio, the probability of error is given by

$$P_e = Q \left(\sqrt{ \frac{3E_s}{N_0} } \ (1 - |\rho|) \right) \tag{22}$$

where ρ, the complex correlation coefficient between a pair of three-symbol waveforms, is defined as

$$\rho = \frac{1}{3T} \int_0^{3T} \bullet^{\,i} \left[\phi_1(t) - \phi_2(t) \right] \, dt \qquad (23)$$

The phases $\phi_1(t)$ and $\phi_2(t)$ are the phase trajectories for each of the worst-case pairs of waveforms. In this case, this phase different is given by

$$\phi_1(t) - \phi_2(t) \quad = \quad \begin{cases} \dfrac{\pi}{4T}\, t & 0 < t < T \\[2ex] \dfrac{\pi}{4T}\,(2T - t) & T < t < 2T \\[2ex] \dfrac{\pi}{4T}\,(t - 3T) & 2T < t < 3T \end{cases}$$

Evaluation of the correlation from Equation (23) yields $|\rho| = \text{sinc}\,(\pi/8)$, which may be used to evaluate the probability of error from Equation (22). This yields an error probability of 10^{-7} at $E_b/N_o = 22.4$ dB, a 5-dB gain over single-symbol noncoherent demodulation.

The symbol error rate performance for coherent and noncoherent demodulation of 4-ary FSK, mod index $1/8$, is plotted in Figure 19 versus E_b/N_o. Also included in Figure 19, for comparison with the performance of the optimum techniques, is limiter-discriminator performance with a 4-pole linear phase IF filter with 3-dB bandwidth equal to the symbol rate. The details of limiter-discriminator performance predictions are treated in Appendix C.

3.2.3   Multiple Symbol Observation

It will be noted from Figure 19 that the ideal performance of the optimum single-symbol receiver is more than a dB short of the design goal. If only 1 dB were allowed for implementation loss, the single-symbol coherent receiver performance would be more than 2 dB from design goal. In addition, as noted above, such a receiver is
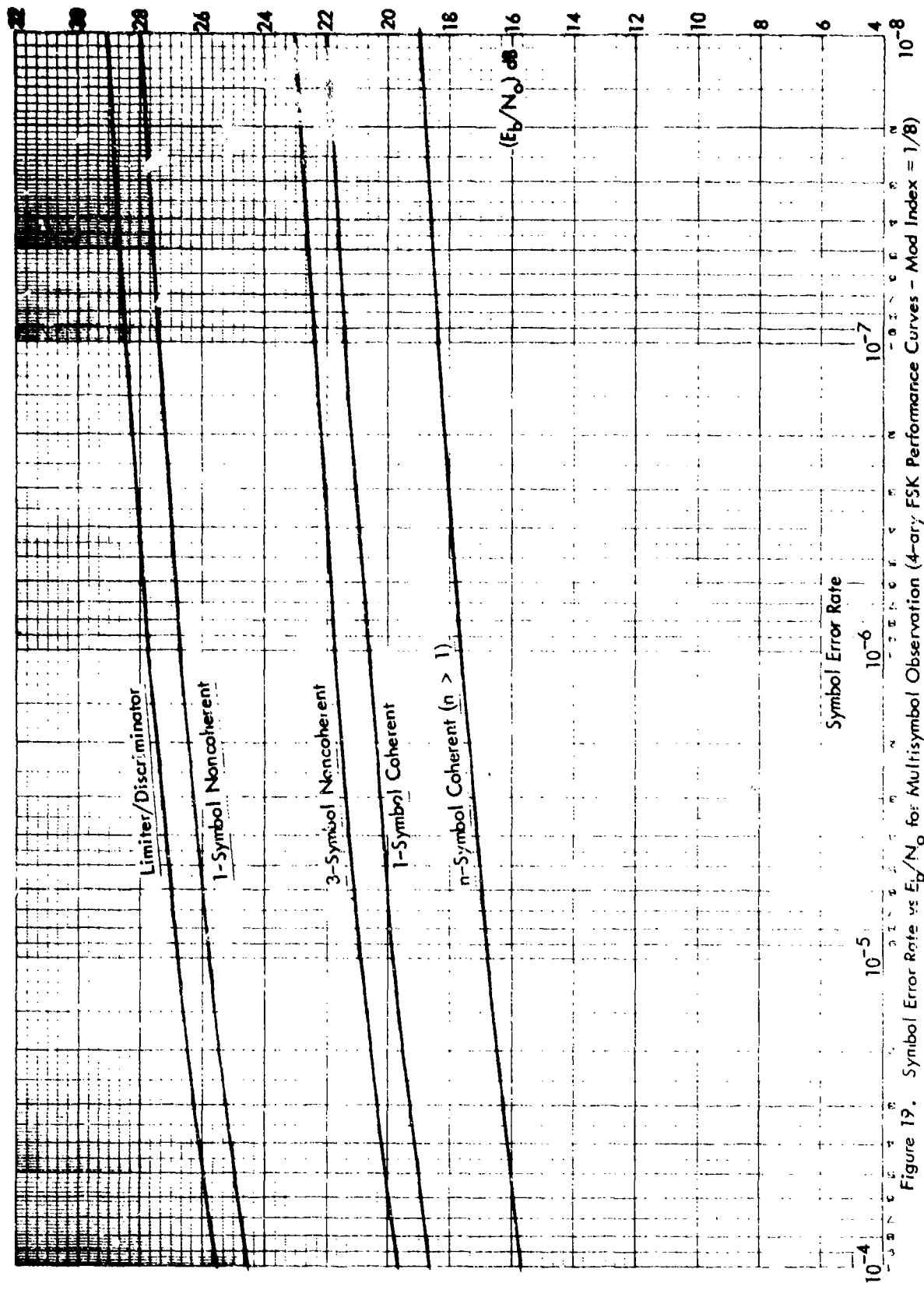
Figure 19. Symbol Error Rate vs E_b/N_o for Multisymbol Observation (4-ary FSK Performance Curves – Mod Index = 1/8)

rather complex to implement. Suboptimum single-symbol approaches would likely lose even more in performance.

It appears clear from the results in Figure 19 that any hope of achieving design goal performance must utilize multisymbol demodulation. That is, the received signal for more than one symbol-time (e.g., for n symbol times) must be used in making each symbol decision. This implies consideration of all possible trajectories over n symbol-times, which leads to implementation complexity and possibly unrealistic speed requirements, as noted earlier. But for any received signal over n symbol-times, many of the possible transmitted trajectories are very unlikely. This consideration leads to a search for simple schemes for eliminating the very unlikely trajectories from further consideration, thus simplifying the final selection of the most likely transmitted trajectory. One such possible scheme for consideration involves first determining the most likely beginning phase (phase at the beginning of each symbol time) for each possible frequency, thus reducing from 32 to 4 the number of symbols for consideration during each symbol-time. This would result in a phase trajectory trellis with four possible symbols per symbol-time, such as that shown in Figure 20.

One way to retain the four most probable symbols each symbol-time is to use the "midsymbol" zero-crossing time to determine the most likely beginning phase for each possible frequency (see Figure 21). It is assumed here that there are roughly two cycles per symbol time for the four symbol frequencies. For any frequency there are eight possible beginning phases, and hence, eight possible sets of zero-crossing times. The time and direction of a zero-crossing then determines the starting phase for any assumed frequency. But with noise the exact zero-crossing times cannot be determined. However, with noise corresponding to $E_b/N_o = 20$ dB, the probability of eliminating the correct transmitted symbol by this procedure is approximately 10^{-14}, which is negligible in relation to available final error rates. This is calculated as follows:

Consider a typical symbol with K cycles per symbol-time (K not necessarily integer), as shown in Figure 21. The slope at a zero crossing is

58
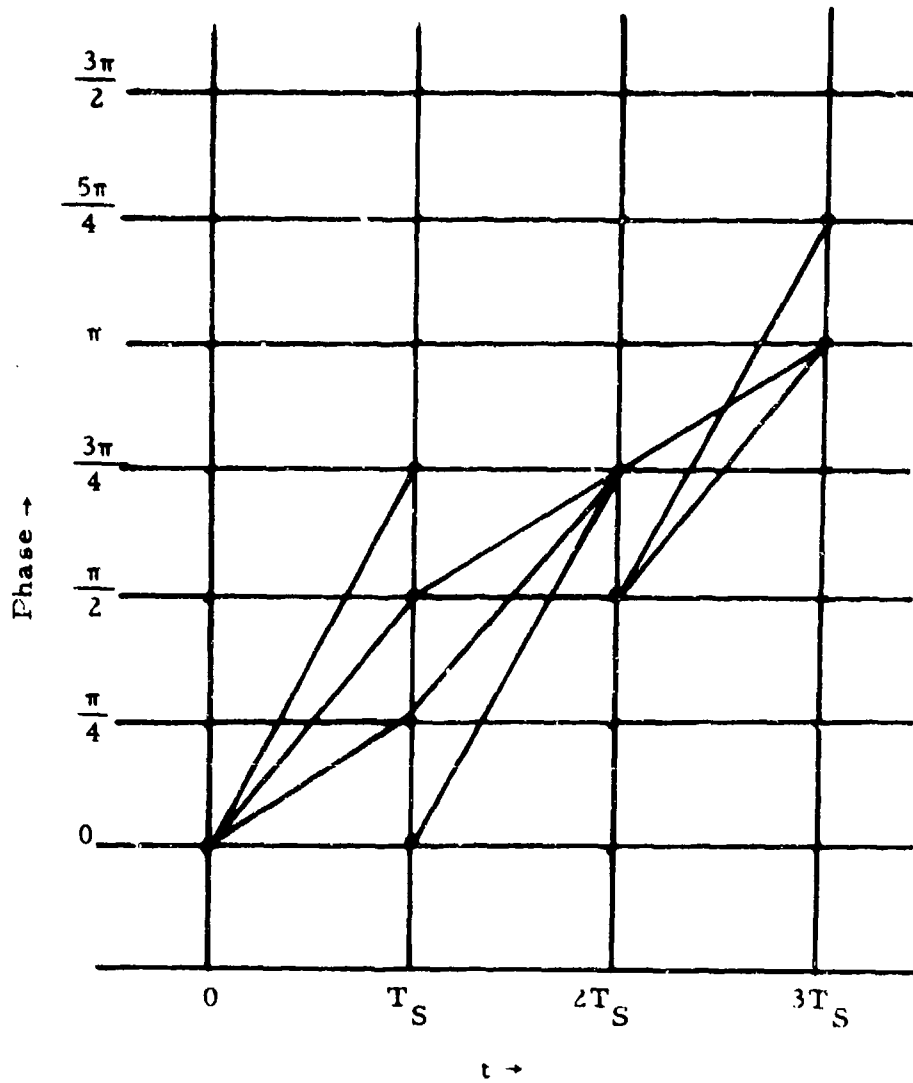
Figure 20. Typical Phase Trajectory Trellis
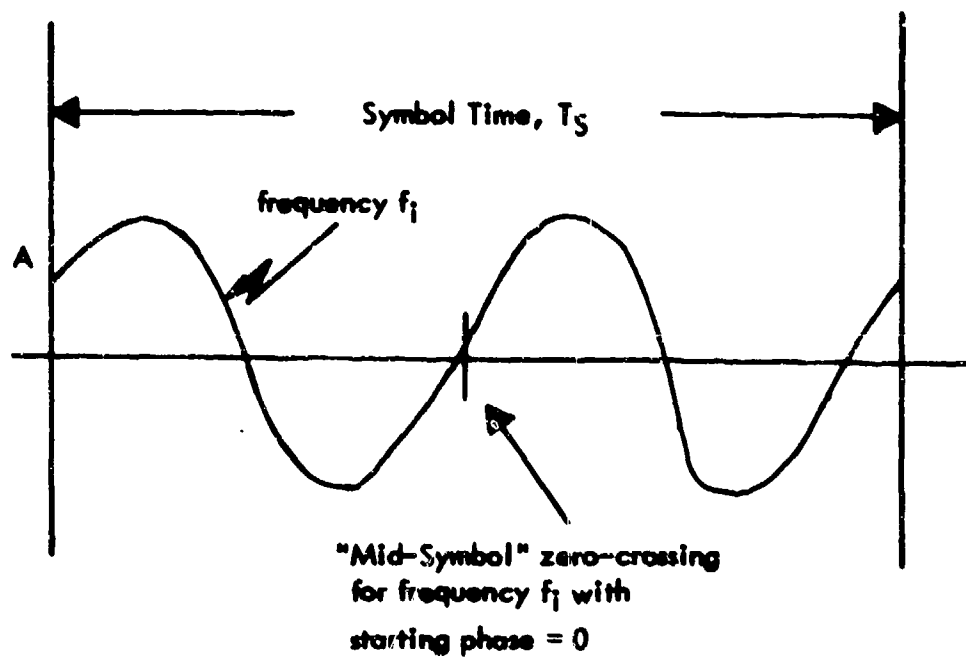
Figure 21. Typical Symbol

$$s = \frac{\pi A/2}{T_S/4K} = \frac{2\pi AK}{T_S}$$

and for high signal-to-noise ratio, the rms phase jitter due to noise variance $\sigma_n{}^2$ is $\sigma_\phi = \sigma_n/s$. But with white noise of spectral height N_o passed through a filter with noise bandwidth = symbol rate,

$$\frac{E_s}{N_o} = \frac{2E_b}{N_o} = \frac{A^2}{2\sigma_n{}^2}$$

$$\therefore \sigma_\phi = 1/4K\pi \sqrt{E_b/N_o} \text{ in symbol-time units.}$$

For any frequency, the eight possible beginning phases differ by 1/8 cycle. And for any frequency, the corresponding zero-crossing locations are known. Therefore, the probability, PE, of selecting the wrong starting phase from a measurement of midsymbol zero-crossing time is equal to the probability that the phase noise exceeds 1/16 cycle. With $E_b/N_o = 20$ dB and Gaussian noise, this is

$$PE = Q\left(\frac{1/16K}{1/40K\pi}\right) = Q\ (7.86) \cong 10^{-14}$$

A conceptual circuit for determining these four most probable symbols each symbol-time, and hence the most probable trellis paths, is shown in Figure 22.

In addition to the "phase noise" considered above, there will be a "measurement noise" due to uncertainties in (noiseless) measurement of zero-crossing time.

As noted above, the rms phase noise in symbol-time units is $\sigma_\phi = 1/4K\pi$ $\sqrt{E_b/N_o}$. For $E_b/N_o = 20$ dB and K = 2 this becomes $\sigma_\phi = \frac{1}{80\pi} = .004$ symbol-times, and this corresponds to PE = Q (7.86) $\cong 10^{-14}$. A PE of 10^{-8}, which corresponds to

61
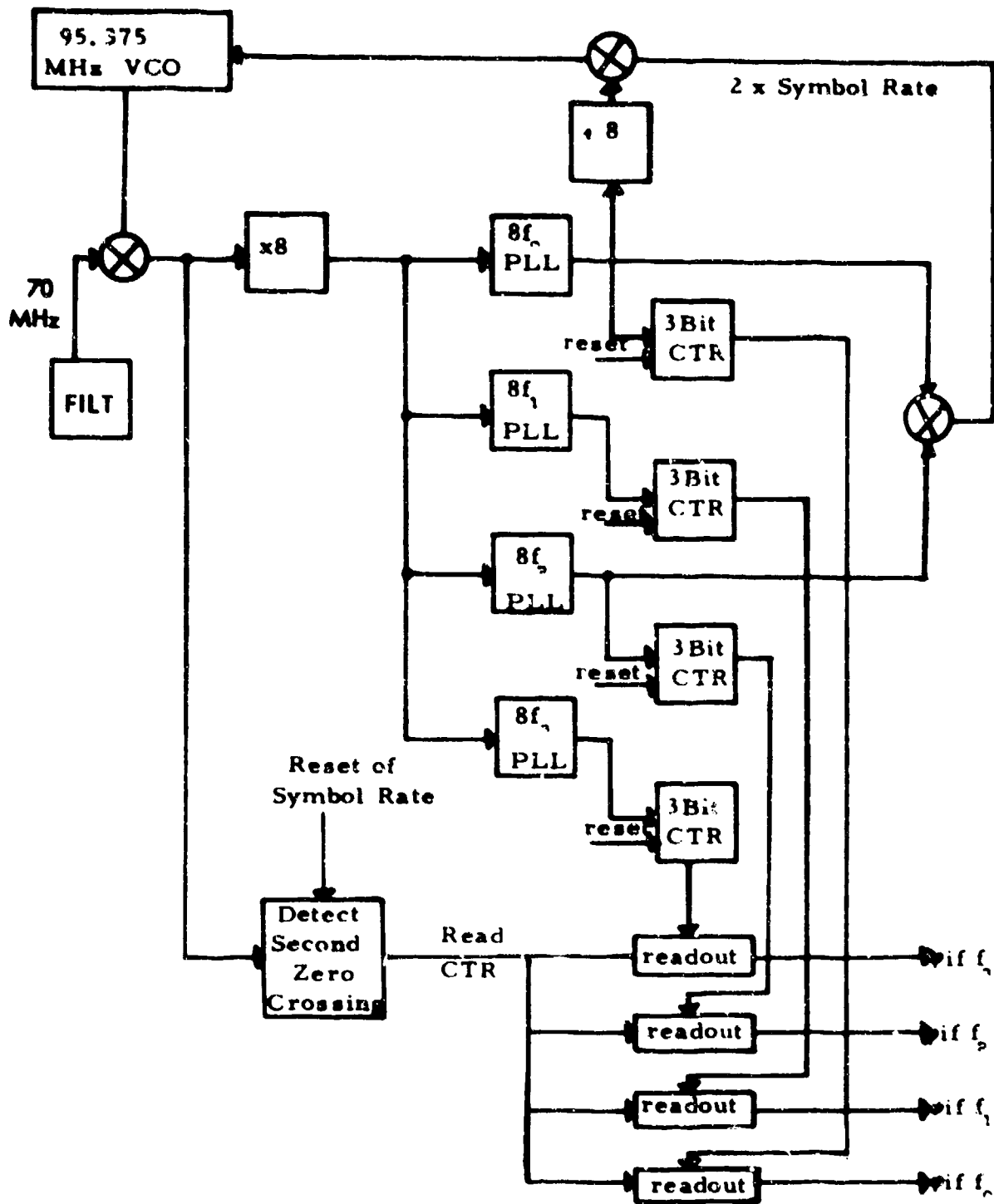
Figure 22. Conceptual Circuit for Obtaining Trellis Symbols

62

Q (5.61) could be tolerated. Since the "phase noise" and the "measurement noise" add together and are considered independent, their variances add. Hence, the variance of the measurement noise, $\sigma_m{}^2$, must satisfy the following equations:

$$\sigma_m{}^2 + \sigma_\phi^2 = \sigma^2$$

and

$$\frac{\sigma}{\sigma_\phi} = \frac{7.86}{5.61} = 1.4$$

$$\therefore \sigma_m = \sigma_\phi = 0.004 \text{ symbol times} \cong 0.3 \text{ nanoseconds}.$$

Therefore, very precise time resolution of zero-crossing time measurements are required. Also, the final selection of trajectories must consider continuity over two or more symbol times of the trellis (Figure 20). Conflicts between trajectories must be resolved by some additional measures such as phase measurements at (or near) symbol transition times (end-phases), making use of intersymbol dependence due to the filtering. The final algorithms and circuitry for accomplishing this were not completed because of the greater promise of the technique of frequency determination from end-phase measurements.

In considering frequency determination from end-phase measurements, it should be noted that if the transmitted phase could be reliably determined at each symbol transition time, the frequency during each symbol time could be reliably determined from the difference in phase at the beginning and end of each symbol time. In fact, at low error rates, one would expect to make two (adjacent) symbol errors each time an error is made in determining this "end-phase." With high signal-to-noise power ratio, S/N, the variance of equivalent phase noise, σ_θ^2, is:

$$\sigma_\theta^2 = \frac{1}{2\,(S/N)} \qquad \text{radians squared}$$

63

If one limits the noise power with a filter with noise bandwidth equal to the symbol rate and neglects the signal attenuation through the filter, the signal-to-noise ratio at the filter output is $S/N = E_s/N_o$, where E_s is signal energy per symbol and N_o is noise-power spectral density. But for 4-ary FSK, $E_s = 2 E_b$.

$$\therefore \quad \sigma_\theta = \frac{1}{\sqrt{4 \frac{E_b}{N_o}}}$$

Assuming this phase noise to be Gaussian, the probability P_ϕ that the phase error due to noise exceeds an angle ϕ is $Q(\phi/\sigma_\theta)$.

$$\therefore \quad P_Q = Q \left[\sqrt{\frac{4E_b}{N_o} \phi^2} \right] \qquad (\phi \text{ in radians})$$

Since transmitted end-phases are separated by 45°, the probability of noise alone causing an error (threshold half-way between phases) is

$$P_{\pi/8} = Q \left(\sqrt{\frac{2 E_b}{N_o} \left[2 \frac{\pi}{8} \right]^2} \right) = Q \sqrt{\frac{2 E_b}{N_o} (.309)}$$

This error-rate performance is only 5.1 dB worse than antipodal signalling (e.g., binary PSK) and corresponds to an error rate of 10^{-7} at E_b/N_o of 16.4 dB. (Antipodal signalling gives an error probability of 10^{-7} at E_b/N_o of 11.3 dB.) This is of course unrealistic, since it ignores filter distortion of the transmitted phase trajectories. Hence, the next step in determining realistic performance predictions for such an approach is to determine realistic phase trajectory distortion by realizable filters.

Several filters were considered and the one which appears to have good phase distortion characteristics is a four-pole modified linear phase filter with noise bandwidth equal to the symbol rate. This is termed a "modified" linear phase filter, since it is not a "standard" bandpass linear phase filter. However, it is realizable and its pole and zero

locations are known. It will be referred to hereafter as the "nominal filter". After adjusting the filter output for a constant time delay and a constant frequency offset, the trajectory distortion of the filter output relative to the input is as shown in Figure 23 for all possible positive frequency transitions. Distortion is symmetrical for negative frequency transitions. No filter distortion of any significance extends over more than one symbol time. From these distortion characteristics it is easily determined that for any two minimum-distance trajectories such as those shown in Figure 24, the filter distortion causes the candidate end-phase to differ by 35°. Hence, if the threshold can be chosen properly (half way between the two distorted phases), the probability of error in deciding between the candidate phases is

$$P_{17.5^{\circ}} = Q\left(\sqrt{\frac{2\, E_b}{N_o}\ (.186)}\right)$$

which is 7.3 dB worse than antipodal signalling and corresponds to an error probability of 10^{-7} with E_b/N_o of 18.6 dB. From the above discussion of optimum coherent reception, recall that the optimum receiver has an error probability of 10^{-7} with E_b/N_o of 18.3 dB.

This performance, only 0.3 dB from optimum, assumes that one can properly locate the decision threshold between two candidate end-phases. But determining the proper threshold location for any symbol transition time (e.g., b in Figure 24) requires knowing the transmitted end-phases on either side of this transition time (e.g., a and c, Figure 24). These phases, of course, are not known; in fact their determination is part of this demodulation process. But an intuitive approach to establishing the thresholds is to make repeated and progressively refined estimates of the transmitted phase at each symbol transition time, using measured phases out of the filter. These phase estimates then provide crosstalk estimates and hence thresholds for more refined phase estimates. Such a process, consisting in principle of three successively refined estimates at each symbol transition time, is described in the following paragraphs.

The first step is to retain a most likely pair of (adjacent) transmitted phases at each point consistent with the measured phase (including noise and filter distortion) at

65
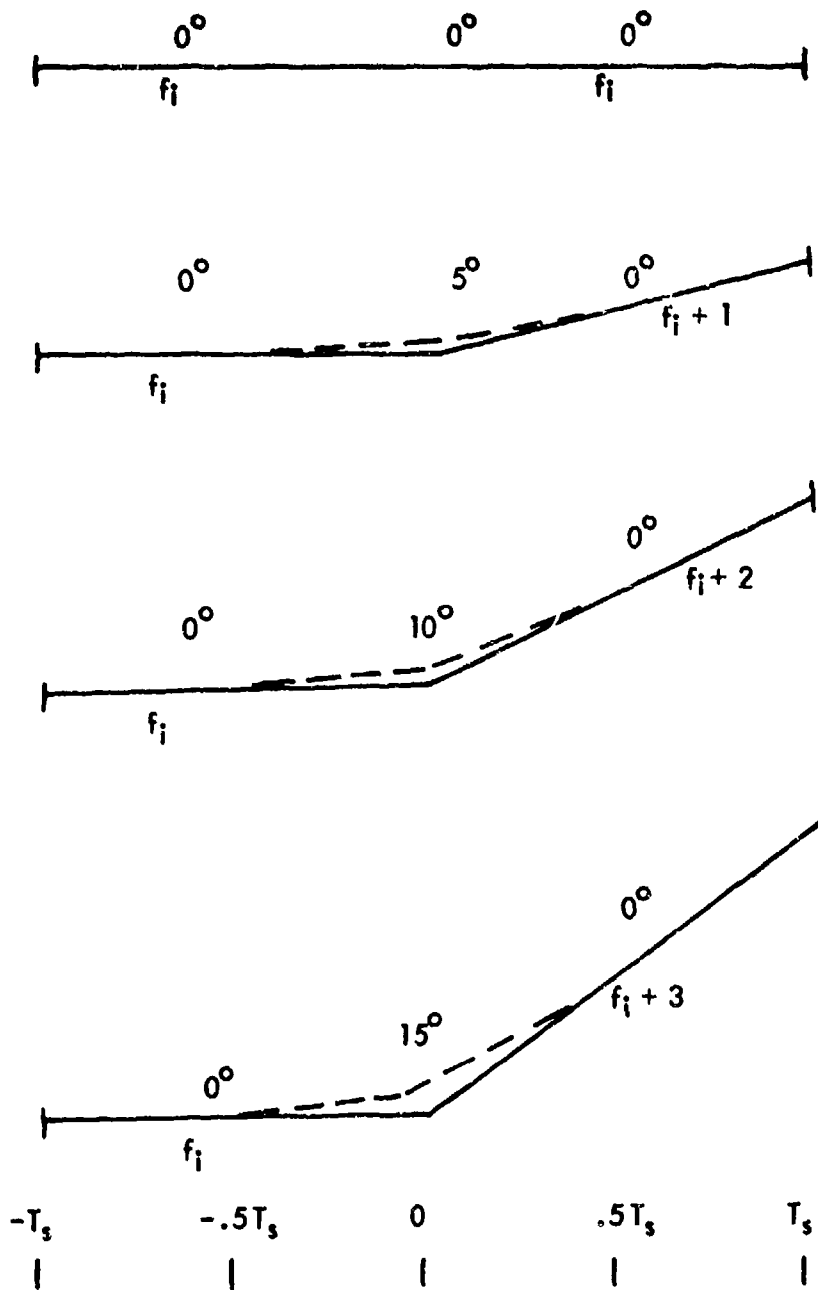
Figure 23.   Phase Trajectory Distortion due to Filtering
with 4th Order Linear-Phase Bandpass Filter

66
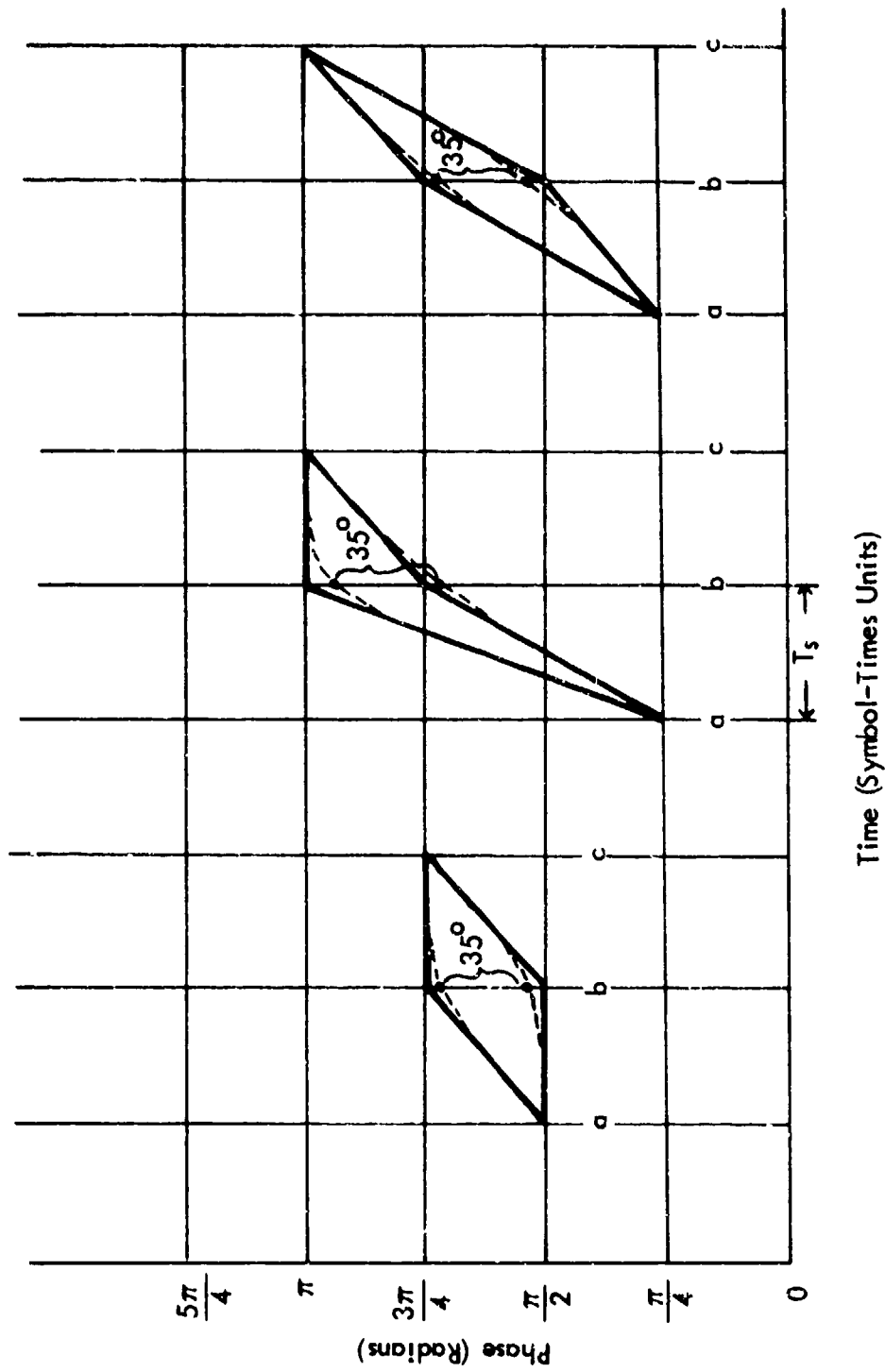
Figure 24. Typical Minimum-Distance Trajectories

67

that point. (See Figure 25.) Since the adjacent transmitted end-phases are separated by 45° and the maximum phase trajectory distortion is 15°, the phase noise must be at least 30° for the measured phase to fall more than 45° away from the transmitted phase. Hence, if the retained pair is the pair nearest the measured phase, the probability that the correct transmitted phase is eliminated by this initial step is

$$P_{30^\circ} = Q \left(\sqrt{\frac{2 E_b}{N_o}} \ (.548) \right)$$

which is about 10^{-17} at $E_b/N_o = 18.3$ dB, the signal-to-noise for which the error probability of the optimum receiver is 10^{-7}. Hence, the probability of eliminating the correct phase is negligible relative to the available demodulator performance.

The task remains, however, of choosing the transmitted phase from each retained pair. The best way to make such a choice (with the assumed Gaussian phase-noise) is to use a threshold midway between the distorted (but noiseless) phase points after filtering. But the amount of distortion, hence the proper threshold location, for the retained pair of phases at any point depends upon the transmitted phase on either side of that point (such as phases at 2 and 4 in Figure 25). If these phases were known, one could determine the proper threshold at 3. But, of course, if all of these phases were known, the thresholds would not be needed. However, a tentative choice of these phases may be made for use in establishing the thresholds for the final phase choices. These tentative decisions are made by using compromise thresholds, considering all possible choices for the phases on either side (such as 2 and 4 in Figure 25). For any retained pairs of phases at points 2, 3 and 4, any combination of the assumed phases at points 2 and 4 will result in one of three adjacent thresholds for deciding between the retained pair at point 3. These three thresholds will be separated by 5° in phase (for the nominal filter). Hence, if we choose the middle threshold of these three for making the tentative decision, the threshold will be off no more than 5°. These tentative decisions at each point are then used to determine the proper threshold for the final decision at each point. If both of the tentative decisions at each point (such as the tentative decisions on either
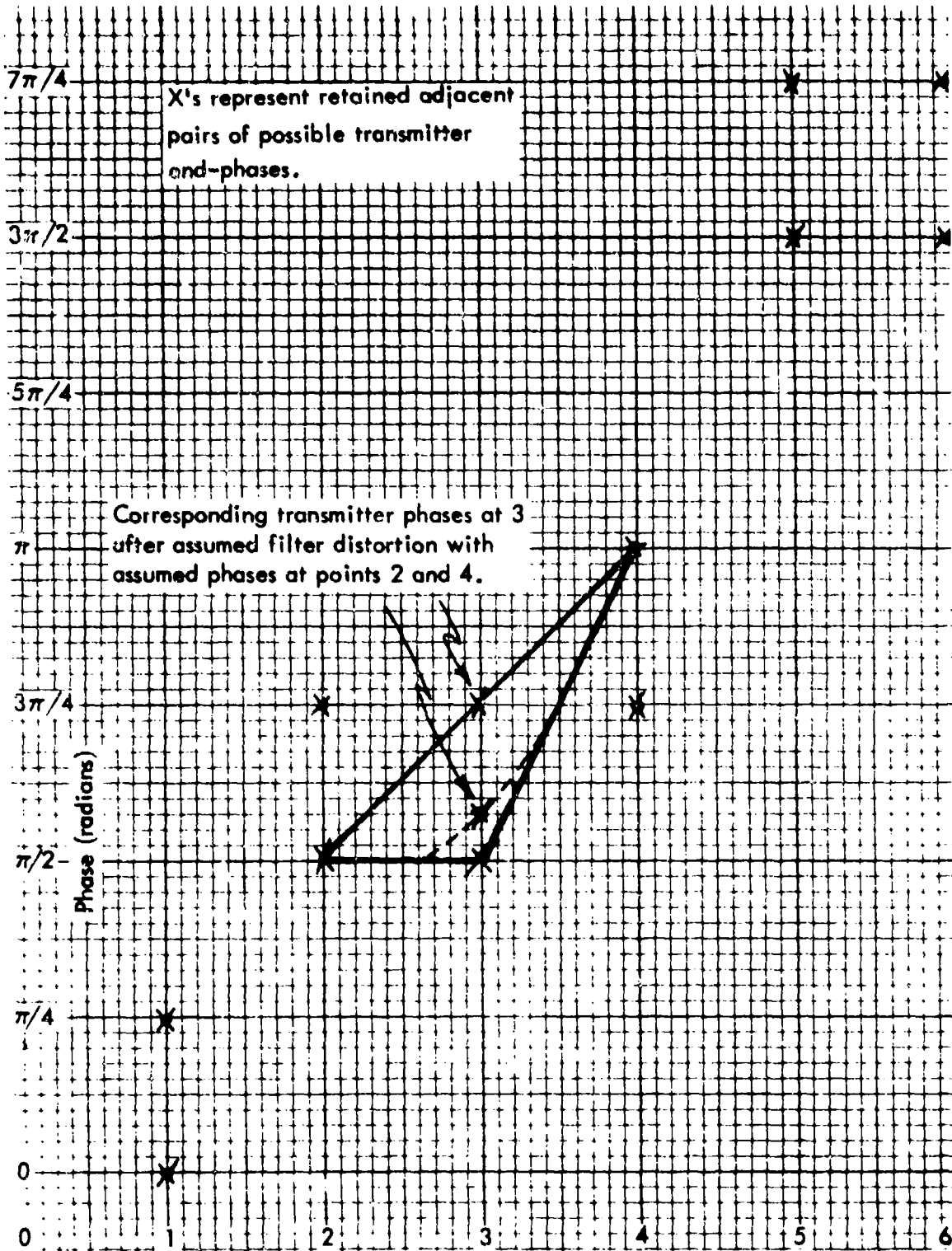
Figure 25. Most Likely Transmitter Phases

side of the point) are made correctly, and hence the threshold for the final decision is established properly, the error probability, as calculated earlier, is

$$P_{17.5^\circ} = Q\left(\sqrt{\frac{2 E_b}{N_o}} \ (.186)\right)$$

As noted earlier, this gives an error probability of 10^{-7} at $E_b/N_o = 18.6$ dB, which is only 0.3 dB from optimum receiver performance. If one of the tentative decisions is in error, then the threshold is 5° off and hence the error probability is

$$P_{12.5^\circ} = Q\left(\sqrt{\frac{2 E_b}{N_o}} \ (.095)\right)$$

The probability of an erroneous tentative decision is also approximately $P_{12.5}$, since the threshold for the tentative decision is also off (most of the time) by 5°. Hence, the probability of making a tentative decision error and an adjacent final decision error at any point is approximately $P^2_{12.5}$, or

$$Q^2\left(\sqrt{\frac{2 E_b}{N_o}} \ (.095)\right) \cong Q\left(\sqrt{\frac{2 E_b}{N_o}} \ (.19)\right)$$

giving a probability of 10^{-7} at $E_b/N_o = 18.3$ dB. Therefore, the overall performance prediction is dominated by $P_{12.5}$, giving an overall error rate of 10^{-7} at about 18.6 dB.

It can easily be seen (by trying all combinations of frequency transitions and considering the crosstalk for any legitimate transition) that for any adjacent pair of legitimate transmitted frequencies there are only five appropriate threshold locations between each adjacent pair of legitimate transmitted end-phases. These are shown in Figure 26 for the nominal filter. Since the transmitted phases are spaced 45° apart, there are only eight possible transmitted phases (modulo 2π) at any symbol end-point, as indicated by the X's in Figure 27. With only five possible threshold locations between each pair, the entire phase space is divided into the 40 regions indicated in Figure 27.
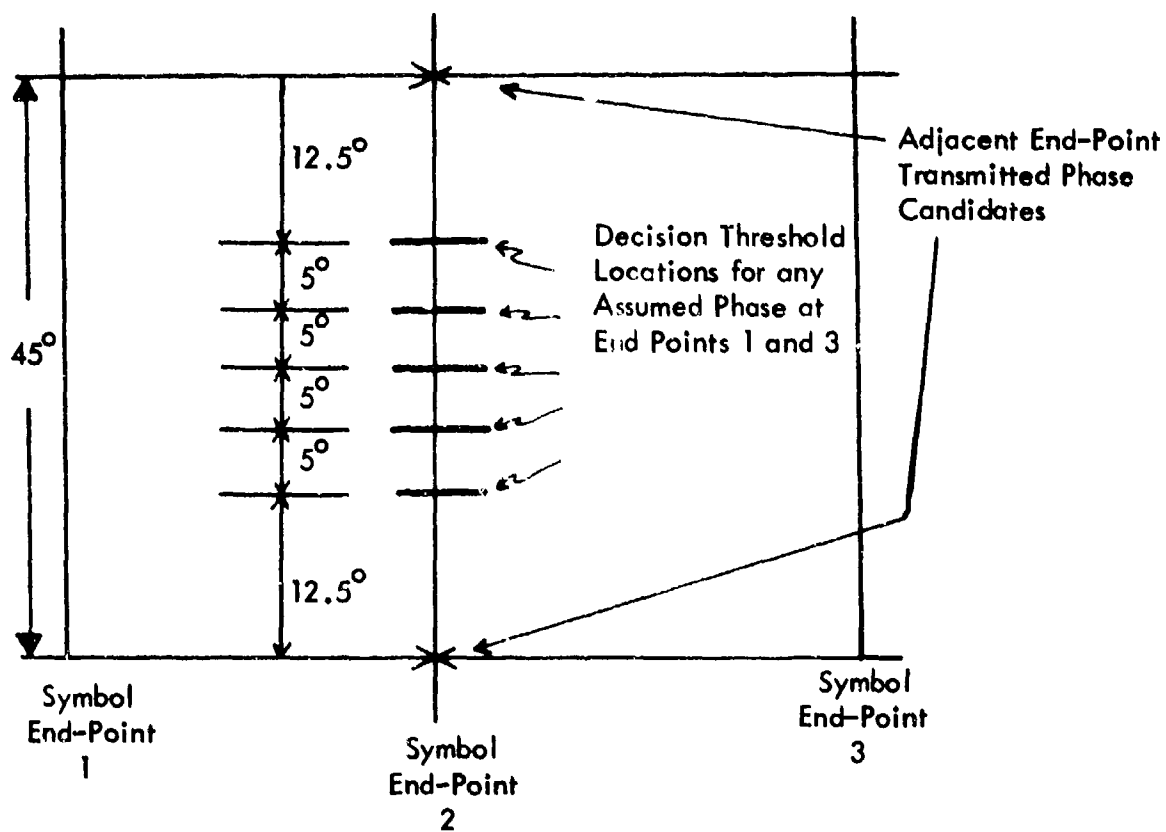
Figure 26. Appropriate Decision Threshold Locations
for the Nominal Filter
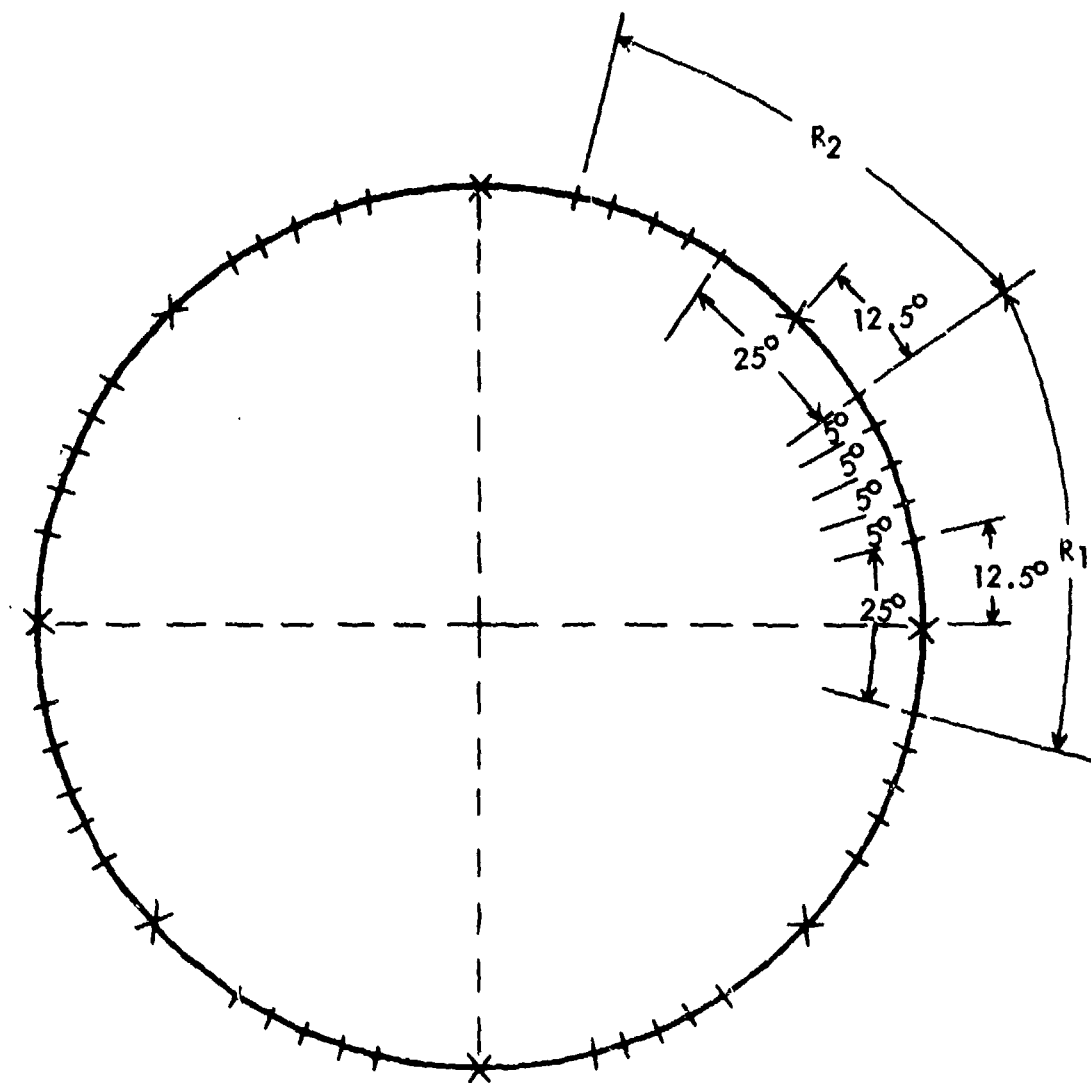
Figure 27.   Phase Locations

It was implied earlier that at any end point, the pair of phases nearest the measured phase at that point were retained. This would require additional thresholds at the transmitted phases (i.e., at the X's) for determining which pair of phases is retained. However, these thresholds are not necessary, since only the 40 thresholds in Figure 27 can be utilized. Phases 1 and 2 (as possible transmitted phases) are retained if the received measurement falls in region R_1, phases 2 and 3 if the measurement falls in R_2, etc. The probability of thus eliminating the correct phase is then easily seen to be $P_{17.5} = 10^{-7}$ at $E_b/N_o = 18.6$ dB, which is the same as the theoretical probability of eliminating the correct phase in the final decision. Therefore, phase measurements must be resolved to within one of the 40 regions between the thresholds of Figure 27 in order to obtain the above performance. As mentioned previously, this performance is within 0.3 dB of theoretical optimum. But even more significantly, if practical implementation losses can be held to 1.4 dB this technique can accomplish the design goal of a 10^{-7} error rate at 20 dB. Hence, this is the technique selected for further investigation and implementation. Further analysis of the performance of this technique and the implementation details are contained in the following section.

3.3 BASELINE RECEIVER

3.3.1 Conceptual Design

Figure 28 is a block diagram of the baseline receiver selected. The filter is nominally a 4-pole modified linear phase filter with a noise bandwidth equal to the symbol rate. The times-eight frequency multiplier following the limiter produces discrete spectral components at eight times each of the four transmitted frequencies. Since the symbol rate is exactly eight times the frequency separation of any two adjacent frequencies, symbol timing can be obtained by locking two oscillators to eight times the lowest frequency (F_0) and eight times the next frequency (F_1), then mixing these oscillators to produce the difference frequency.

As previously discussed, the receiver must subdivide the phase of the received signal at the end of a symbol time into 40 segments. This is accomplished by the three
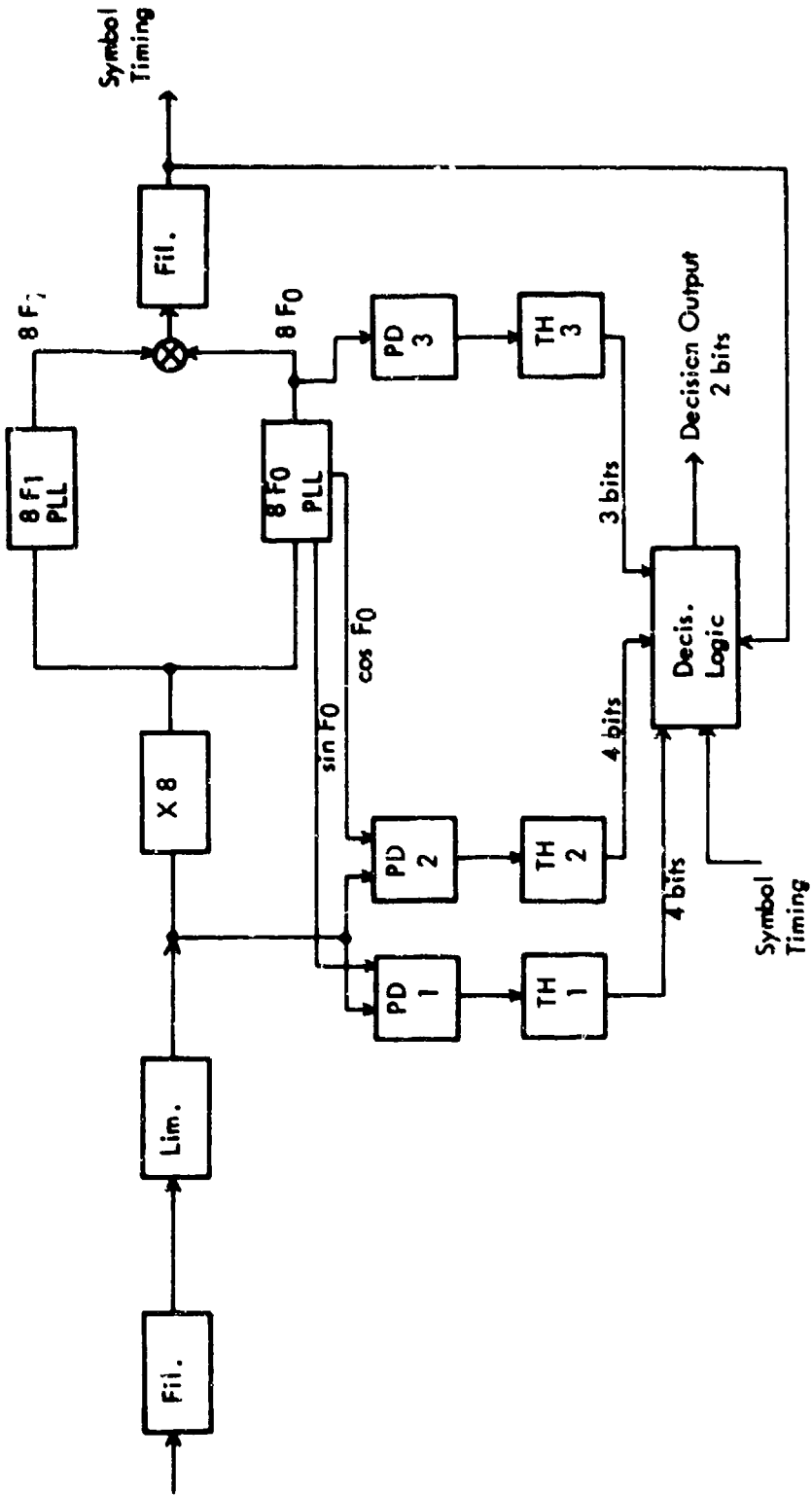
Figure 28. Baseline Receiver Block Diagram

phase-detector threshold units shown. Let the phase displacement caused by the crosstalk produced when two adjacent frequencies are successively transmitted (such as F_1 followed by F_0) bc θ. In this case the receiver must provide thresholds at phases of

$$\pi/8 + n\pi/4,$$

and
$$\pi/8 + n\pi/4 \pm \theta$$
$$\pi/8 + n\pi/4 \pm 2\theta$$

where n takes on values 0 through 7. These locations are shown in Figure 29. The sixteen thresholds located at $\pi/8 + n\pi/4 \pm 2\theta$ are provided by the two phase detectors, PD1 and PD2. Each of the two phase detectors has four threshold devices on its output. Phase detector PD1 measures the phase difference between the input and sine of F_0, as obtained from the phase-locked loop at eight F_0. Phase detector PD2 measures the phase difference between the input and the cosine of F_0. As illustrated in Figure 29a and Figure 30, this subdivides the phase region from 0 to 2π (relative to the phase of F_0) into 16 parts. In both figures it is assumed that 4θ is approximately $22.5°$, which is approximately true for the filter proposed in the baseline design. As can be seen from Figure 30, the four threshold voltage levels for TH 1 and TH 2 are the same and are symmetrically spaced about zero. The two digit numbers identifying the 16 phase regions in Figure 29a will be explained when the detailed logic diagram is explained.

The remaining 24 thresholds shown in Figure 29a are supplied from the three threshold levels on PD3. Since the third phase detector, PD3, compares the phase of eight times the input to eight F_0, the three levels appear modulo $\pi/4$. The levels are shown in Figure 29b. As is shown, the $45°$ phase region, which appears as $360°$ after the frequency multiplication, is basically divided into five segments by the three thresholds associated with PD3 and the appropriate two thresholds from PD1 and PD2.

The 11 binary outputs from the 11 threshold devices are sampled every symbol time and supplied to a logic network to make the decision as to the transmitted frequency. Figure 31 illustrates the logic functions required to carry out the operations described previously which are necessary to make near optimum frequency decisions.
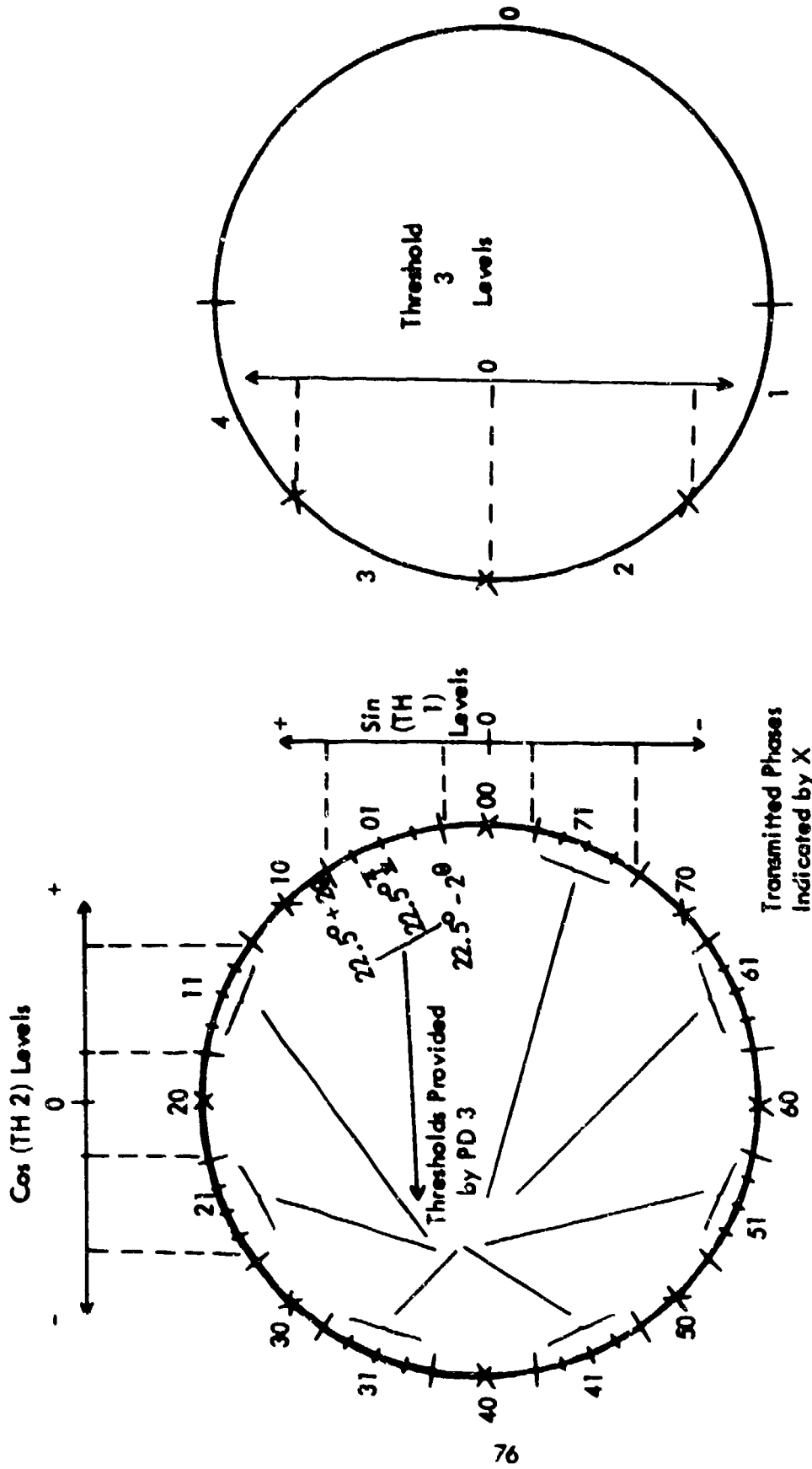
(29a) Phase Locations

(29b) Threshold 3 Settings

Figure 29. Threshold Settings

76
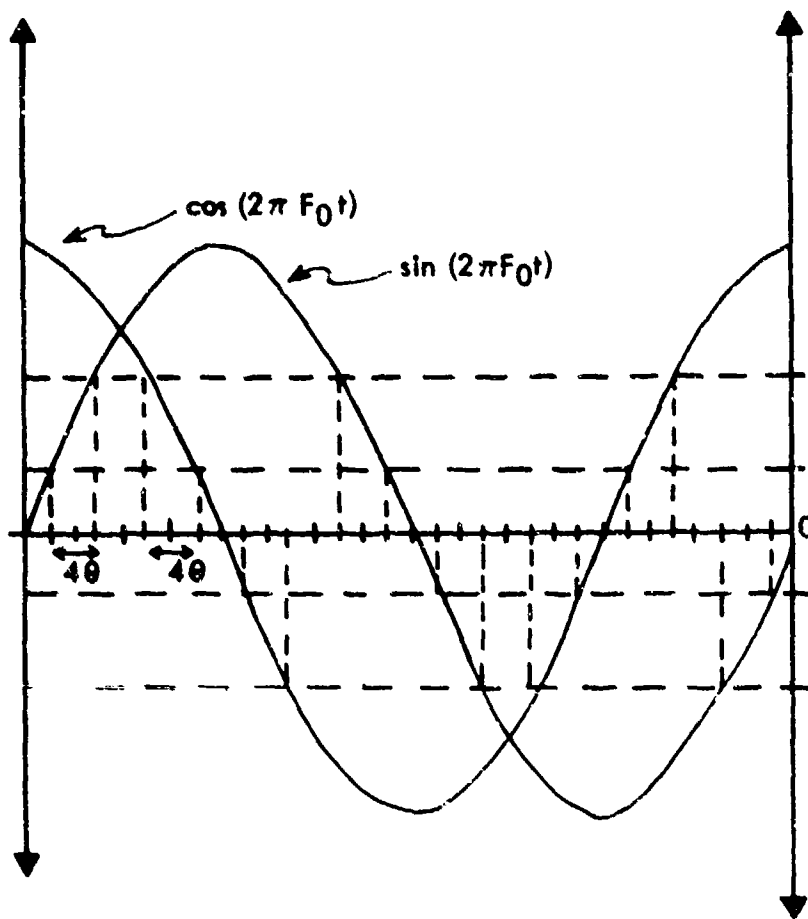
Figure 30. Setting of Thresholds for TH 1 and TH 2

77
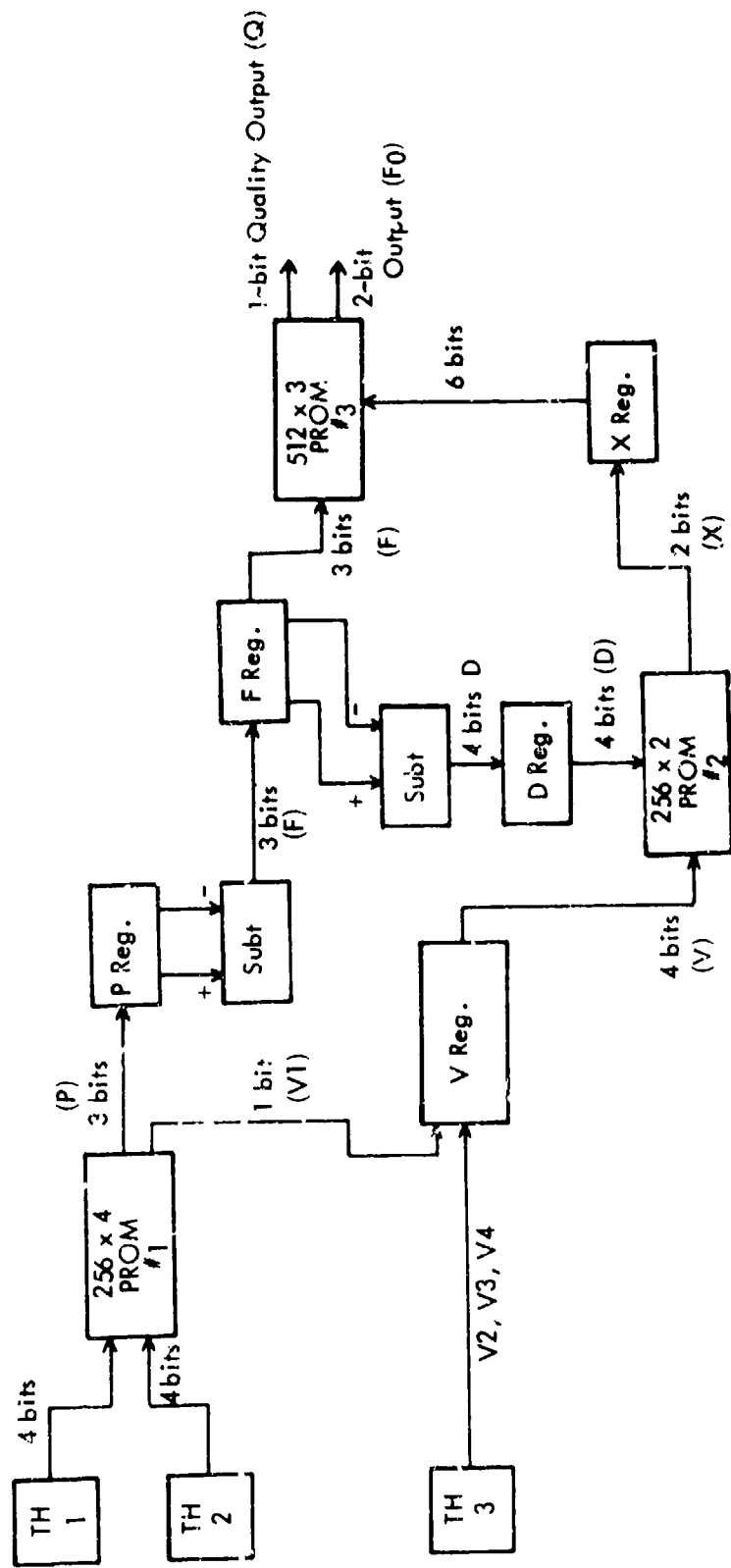
Figure 31. Detailed Logic Diagram

The eight bits from the eight threshold devices associated with TH 1 and TH 2 are converted to a 3-bit binary number corresponding to the estimated transmitted phase and a 1-bit binary number designating whether or not the received phase is close to a legitimate transmitted phase. These two numbers are shown in Figure 29a, with their corresponding phase region. Table 2 presents a truth table showing the conversion which must take place between the eight bits from the threshold detectors and the three phase-identification bits (P) and the vernier bit (V1). In Figure 31 this operation is shown as being accomplished by a PROM or ROM, although it could be accomplished by straight-forward logic as well.

The three phase bits are fed to a two-stage (3-bit) shift register (P register). These two values are subtracted to produce a 3-bit estimate of the frequency (F). Although the actual transmitted frequency is limited to one of four values, F_0 through F_3, noise conditions can easily produce an estimated frequency of minus one or plus four. Hence, three bits are used to represent the frequency in the F shift register. The first two frequencies in the F register are subtracted to a 4-bit, D, value which represents the difference between the two frequencies. Since each frequency can be one of six values, the difference needs to be represented as a 4-bit number which is stored in the D register.

The difference in estimated frequencies, D, is then supplied, along with the four vernier bits, V, from the V register to produce a 2-bit value, X, which carries the information for both the tentative and final decisions in a differential form. That is, the MSB of the X word is zero if the tentative decision indicates that the initial value of P should be tentatively selected and is one, if the phase P+1 should be tentatively selected. Since the threshold setting for the final decision differs from that of the tentative decision by, at the most, one threshold location (on Figure 29a), the LSB of the X word carries all of the information necessary to make the final decision from a set of tentative decisions. The four bits from the V register indicate the location of the phase measurement in the 45° segment corresponding to a particular value of P, which places it in one of the five regions shown in Figure 29b.

TABLE 2. PROM 1 TRUTH TABLE - THRESHOLD OUTPUTS VS. PHASE (P) AND VERNIER (V1) OUTPUTS OF PROM 1

TH 1	TH 2	P	V1
1100	1111	000	0
1110	1111	000	1
1111	1111	001	0
1111	1110	001	1
1111	1100	010	0
1111	1000	010	1
1111	0000	011	0
1110	0000	011	1
1100	0000	100	0
1000	0000	100	1
0000	0000	101	0
0000	1000	101	1
0000	1100	110	0
0000	1110	110	1
0000	1111	111	0
1000	1111	111	1

Table 3 presents the truth table for PROM number 2. The four bits from the V register are shown as the designation bit V1 from PROM number 1, and the three bits from TH 3, along with the corresponding 5-ary value of V, as shown in Figure 30. The two X bits are shown as a function of the frequency difference, D, for difference values of ±4. Values of D larger or smaller than these values should not occur unless noise is large, but should be ascribed the values of X corresponding to either plus or minus four, depending on the sign of D. The left-hand bit in Table 3 is considered the MSB, and hence corresponds to the tentative decision.

The MSB of Table 3 can be deduced directly from the principles of operation previously discussed when one takes into account the dependence between the tentative threshold decision setting and the frequency difference (which is proportional to the crosstalk). It is important to note that the threshold should not move beyond the range in a particular 45° segment. The LSB simply carries the information as to what final decision would be made if the threshold is to be moved up or down one from the tentative decision in the final decision process.

A delay of five symbol times is provided in the V shift register, since it is assumed that five symbol times are necessary to provide a legitimate D value. This assumes that each PROM and subtract operation has one symbol time to settle. The X values are supplied to a four-sample shift register. The two MSB values of the first and last stage are supplied, along with both values of the middle two stages, to PROM number 3. These six bits are sufficient to determine two successive final decisions on phase, and hence, one final frequency decision in a differential form (that is, whether the stored frequency should be advanced or reduced by one, or left alone). Table 4 provides the truth table for this decision. Only the conditions which require a change in the frequency value are listed. The PROM accepts the 3-bit frequency number and provides an output which advances or retards the frequency as indicated by the six bits from the X register and the truth table of Table 4. Since only four values of frequency could be transmitted, the PROM would select the closest legitimate frequency when a value outside the range 0 to 3 is called for. For convenience, a quality bit Q could be provided to indicate this event.

VI	TH 3	V	D								
			-4	-3	-2	-1	0	+1	+2	+3	+4
0	0 0 0	0	1 1	1 1	1 1	1 1	1 1	1 0	0 1	0 0	0 0
1	0 0 0	1	1 1	1 1	1 1	1 1	1 0	0 1	0 0	0 0	0 0
1	1 0 0	2	1 1	1 1	1 1	1 0	0 1	0 0	0 0	0 0	0 0
1	1 1 0	3	1 1	1 1	1 0	0 1	0 0	0 0	0 0	0 0	0 0
1	1 1 1	4	0 0	0 0	0 0	0 0	0 0	0 0	0 0	0 0	0 0

TABLE 4. PROM 3 TRUTH TABLE – F_0 OUTPUT VS. X AND F INPUTS

-	0	2	1		
X_1 (MSB)	X_2	X_3	X_4 (MSB)		
0	0	1	0		
1	2	3	1		
1	0,1	1	0	$F_0 = F+1$	If $F_0 > 3$, $F_0 = 3$
1	2	2,3	0		
-	0,1	2,3	0		If $F_0 < 0$, $F_0 = 0$
0	1	0	0		
1	3	2	1		
0	1	0,1	1	$F_0 = F-1$	
0	2,3	2	1		
-	2,3	0,1	-		

All other combinations $\quad F_0 = F$

If a second layer of final decision is desired, a second register and an additional PROM will be required over that shown in Figure 31. An additional stage in the F register will also be required to allow for the additional delay. An alternative hookup for providing "final - final" decisions based on surrounding final decisions is shown in Figure 32. The truth table for making final decisions from surrounding tentative decisions and a middle value of X is given in Table 5. The same table applies to making "final - final" decision from surrounding final decisions and a middle value of X where the final decisions take the place of X_1 and X_3. The logic shown in Figure 32 implements this table and applies the appropriate correction to the frequency word. It does not, however, account for final frequency estimates outside the range of 0 to 3.

3.3.2   Performance Estimates

In this section, performance estimates for the baseline configuration are presented. The sensitivity of performance to various conditions of link and equipment imperfection was investigated. The specific areas investigated were as follows:

1.   Selection and sensitivity to variations of the input filter.

2.   Sensitivity to additional filtering in the radio.

3.   Sensitivity to threshold setting variations.

4.   Sensitivity to phase jitter from the link and from the equipment.

5.   Sensitivity to symbol timing variations.

6.   Sensitivity to frequency offset.

7.   Sensitivity to adjacent and cochannel interference.

8.   Sensitivity to multipath reflections.

Because of the large number of parameters to be varied, the procedure taken was to establish a baseline for all parameters which was felt to represent a nominal operating condition. The parameter in question was then varied from that point, with all other perturbances set at their nominal value. In this manner, it is felt that the performance estimates provided should represent performance predictions for the constructed device rather than bounds which the equipment could not surpass.
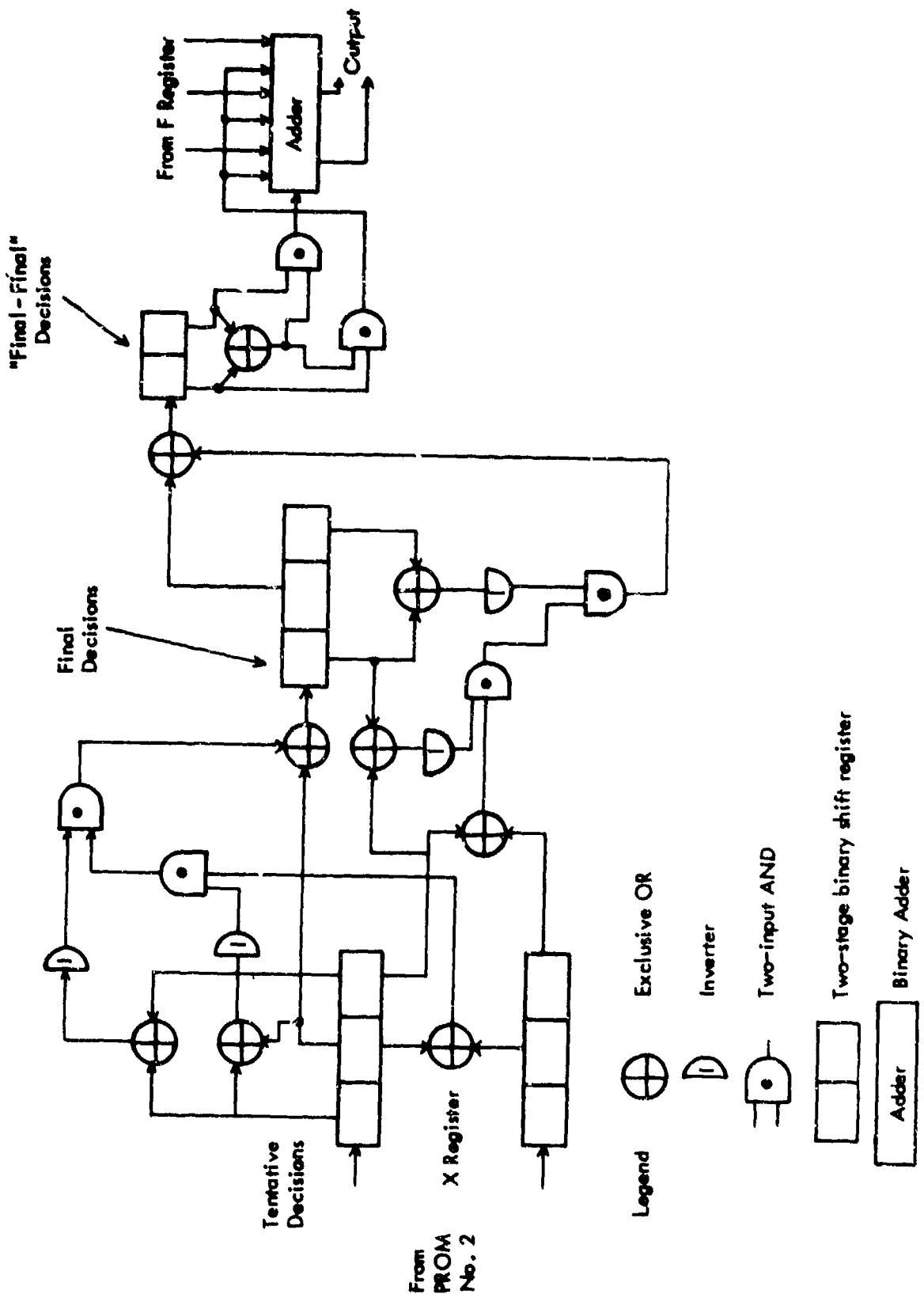
Figure 32. Alternative Logic for Two-Layer Final Decision

Legend

Exclusive OR

Inverter

Two-input AND

Two-stage binary shift register

Binary Adder

TABLE 5.   TRUTH TABLE RELATING VALUES OF X TO FINAL DECISION

X_1 (MSB)	X_2	X_3 (MSB)	Final Dec.
0	1,2,3	1	1
0	0	0	0
0	2,3	1	1
0	0,1	0	0
1	2,3	1	1
1	0,1	0	0
1	3	1	1
1	0,1,2	0	0

3.3.2.1 Computer Program

Before presenting the performance results it is desirable to first briefly desribe the computer program which was used to obtain these.

The performance was calculated in terms of symbol error rate for a specified E_b/N_o for the configuration presented in Figures 28 and 31. The error rate prediction is based on a combination of simulction and analysis. This combination was necessitated by the fact that the crosstalk effects are too complex for analysis and the error rates with noise are too small to obtain from a simulation of reasonable length. The approach, therefore, was to calculate the instantaneous phase (relative to the phase of F_0) and envelope of the signal out of the input filter of Figure 28 when a representative transmit signal sequence is sent. The representative transmitted sequence was selected as a 64-symbol sequence which goes through all combinations of three successive 4-ary frequency symbols. Since the intersymbol interference does not significantly change beyond adjacent symbols, this sequence was felt to be representative of random symbol transmission.

The received phase at the end of symbol time was assumed to be the instantaneous phase calculated for that time plus a zero mean Gaussian random variable whose variance depended upon the assumed value of E_b/N_o, the assumed noise bandwidth of the filtering, and the instantaneous envelope of the noise-free received signal at that time. It was felt that the Gaussian assumption was justifiable because the range of IF signal-to-noise ratios of interest did not include small values. With these assumptions, the probability of the received phase falling in a particular threshold region (relative to the transmitted phase) was calculated. Eleven regions around the transmitted phase were considered, as illustrated in Figure 33. If the transmitted phase was that corresponding to P equal to zero, the eleven threshold regions ranging from P equal to one and V equal to zero, to P equal to seven and V equal to zero, were considered. The probability that the received value was beyond the outside regions (which was quite small for the cases calculated) was lumped into the probability of being in the outside region. Since in either case a symbol error is almost certain, this simplification should have little effect on the error rate.
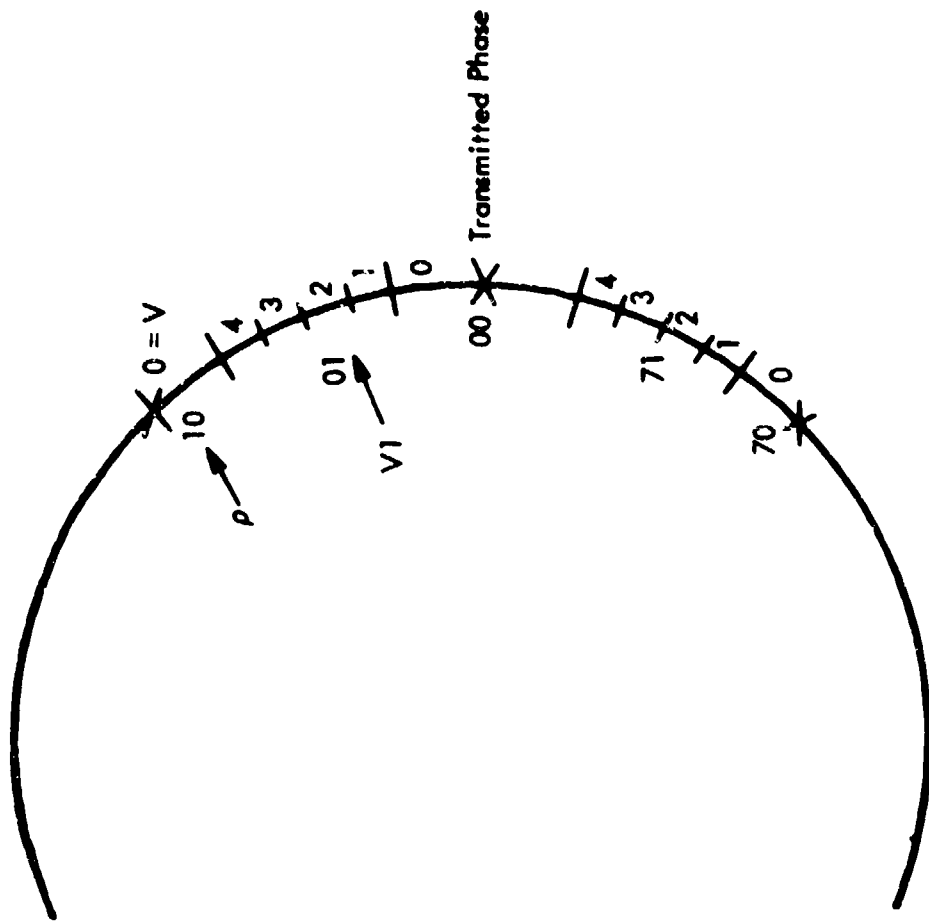
Figure 33. Regions used in Error Rate Calculations

Thus, the probability of lying in each of eleven threshold regions around each transmitted phase was obtained. Each frequency estimate from the logic configuration of Figure 31 depends upon exactly six phase measurements. Therefore, each of the 11^6 combinations of threshold regions was tested to ascertain if a symbol would occur, and the probability of all combinations causing error was summed. It should be noted that the logical configuration of Figure 31 is such that the threshold regions can be lumped together in many cases, and considerably less than 11^6 calculations are necessary to obtain the final error probability.

The calculation for the instantaneous phase and envelope is such that variation in filter parameters and input signal tuning can be accommodated. In addition, the signal into the filters can consist of more than one FSK signal with different center frequency and time reference so that cochannel and adjacent channel crosstalk and multipath can be examined. Additional phase jitter appears as a term which adds to the Gaussian phase noise assumed to be present from the additive link noise. The additional phase noise was usually assumed to be normally distributed. However, the case of uniform distribution for this noise was also investigated. Variation of the threshold settings could be accommodated by varying the probability of the received phase falling in a region.

To determine the appropriate time to sample the receiver output, the phase shifts of the filter to F_0 and F_1 were calculated and the time of the zero crossings of the difference frequency from $8F_0$ and $8F_1$ was determined. Since this corresponds to the method proposed for symbol timing, the effect of filter variation upon the timing was automatically checked. A means of varying the sampling time about the value calculated in this manner was provided.

3.3.2.2   Results

As previously stated, the approach used to obtain results was to choose nominal values for the parameters to be varied and to vary one at a time with the others equal to their nominal value. The values chosen as nominal were the following:

1. Input filter: 4-pole modified linear phase - Bandwidth equal 14 MHz

2. Radio filters: 3-pole 0.1-dB ripple TBY - Bandwidth equal 30 MHz;

   3-pole Butterworth - Bandwidth equal 30 MHz

3. Threshold settings: $\theta = 4.5^\circ$ (best setting within 0.5°)

4. Phase jitter: 0.6° rms

5. Symbol Timing: 1 percent of symbol from best location

6. Frequency Offset: None

7. Interference: None

8. Multipath: None

The performance for this nominal configuration is shown in Figure 34 along with the bound for multisymbol coherent 4-ary FSK with a deviation ratio of 1/8. As can be seen, the symbol error rate tracks the bound reasonably well over a wide range of E_b/N_o. As can also be seen, the value of 19.7 dB is required for 10^{-7} symbol error rate, which is approximately 1.4 dB away from the bound. The performance diverges slightly from the bound at both higher and lower error rates, being about 1.6 dB away at 10^{-13} and 1.9 dB at 10^{-2} symbol error rate.

Figure 35 shows the performance over a smaller range of E_b/N_o. As can be seen, the rough performance estimates based on minimum distance alone for the filter used predicted performance approximately 0.7 dB away from the bound. As is also apparent, the performance predicted for the unit back-to-back (without the radio filter) and with no jitter is quite close to the minimum distance prediction. Thus, the strategy of using tentative decisions comes very close to the best performance available from the filter. Also shown are the results with back-to-back operation and 0.50 rms jitter (omitting the link jitter). Thus, one might conclude that roughly 0.7 dB difference from the bound is fundamental to the filter-limiter approach and the remaining 0.7 dB is due to anticipated equipment and link impairments.
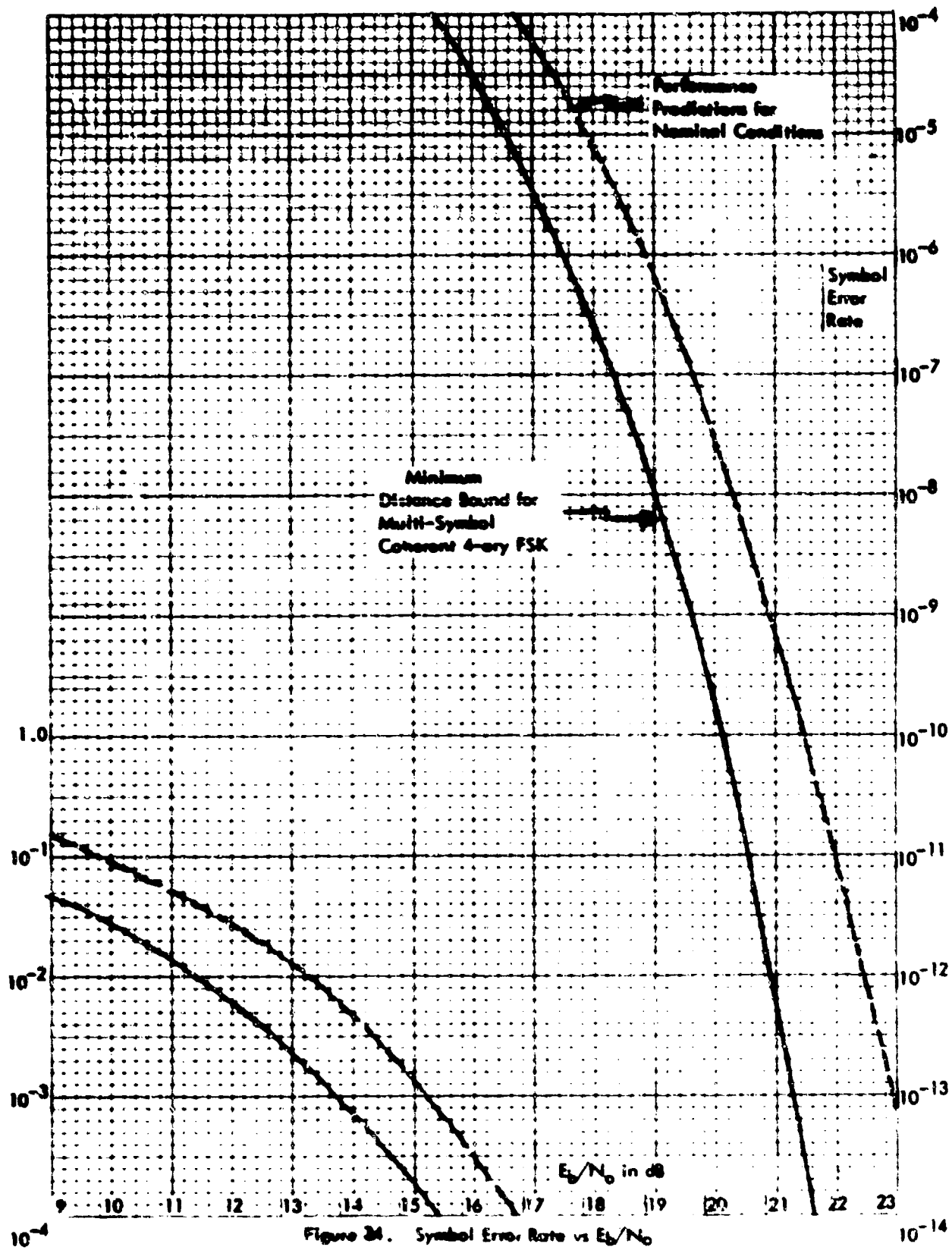
Figure 24. Symbol Error Rate vs E_b/N_o
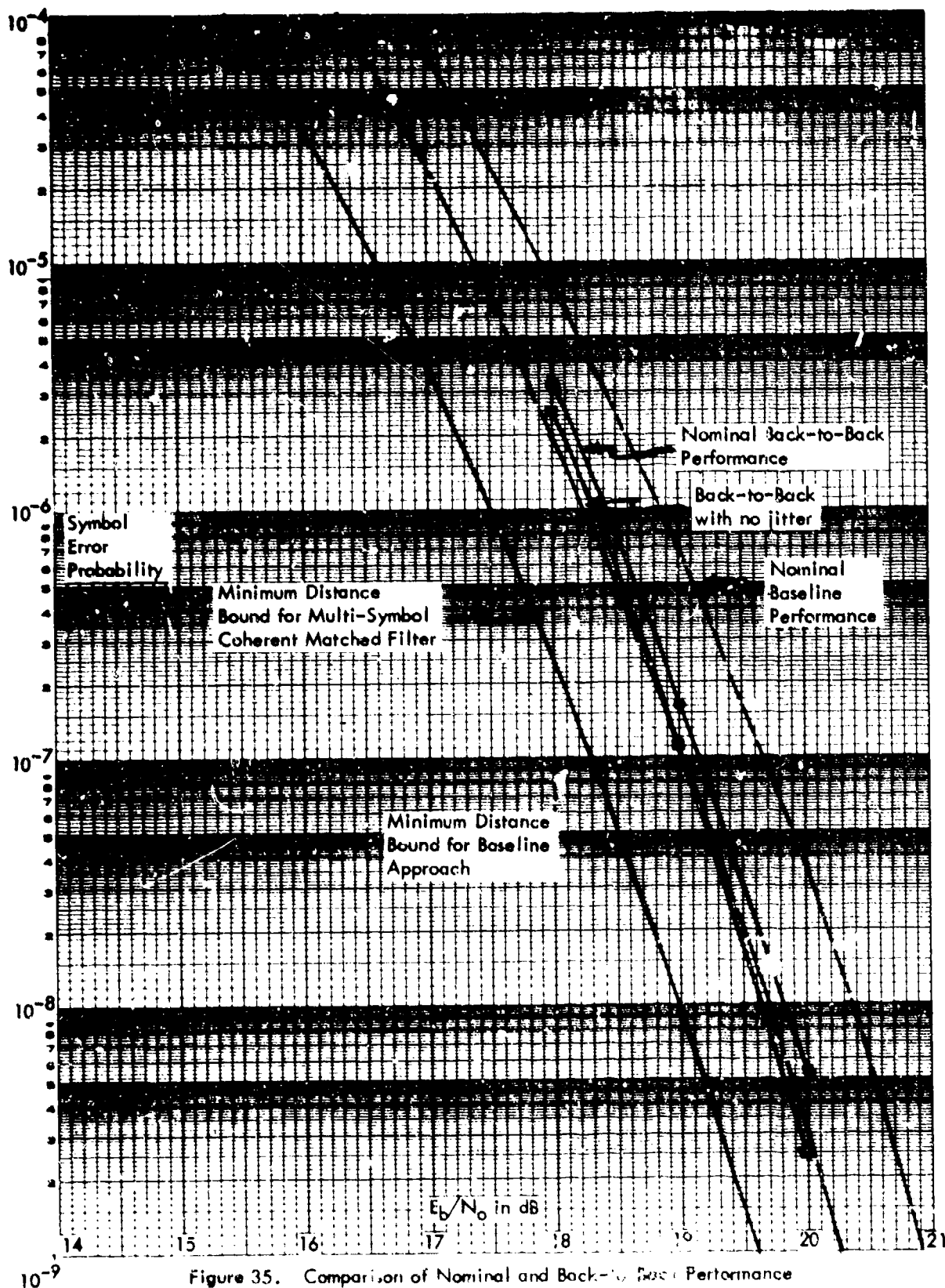
Figure 35. Comparison of Nominal and Back-to-Back Performance

3.3.2.3 Filter Selection

The process employed in selecting the characteristics of the nominal filter involved trying a variety of filters and observing their performance. Table 6 lists the E_b/N_o necessary to achieve 10^{-7} symbol error rate for a variety of different front-end filters. All of these figures assume the nominal conditions other than the input filter. As can be seen, using a modifed linear phase filter provides a reasonably significant gain over that available from standard four-pole filters which utilize the standard frequency translation. The performance variation for different bandwidths and different numbers of poles for the modified linear phase configuration, however, is quite small.

In order to test the sensitivity of the performance to filter drift, each pole of the modified linear-phase (MLP) filters was shifted by an amount randomly chosen from a uniform distribution corresponding to ± 5 percent of the Q of the pole and 1 percent of the center frequency. The results are shown in Table 7, where each filter was perturbed with four independent trials. As can be seen, little loss occurs except in the narrower bandwidth case.

3.3.2.4 Radio Filter Variation

It was anticipated that the narrower and higher order MLP filters would provide better protection against variation in the radio filters. Table 8 shows the E_b/N_o necessary for 10^{-7} symbol error rate when the 3-pole Butterworth radio filter is changed to a 1-dB ripple Tchebycheff filter. Although loss occurs in all cases, the difference is not great.

3.3.2.5 Threshold Settings

Figure 36 shows the E_b/N_o necessary to obtain 10^{-7} symbol error rate versus the spacing of the threshold settings in degrees.

TABLE 6. FILTER CHARACTERISTICS VS. E_b/N_o

Characteristic	#Poles	BW/SR	E_b/N_o for 10^{-7}
0.1 dB Ripple TBY	4	1.0	22.3
Linear Phase	4	0.8	20.9
Mod. Linear Phase	2	0.8	20.6
"	2	1.0	19
"	2	1.2	19.8
"	4	0.8	20.0
"	4	1.0	19.7
"	4	1.2	19.9
"	6	0.8	20.0
"	6	1.0	19.8
"	6	1.2	19.9
"	8	0.8	20.0
"	8	1.0	19.7
Mod. Linear Phase	8	1.2	19.9

TABLE 7. FILTER PERTURBATIONS VS. E_b/N_0 - MODIFIED
LINEAR PHASE FILTERS

#Poles	BW	Stand.	Var. 1	Var. 2	Var. 3	Var. 4
2	0.8	20.6	21.2	20.5	20.8	20.3
2	1.0	19.8	19.8	19.6	20.2	20.0
2	1.2	19.8	19.8	19.9	19.9	20.0
4	0.8	20.0	19.7	19.9	20.6	20.6
4	1.0	19.7	19.5	19.6	19.5	19.6
4	1.2	19.9	19.7	19.7	19.7	19.6
6	0.8	20.0	20.0	20.6	20.3	19.9
6	1.0	19.8	19.9	20.0	20.2	20.2
6	1.2	19.9	20.0	19.8	19.9	19.8
8	0.8	20.0	19.9	19.9	19.9	20.0
8	1.0	19.7	19.6	19.6	19.7	19.8
8	1.2	19.9	19.8	20.1	19.8	19.9

TABLE 8.   EFFECT OF CHANGING 3-POLE BW TO 1 dB RIPPLE TBY

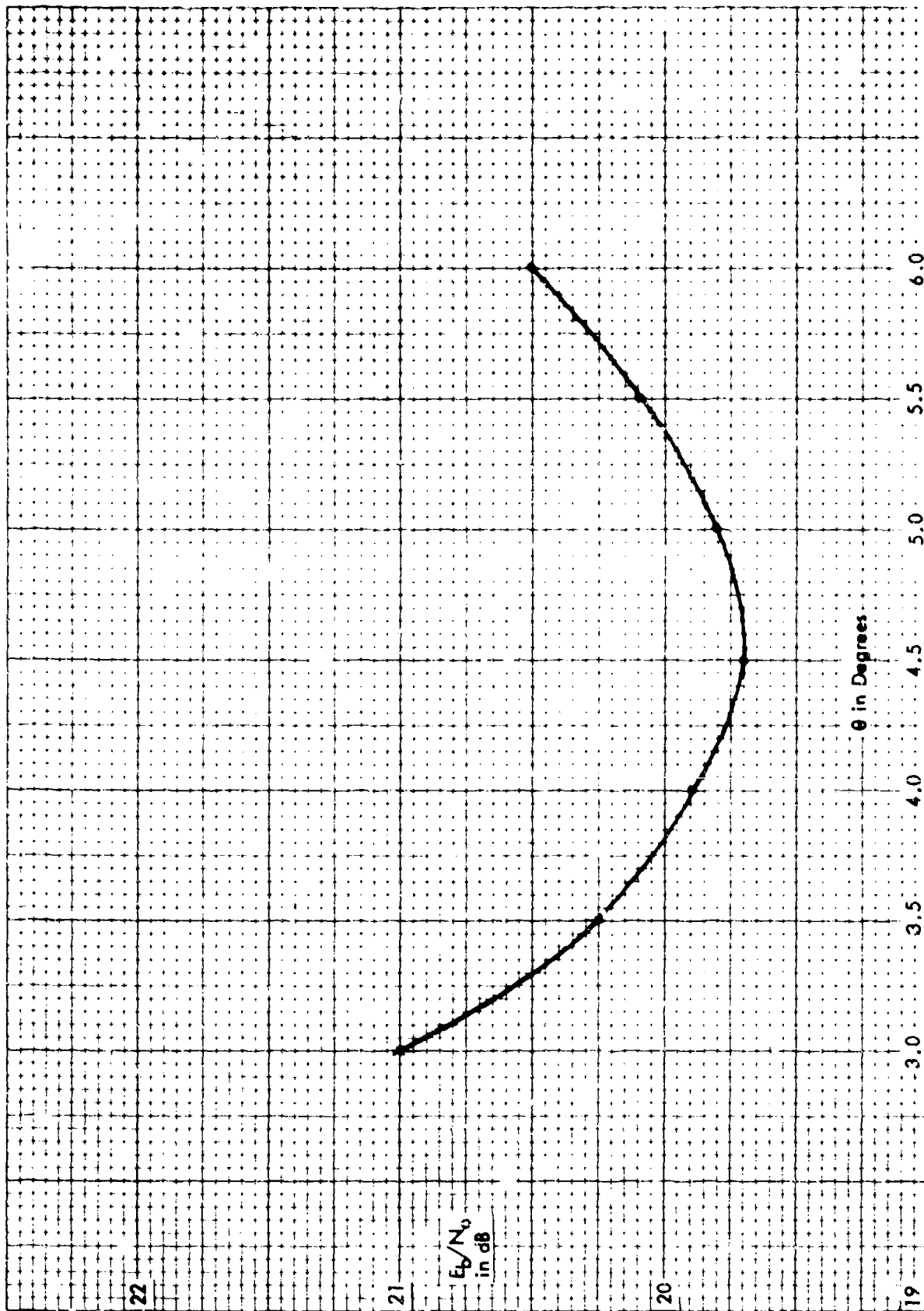| #Poles	BW	Stand. Conf.	Perturbed
2	0.8	20.6	22.1
2	1.0	19.8	20.7
2	1.2	19.8	20.9
4	0.8	20.0	20.9
4	1.0	19.7	20.4
4	1.2	19.9	20.4
6	0.8	20.0	20.8
6	1.0	19.8	20.3
6	1.2	19.9	20.4
8	0.8	20.0	20.4
8	1.0	19.7	20.5
8	1.2	19.9	20.9

Figure 36. Effect of Threshold Variation

3.3.2.6   Phase Jitter

Figure 37 shows the performance versus phase jitter for both uniform and Guassian density functions for the phase.

3.3.2.7   Symbol Timing

Figure 38 shows the performance versus variation in symbol time. As can be seen, the performance is quite sensitive to symbol time variation. The symbol time deduced by the computer and used in the nominal case, however, is not as good a location as that available from a symbol time "tweak knob."

3.3.2.8   Frequency Offset

Figure 39 shows the performance versus frequency offset of the received signal.

3.3.2.9   Interference Rejection

Figure 40 presents the interference performance of the nominal baseline system when an interfering signal identical in nature, but with a different PN sequence, is present. The different curves represent the performance versus the frequency separation of the two signals in units of the symbol rate. The curve for zero separation represents the case of cochannel interference. The horizontal line represents the symbol error rates corresponding to degradations of 1 dB, 2 dB, and 3 dB from the interference-free performance at 20-dB E_b/N_o.

Table 9 lists the signal-to-interference ratios corresponding to the various frequency separations and degradation values.

Figure 41 shows the symbol error rate for an E_b/N_o of 20 dB and a frequency separation of two symbol rates for various input filter choices. As can be seen, little performance difference exists among the filters. This would seem to argue that the predominant cause of errors from interfering signals with this spacing is the cochannel component of the adjacent-channel signal.

97

Figure 37. Effect of Phase Jitter
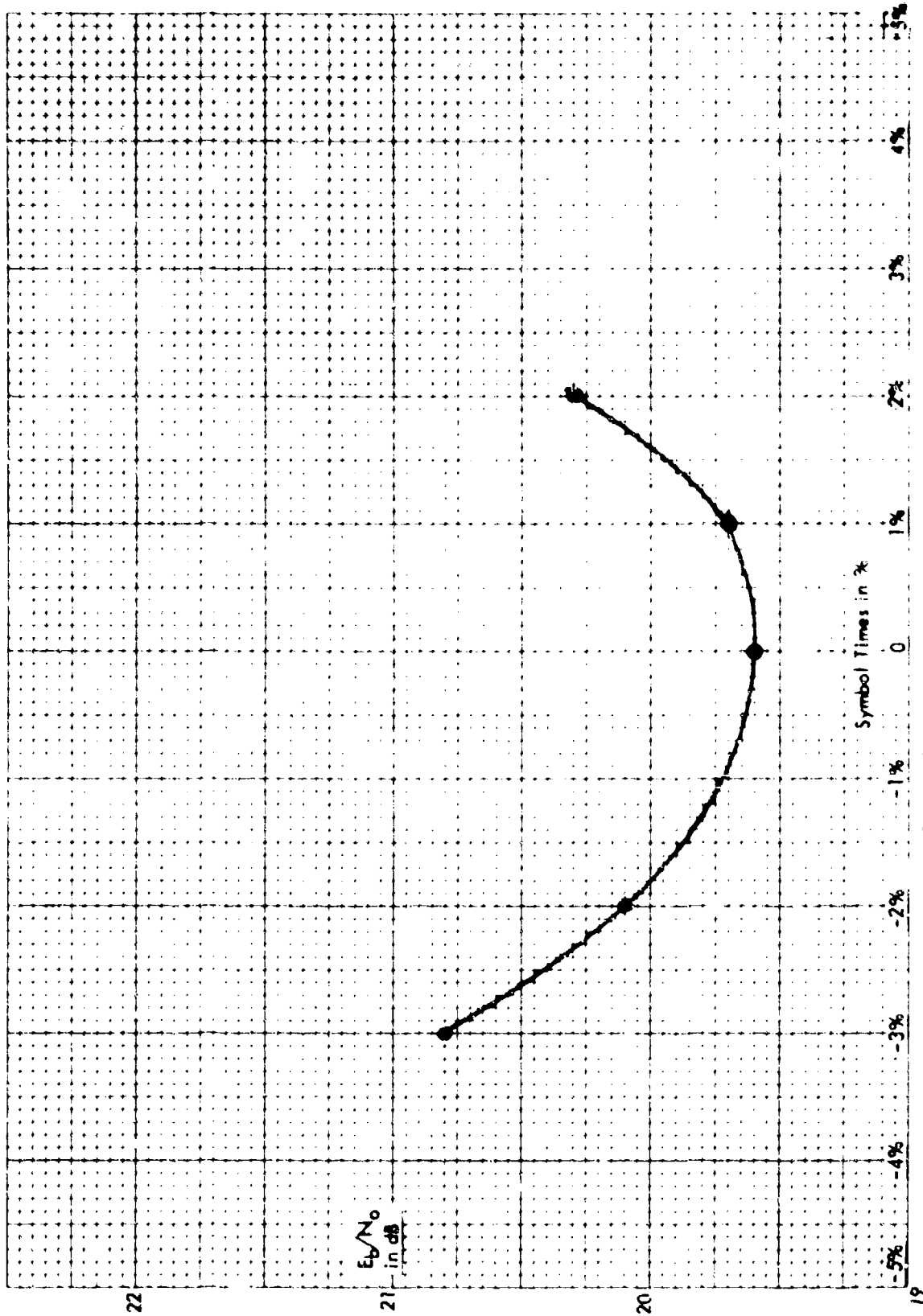
Figure 38. Effect of Symbol Timing Error
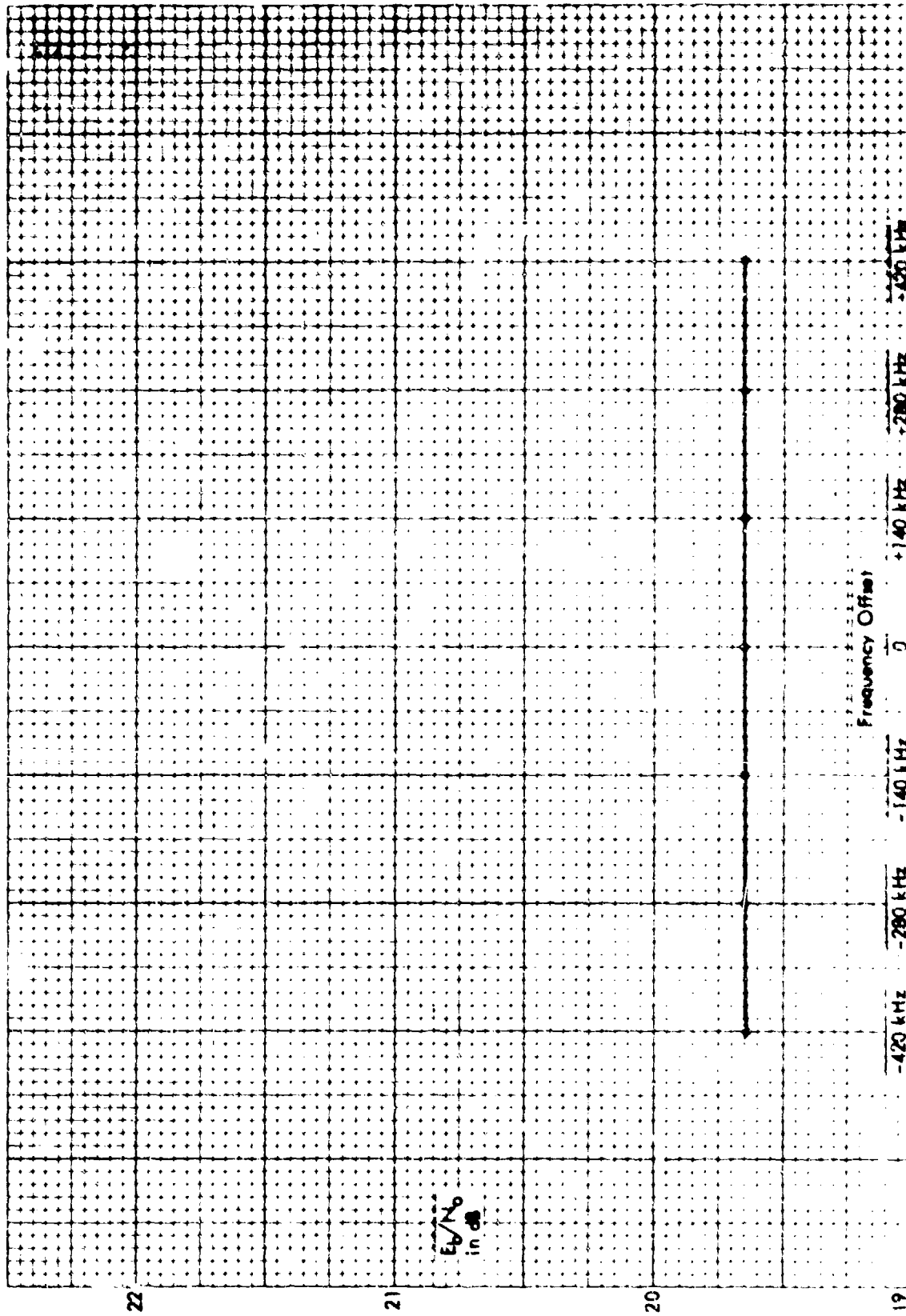
Figure 39. Effect of Carrier Detuning

100
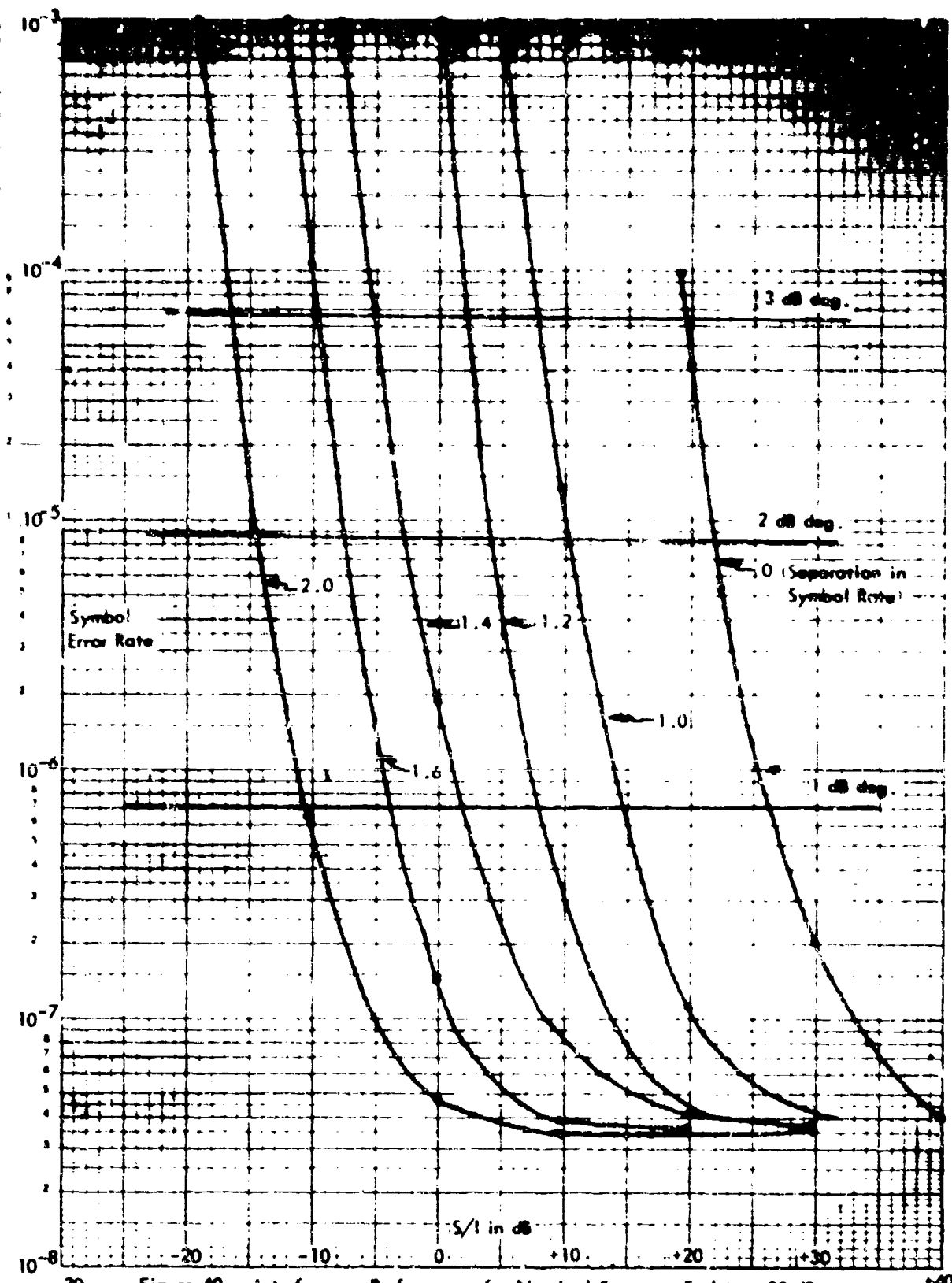
Figure 40. Interference Performance for Nominal System - E_b/N_o = 20 dB

TABLE 9.   S/I IN dB FOR SPECIFIED DEGRADATION

Separation (Symbol Rate)	Degradation			
	1 dB	2 dB	3 dB	
2.0	-10.5	-14.3	-16.5	E_b/N_o 20 dB
1.6	-3.5	-7.5	-9.6	Nominal System
1.4	+2.1	-2.5	-5.1	
1.2	+8.1	+4.3	+2.2	
1.0	+14.8	+10.5	+7.8	
0	+26.2	+21.8	+19.5	

Figure 41. E_b/N_0 Interference Performance vs Filter Choice Spacing = 2.0 x Symbol Rate

Section IV

HARDWARE DESCRIPTION

A breadboard modem incorporating the baseline concepts described in Section III was constructed. The actual hardware is described in this section.

4.1 MODULATOR

The modulator is packaged in a 5-inch chassis with integral power supplies. The unit accepts data and return clock and provides a modulated 70-MHz signal at a nominal level of +1 dBm. Figure 42 is a block diagram of the modulator.

The four tones are generated by mixing the crystal oscillator with bit rate and symbol rate. This results in four frequencies with spacing exactly equal to the symbol rate and differing by an integral number of cycles per symbol time. The input data is blocked into two bit words which control the selection of one of the four frequencies during each symbol time. This forms a mod index equal 1, FSK signal centered at 225 MHz. The phases of the tones are statically adjusted such that all have the same phase at the beginning of a symbol time.
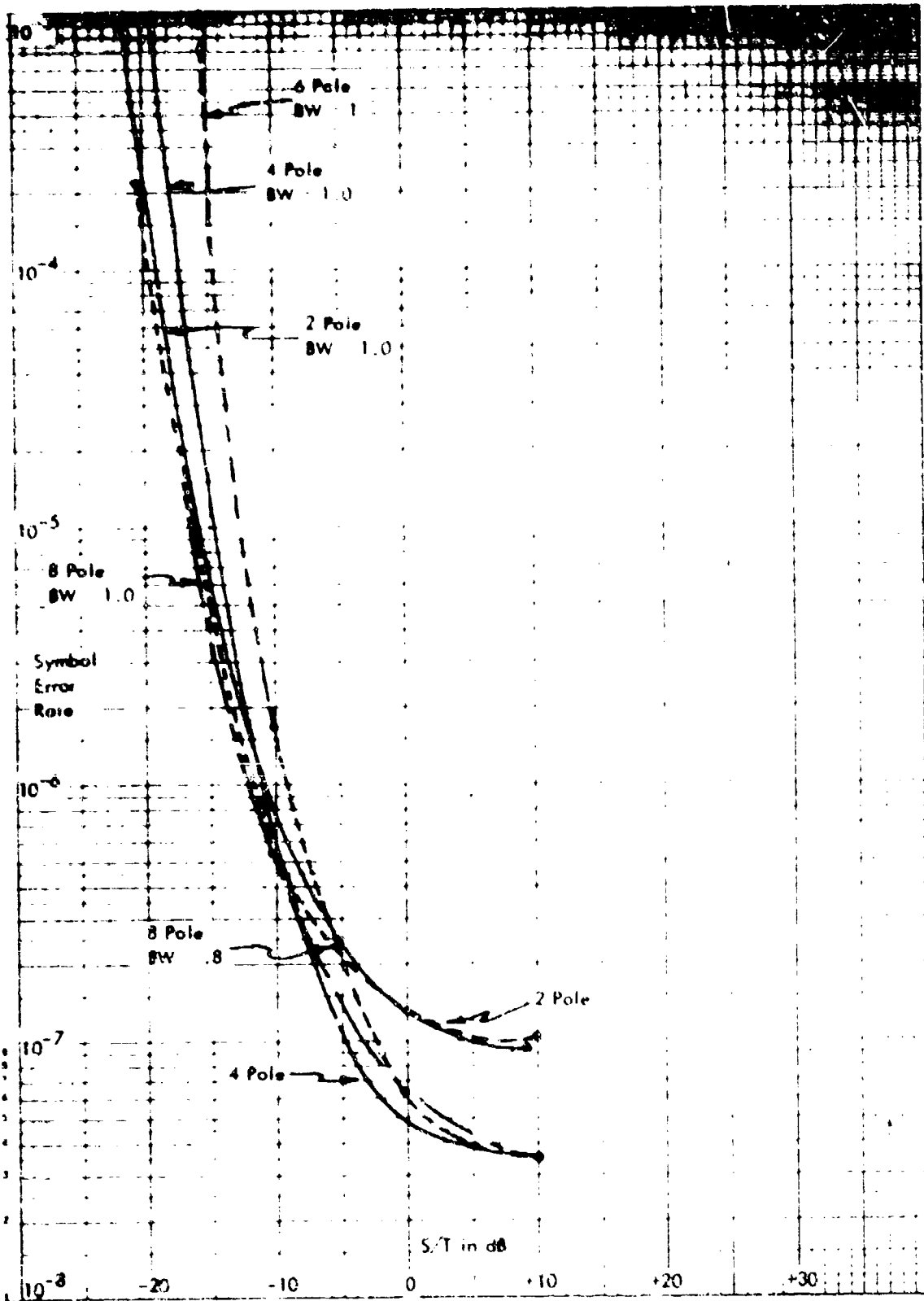
The mod index 1 signal is divided by 8 to generate the desired mod index 1/8 signal at 28.125 MHz. This signal is buffered, filtered, and translated to 70 MHz by mixing with a 98.125-MHz oscillator. The necessity for conversion results from the implementation difficulties associated with the divide-by-8 function and frequency selector. Direct generation requires the divide-by-8 and multiplier to operate at 8 x 70 MHz, or 560 MHz. Although this is within the state-of-the-art, it was felt that the risk and difficulty did not outweigh the cost of the additional circuits.

No significant conceptual difficulties were encountered in the design, construction, and test of the modulator.
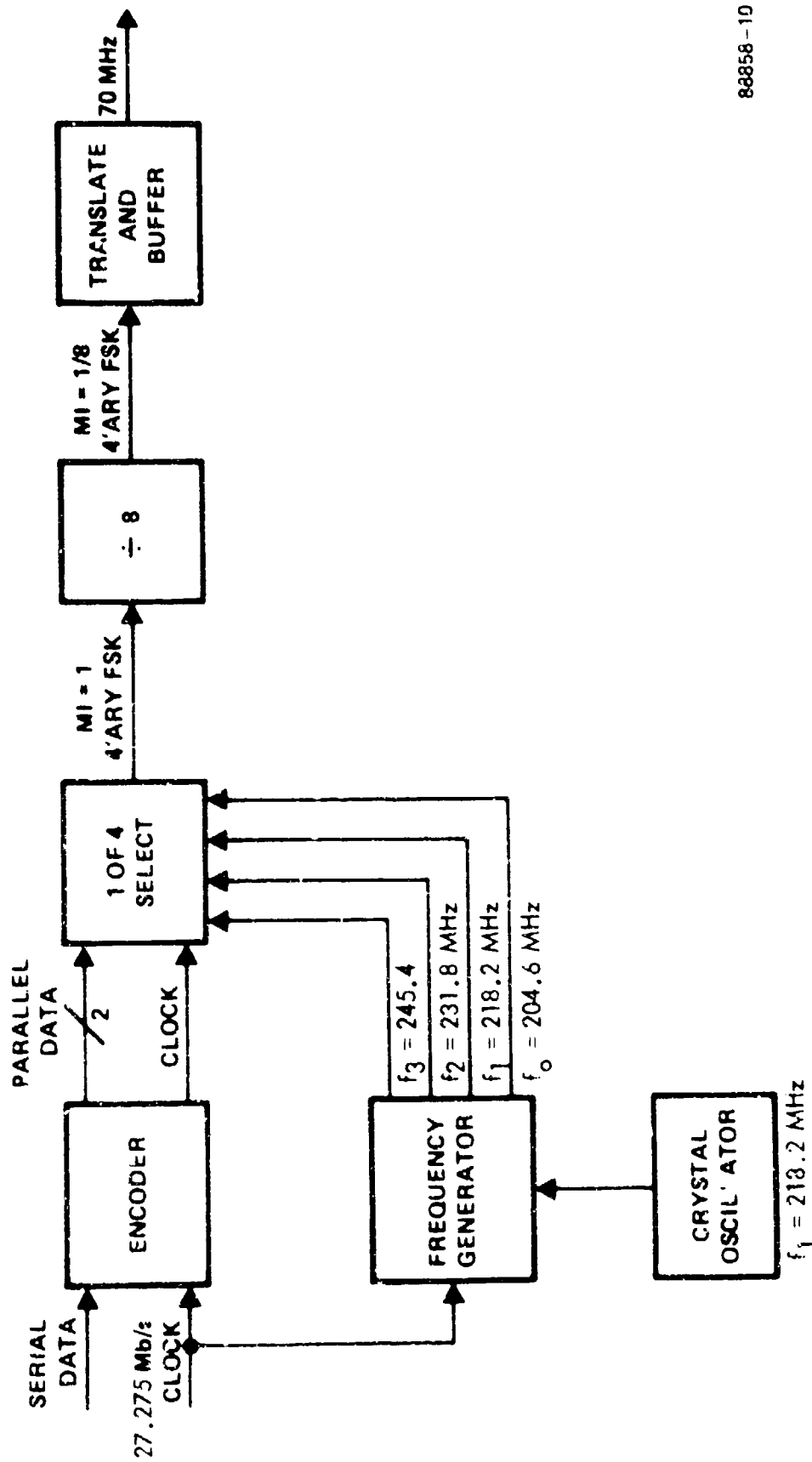
Figure 42. Modulation Index 1/8, Continuous Phase, 4-ary FSK

88858-10

4.2 DEMODULATOR

The demodulator is packaged in a 7.25-inch chassis with integral power sup-
plies. The unit accepts a +1 dBm nominal signal at 70 MHz and provides data and clock.
Figure 43 is a block diagram of the demodulator.

The operation of the unit is described in detail in Section III. The received
signal is filtered and limited. The input filter approximates a symbol-rate-wide modified
linear phase design with a generalized 4-pole-pair bandpass followed by two sections of
phase equalization. The composite delay distortion was less than 5 ns. The required
carrier reference is generated by downconverting and multiplying by 6 to generate a
mod index 1 signal with discrete frequencies. The purpose of downconverting is to allow
the use of readily available, low risk, voltage-controlled oscillators in the phase-locked
loops. The two loops lock to the two lowest frequencies. The bottom frequency is divided
by 8 and translated coherently to 70 MHz to serve as a reference for demodulation. The
upper frequency is mixed with the lower frequency to produce symbol rate.

A single pair of quadrature phase detectors is used to measure the ending
phases. The second phase detector described in Section III was eliminated by adding the
appropriate thresholds to the quadrature units. The phase detectors are sampled at the end
of the symbol time and the result processed by the logic. The detailed operation of the
logic is described in Para. 3.3.1.

No significant conceptual problems were encountered in the design, con-
struction, and test of the demodulator.
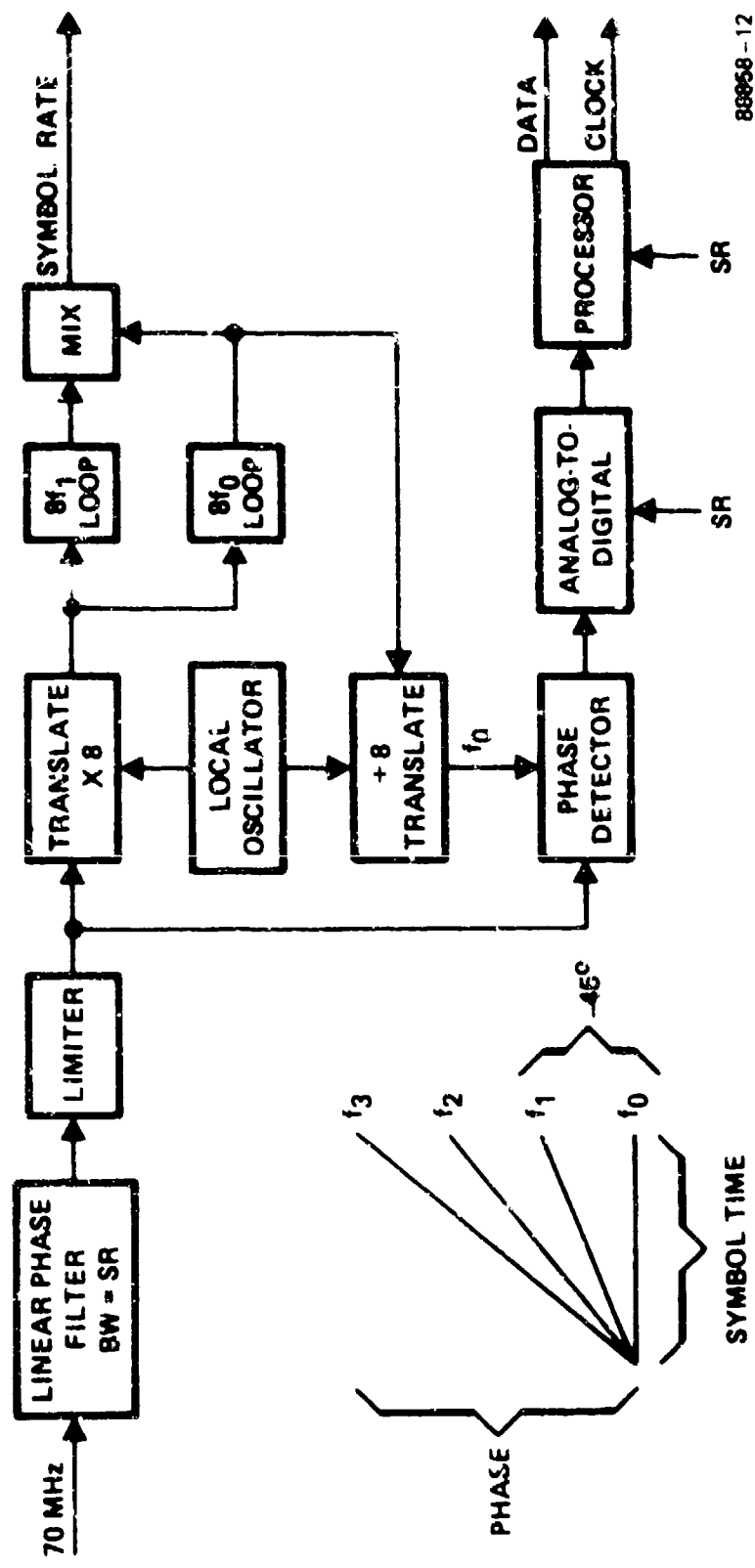
Figure 43. Coherent Detection, Multisymbol Observation

88958-12

108

Section V

TEST RESULTS

The test program includes tests at Harris ESD in Melbourne, Florida, and at RADC in Rome, New York. The in-plant tests were designed to provide a performance baseline from which to interpret results from later radio and link tests and to verify the characteristics of various internal parameters. These tests were performed with the modem looped back at 70 MHz with additive thermal noise. The RADC tests included both back-to-back tests with the LC8D radio and simulator and link tests utilizing the Stockbridge radio. The Test Plan is included in this report as Appendix D.

In this section, the test results are presented. The modem performed quite well and met or exceeded the design objectives in all cases.

5.1   BER vs E_b/N_o

The design objective for the modem was an error rate of 10^{-7} or less at an E_b/N_o of 20 dB. The BER was measured in a variety of configurations, as described below. Details of the test configuration and calibration are in Appendix D.

5.1.1   Back-to-Back Results

For this test, the modulator and demodulator were connected directly at 70 MHz. At the demodulator input, thermal noise with an equivalent bandwidth of 30 MHz was added at 70 MHz. A typical BER curve is shown in Figure 44. The minimum-distance bound curve represents the performance theoretically attainable with the 4-ary FSK signal structure used. In the vicinity of a 10^{-7} BER, the measured data is approximately 1.7 dB from this bound. Referring to Figure 34, the bound for the baseline approach is approximately 0.7 dB from the theoretical bound. This implies an implementation loss of 1 dB for the modem as constructed. The most probable sources of this degradation are the input modified linear phase filter and timing jitter. It should
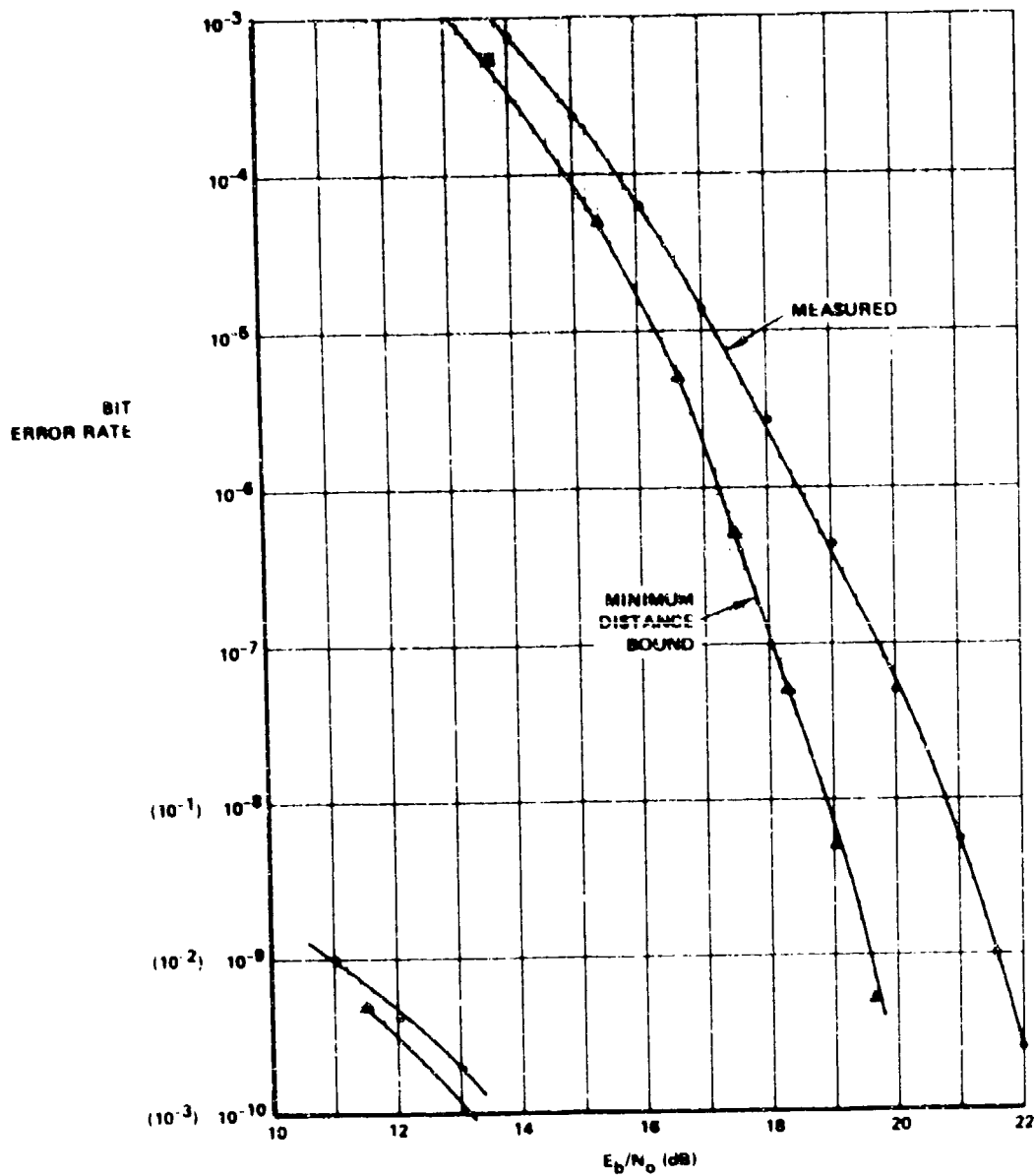
Figure 44.   Typical Back-to-Back Performance

be noted that an additional 0.5 dB in performance is available by implementing the second layer of tentative decisions described in Para. 3.3.1.

5.1.2 Microwave Radio Simulator Results

The microwave radio simulator consists of two LC8D radios configured to facilitate testing in various modes. The modem interfaced the radio at 70 MHz. The radio was then looped back at 8 GHz via a coupler and the receive level was varied to produce the curves of Figure 45.

The open-circle curve was taken with no IF filtering in the radio. The nominal bandwidth in this mode is 50 MHz. A BER of 10^{-7} was achieved at an E_b/N_o of 20.3 dB. The measured data is 0.6 dB worse than typical laboratory measurements made at 70 MHz. The amplitude response and delay distortion of the simulator were measured. The amplitude characteristic varied by +0.5/-0.9 dB over the 14-MHz active band. The delay distortion was +2/-4 ns over the band, or 6 ns peak-to-peak. The conclusion was reached that the delay distortion was probably the major contributor to additional degradation.

The remaining plots were made with either a 25-MHz, 3 pole-pair, equalized Butterworth or a 30-MHz, 0.1 dB, 3 pole-pair Tchebycheff preceding the demodulator. In the vicinity of a 10^{-7} BER, the Butterworth filter resulted in a loss of approximately 0.8 dB, while the Tchebycheff loss was approximately 1.0 dB worse. Although the Tchebycheff has a wider bandwidth, the additional loss was expected due to the poorer phase characteristic. A loss of 0.7 dB was predicted by Table 8 for replacement of the Butterworth with a 1-dB Tchebycheff. The measured 0.2 dB difference appears consistent with the experiment, which utilized a 0.1-dB Tchebycheff with a 30% greater bandwidth.

5.1.3 Link Results

Measurements over a 36-mile, 8-GHz, microwave link were also made. This was accomplished by looping the remote radio at 70 MHz and retransmitting
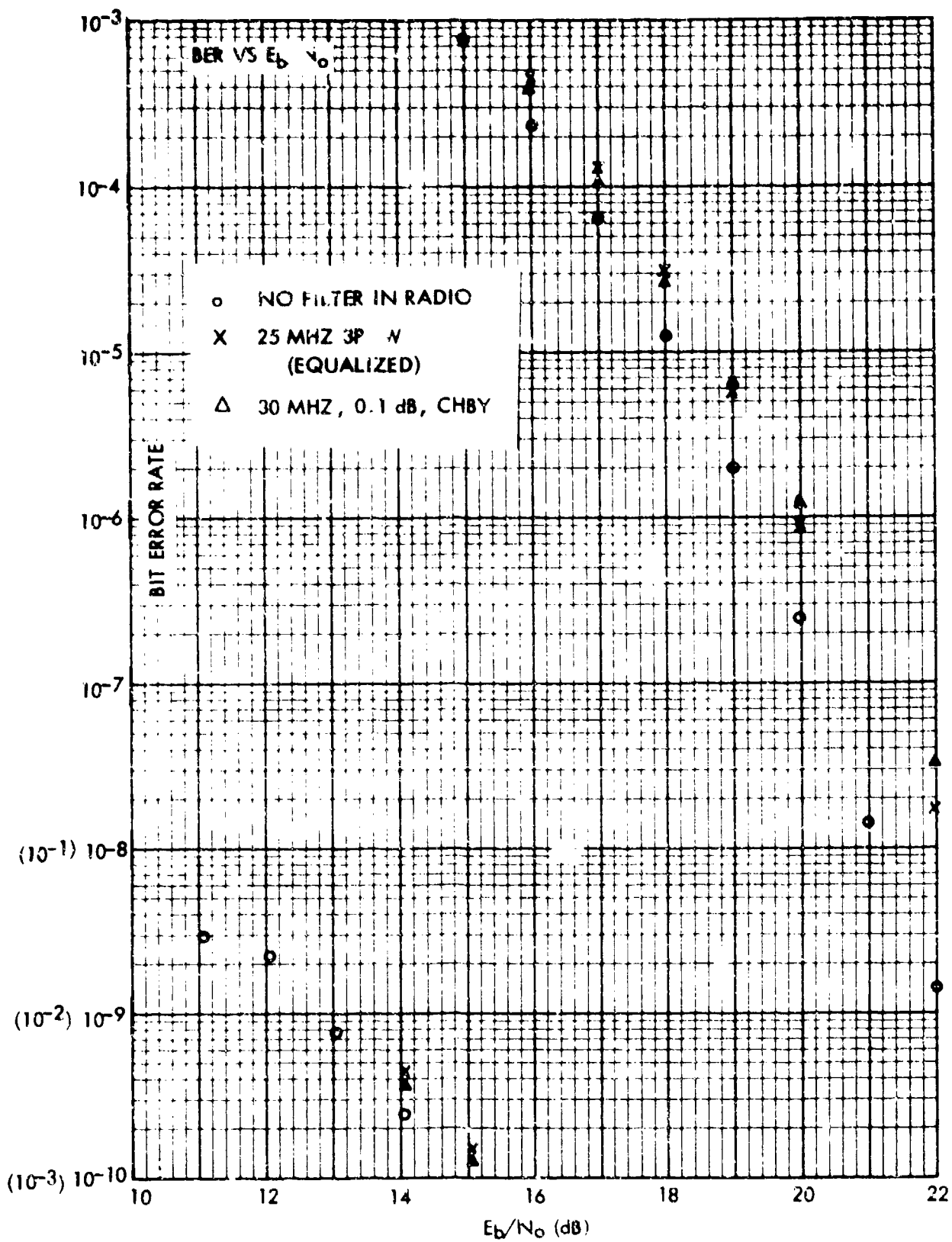
111

Figure 45. Microwave Radio Back-to-Back Performance

112

to the simulator on a second frequency. The results of this experiment are plotted in Figure 46. The measured performance at a 10^{-7} BER is 21.6 dB. This represents a degradation of 1.3 dB over the unfiltered simulator result. The amplitude response of the remote radio was measured and found to be worse than that of the simulator. The amplitude was +0.0/ -1.8 dB and the delay distortion was +2 ns/ -6 ns, or 8 ns peak-to-peak. The additional distortion is probably the major contributor to the additional degradation.

5.2   INTRINSIC BER

The E_b/N_0 was set at 30 dB and the BER observed for an extended period to estimate the intrinsic BER of the modem-radio combination. A 2-hour period on the simulator and on the link resulted in no errors. The number of error-free bits processed in this period is approximately 2×10^{11}. Based on this experiment, and after examining the slope of the measured data in the 10^{-9} region, it was concluded that the intrinsic error rate is certainly less than 10^{-11} and probably less than 10^{-12}.

5.3   SPECTRAL OCCUPANCY

The design objective was to achieve a 99-percent power bandwidth of 0.5 times the bit rate. The predicted and measured spectra are shown in Figure 47. The calculated spectrum has a 99-percent power bandwidth of 0.5. A comparison with the measured data indicates the actual spectrum is 0.5 or slightly less. The indicated increase in the measured spectrum near 1.0 results from the addition of the upper sideband from the final translation. This was removed by a bandpass filter within the modulator at 70 MHz.

A series of experiments was run with the simulator to determine the effects of filtering and limiting the FSK spectrum. It was felt that this data would be useful in determining the best strategy for complying with the stringent emission requirements of FCC Docket 19311. This requirement specifies that the power in a 4-KHz bandwidth at the band edge (0.25) be 50 dB below the total power and that an ultimate floor of 80 dB
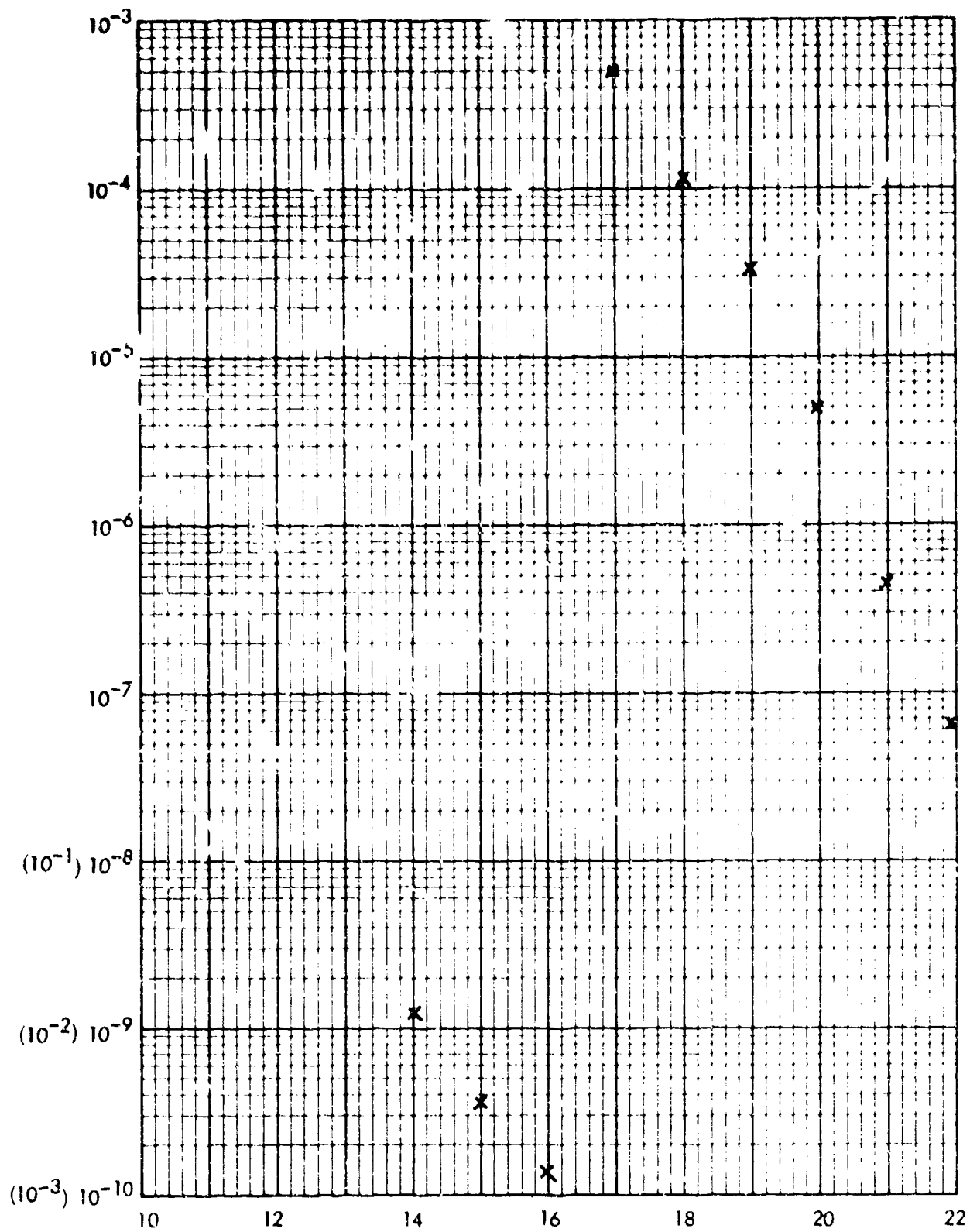
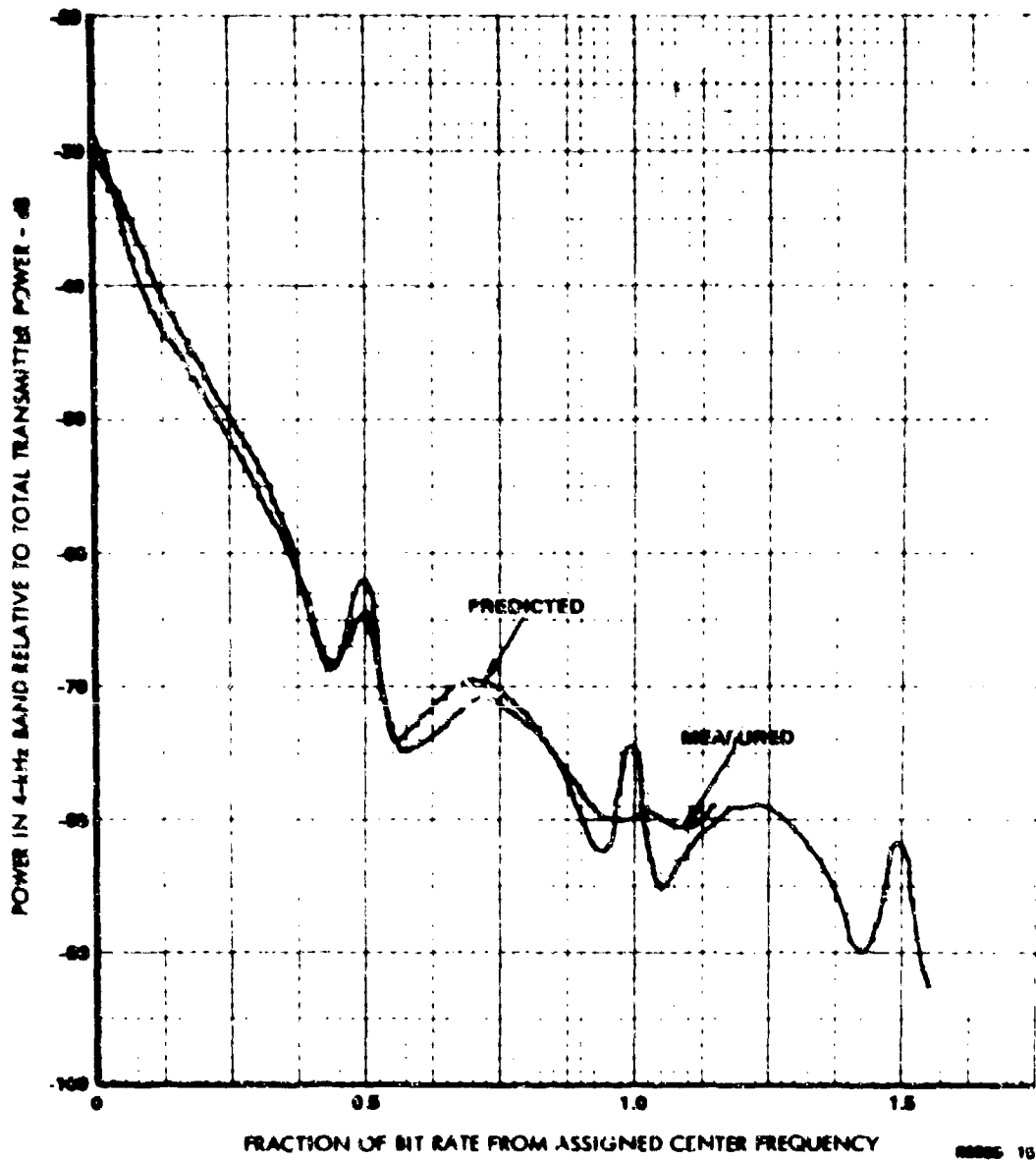Figure 46. Stockbridge Loop Performance

114

Figure 47. Predicted and Measured Spectra at 70 MHz

be reached at 0.45. As shown in Figure 47, the unfiltered spectrum meets the -50 dB requirement at 0.25. The mask from -50 dB to -80 dB is missed by a maximum of 16 dB in the vicinity of 0.45.

For experimental purposes, the modified linear phase filter in the demodulator was configured as a transmit filter. Figure 48 is a spectrum analyzer plot of the unmodified modulator 70-MHz output. Note that this plot has the same shape as that of Figure 47, but the absolute level is different by as much 6 dB. This resulted from the use of the video filter with the log mode and a 3-kHz rather than a 4-kHz IF. The plot of Figure 47 represents the average logarithm rather than the average power, and hence indicates a larger absolute level. However, for the purpose of observing the relative spectrum restoration resulting from limiting, the plots are quite adequate.

The nominal 8-GHz output spectrum is shown in Figure 49. In Figures 50 and 51, the spectra were measured with the linear phase filter inserted at 70 MHz. Comparing Figures 48 and 50, it can be seen that the side-lobe level has been reduced by approximately 17 dB. Comparing Figures 49 and 51, the side-lobe level is reduced by more than 9 dB. This result indicates that a significant portion of the filtering necessary to comply with the FCC requirements can be accomplished at IF, with relatively inexpensive and easy to replace filters.

5.4 INTERFERENCE REJECTION

The BER performance at selected E_b/N_o's was measured with both cochannel and adjacent-channel interference. The interference was identical to the desired signal, as described in Appendix D.

5.4.1 Cochannel Interference

The results of the cochannel interference test are listed in Table 10. In this table, CIR is the ratio in dB of the desired signal to the interfering signal. The degradation is calculated by reading from Figure 45 the difference in E_b/N_o between the BER with interference and the BER without interference.
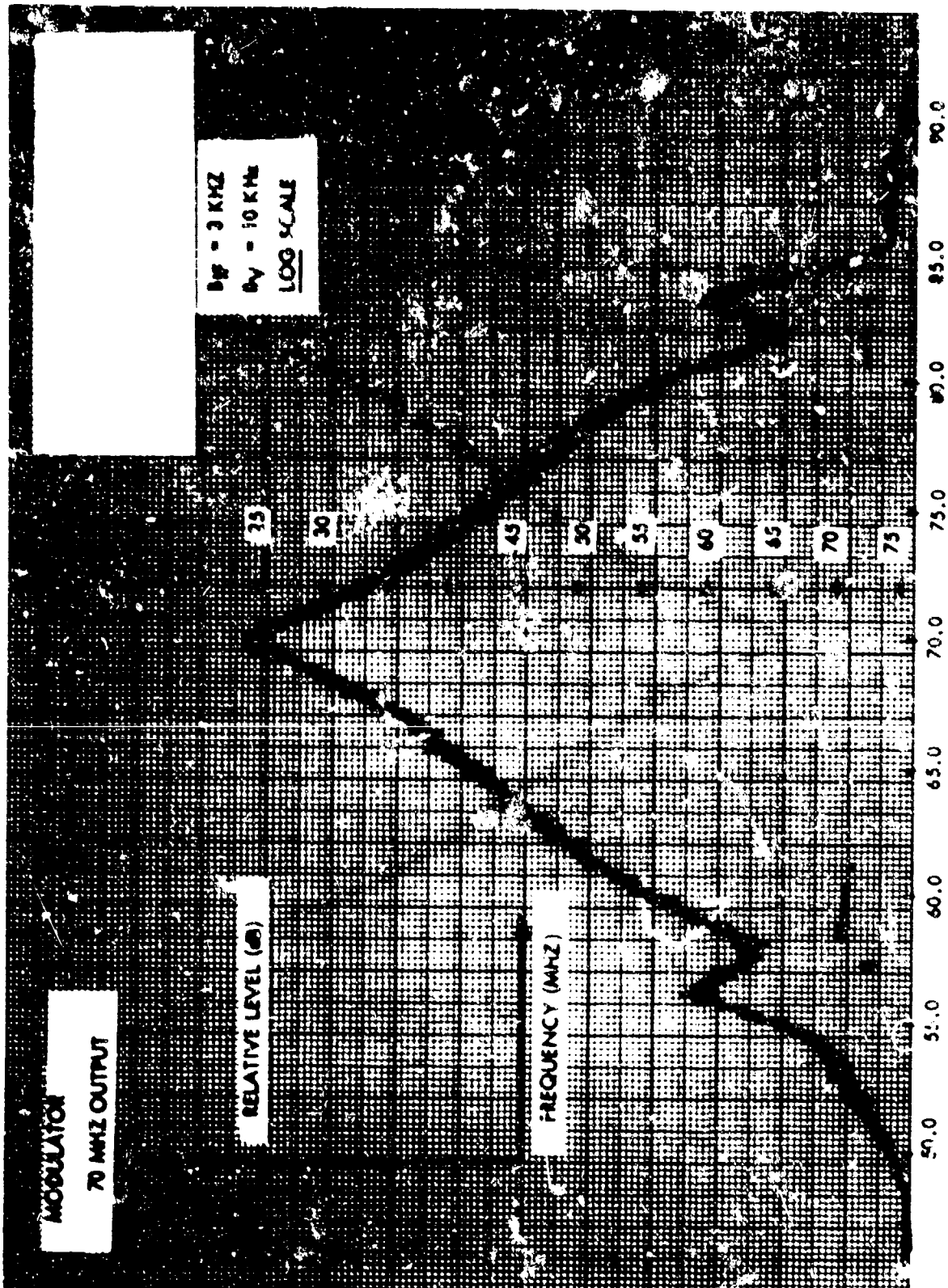
Figure 48. Unfiltered 70 MHz
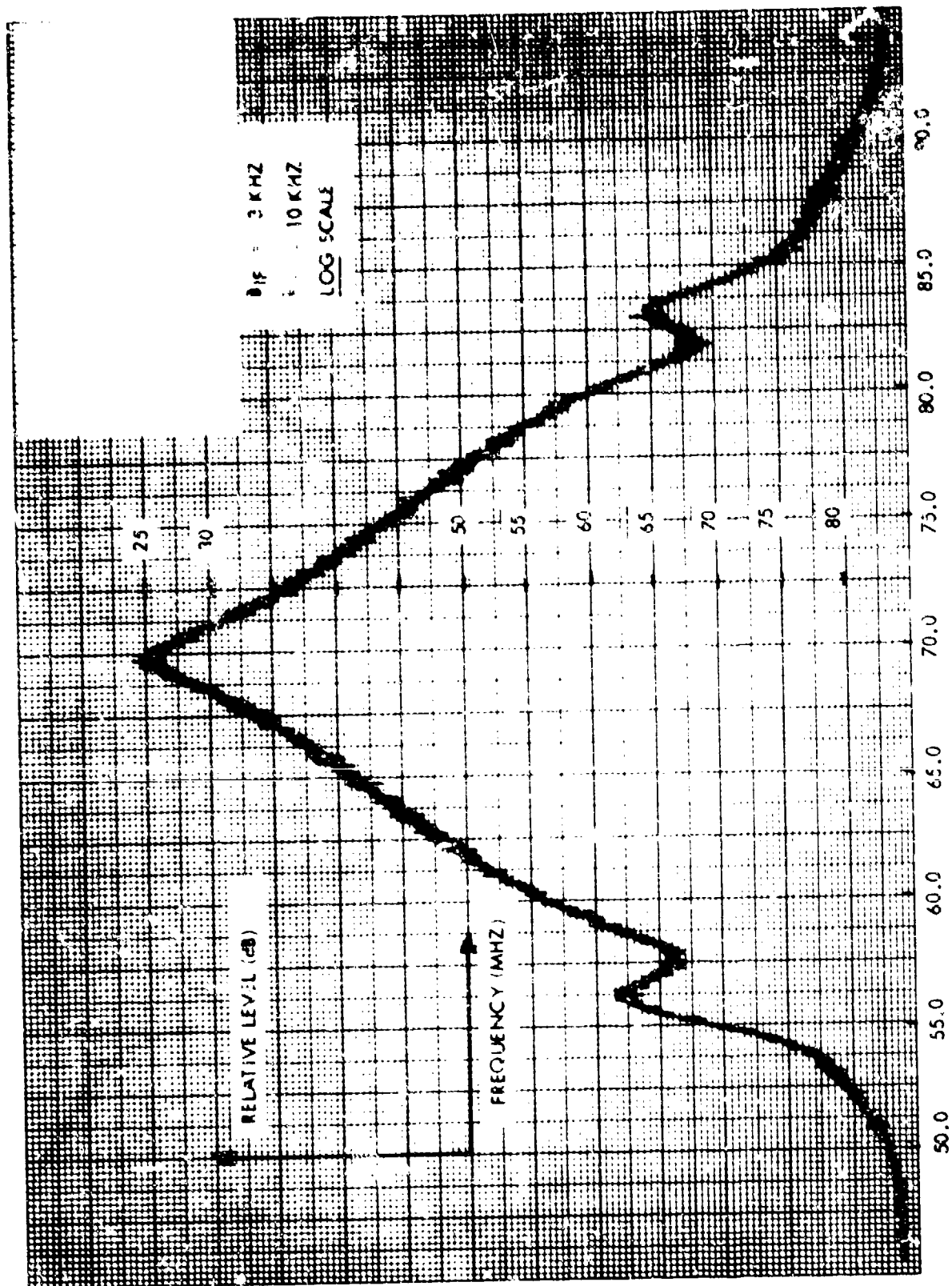
Figure 49. 8-GHz Spectrum After Limiting – No Filter
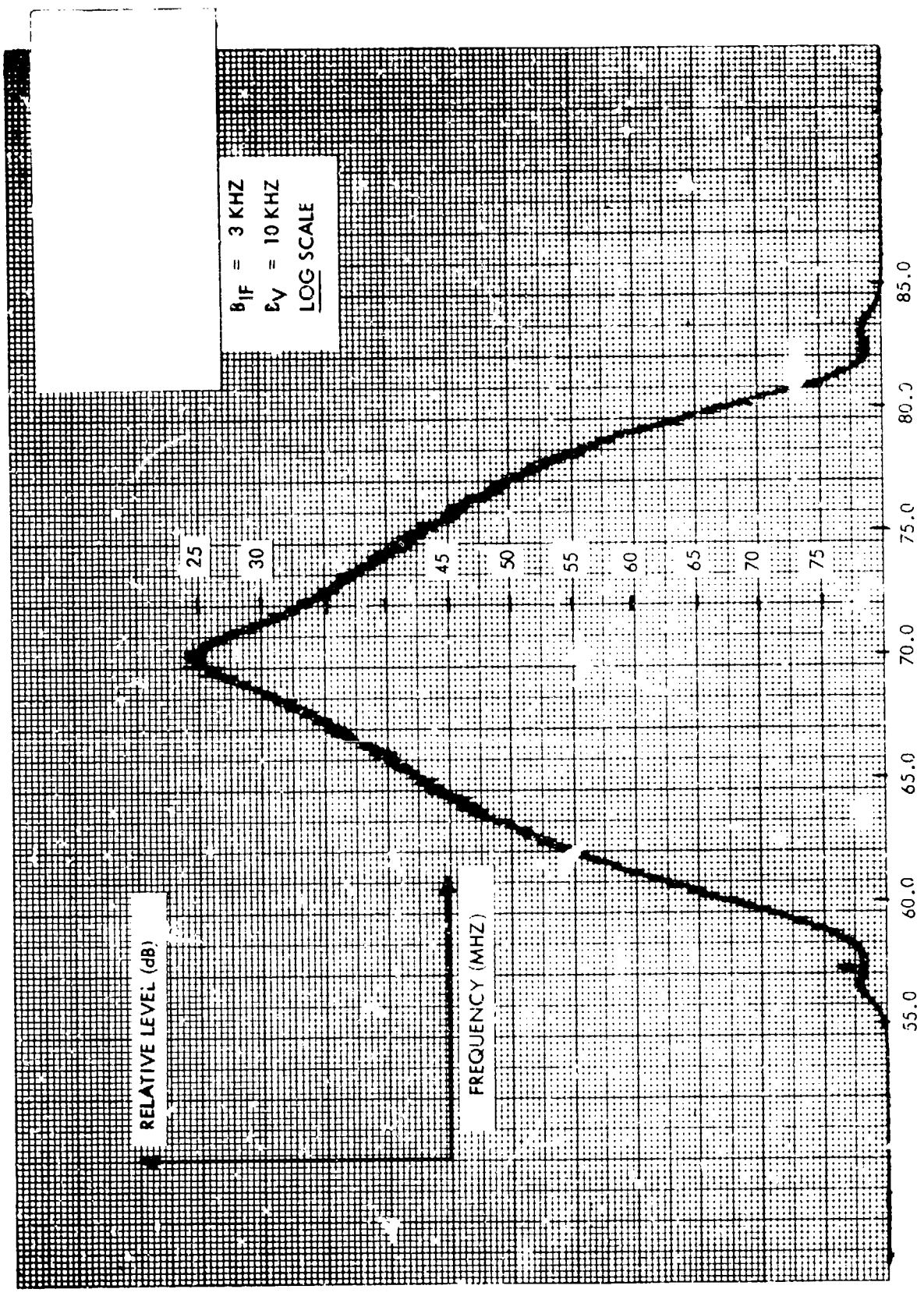
Figure 5C. Filtered 70-MHz Spectrum
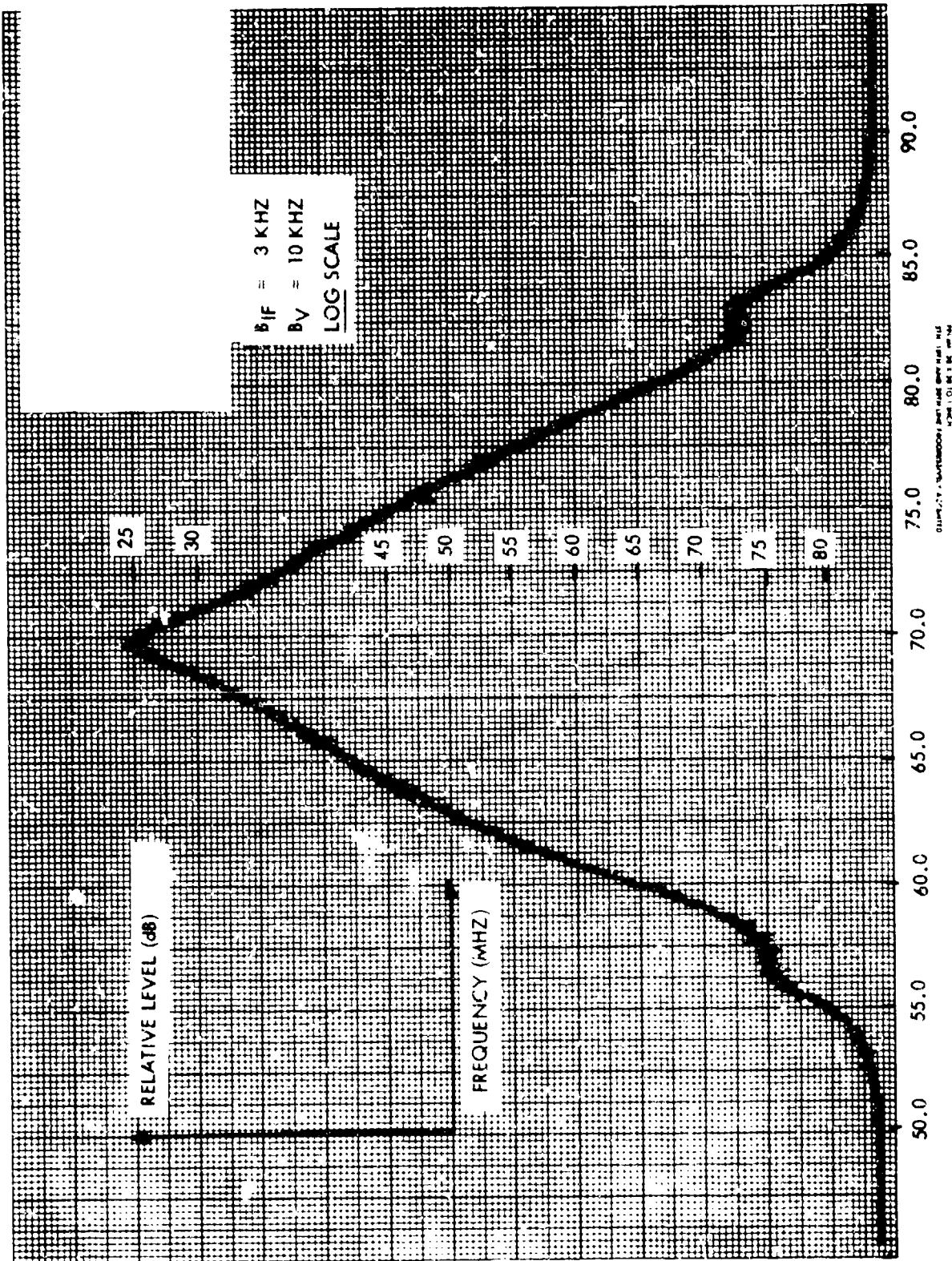
Figure 51. 8-GHz Spectrum After Limiting with IF Filter

B_{IF} = 3 KHZ
B_V = 10 KHZ
LOG SCALE

RELATIVE LEVEL (dB)

FREQUENCY (MHZ)

120

TABLE 10.   DEGRADATION FROM COCHANNEL INTERFERENCE

E_b/N_o (dB)	CIR (dB)	Degradation (dB)
15.0	27.4	0.2
	24.4	0.3
	21.4	0.4
20.0	27.4	0.4
	24.4	1.6
	21.4	3.4
23.0	27.4	1.7
	24.4	2.0
	21.4	3.2

5.4.2   Adjacent-Channel Interference

A similar experiment was performed with the interfering signal placed in the upper and then the lower adjacent channel. The center frequency of the interference was set at ± 7 MHz relative to the band edge of the center channel. The results are listed in Table 11.

TABLE 11. DEGRADATION FROM ADJACENT-CHANNEL INTERFERENCE

	E_b/N_o (dB)	CIR (dB)	Degradation (dB)
	20	21.4	0.4
(Low)		18.4	0.6
	23	21.4	0.4
		18.4	0.8
	20	21.4	0.0
(High)		18.4	0.3
	23	21.4	0.0
		18.4	0.4

Section VI

CONCLUSIONS AND RECOMMENDATIONS

6.1   CONCLUSIONS

A practical modem technique providing the desired bit error rate and spectral occupancy with hard-limiting radio sets was constructed and successfully tested. The modem implements a new technique for coherent, multisymbol detection of 4-ary FSK which performs within 0.7 dB of optimum and is significantly less complex than the classical demodulator.

The analytical and experimental results indicate that the modem provides a bandwidth efficiency of 2 bits per hertz and an error rate of 10^{-7} or less at an E_b/N_o of 20 dB. It was concluded that the modem provides a practical and efficient mechanism for converting an analog FDM-FM line-of-sight microwave system to high-density digital operation by replacement of the modulation elements.

6.2   RECOMMENDATIONS

It is recommended that a program be undertaken to refine the breadboard design toward operational hardware to facilitate additional test and evaluation. This program should focus on optimizing the cost performance and operational characteristics of the modem. Performance features to be evaluated include acquisition, a second layer of decision processing, 1-bit-per-hertz operation, and emission-control techniques.

APPENDIX A

CONSTANT ENVELOPE M-ARY SIGNALLING POWER SPECTRA

In this Appendix the general expressions for spectra of constant envelope digital angle modulation signals are developed. These are the expressions used in the signal design effort of the study.

Form of Constant Envelope Signals Considered

The signals we consider are of the form:

$$s(t) = A \cos (w_c t + \phi(t))$$
(A-1)

where

A = constant amplitude

w_c = carrier frequency

$\phi(t)$ = information-carrying angle modulation

We assume that $w_c >>$ frequencies of $\phi(t)$. Under this condition it becomes much easier in the sequel to work with the low-pass equivalent complex signal

$$z(t) = A e^{i \phi(t)}$$
(A-2)

We restrict our consideration of $\phi(t)$'s to the following type. $\phi(t)$ must be made to vary in response to a sequence of digital symbols which we denote by $\{a_0, a_1, a_2 \ldots \}$ where a_i is allowed to be an M-ary symbol, $a_i \epsilon [1, M]$. We shall allow $\phi(t)$ in the ith symbol interval to be of the form

$$\phi(t) = \phi_{a_i} (t - iT) + \theta_i, \quad iT < t < (i+1) T$$
(A-3)

where

T = M-ary symbol time

$\phi_{a_i}(t) \in \left[\phi_1(t), \; \phi_2(t) \; \ldots \; \phi_M(t) \right]$, a set of M phase shapes

defined over time interval $\left[0, \; T \; \right]$. We will call these ϕ_{a_i}'s the

phase trajectories.

θ_i = an initial starting phase at the beginning of the ith symbol defined

by the recursion:

$\theta_i = \theta_{i-1} + \Delta_{ai-1}$

Δ_{ai} = net phase increment relative to carrier incurred when symbol a_i

is transmitted.

The form of $\phi(t)$ specified in Equation (A-3) requires that the shape of the phase function
during each symbol time be selected from one of M basic shapes (the ϕ_{a_i}'s) depending
upon a_i. In addition, the beginning phase is always the net accumulated phase caused
by all preceding symbols. With this form we can treat all forms of continuous and dis-
continuous phase angle modulation signals. As an example, Figure A-1 shows the two
ϕ_{a_i}'s for binary mod index = h continuous phase FSK. We note with regard to Figure
A-1, and for all continuous phase signals in general, all $\phi_{a_i}(0)$ must equal 0.

Figure A-2 shows binary PSK phase trajectories as an example of a discontin-
uous phase trajectory angle modulation. Figure A-3 shows arbitrary discontinuous binary
phase trajectories.

Derivation of Power Spectra

Now that we have detailed the type of constant envelope signalling we are
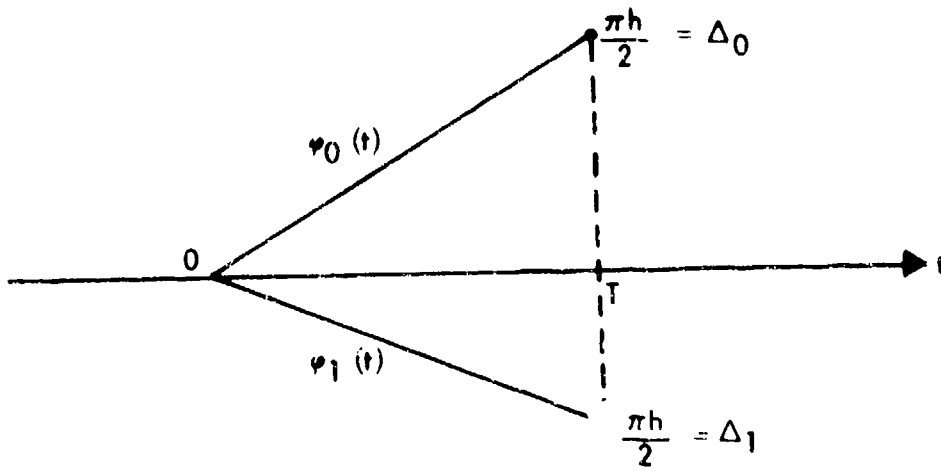considering, we derive here the spectral density for such signals. Consider an N-symbol

Figure A-1. Binary FSK Phase Trajectories
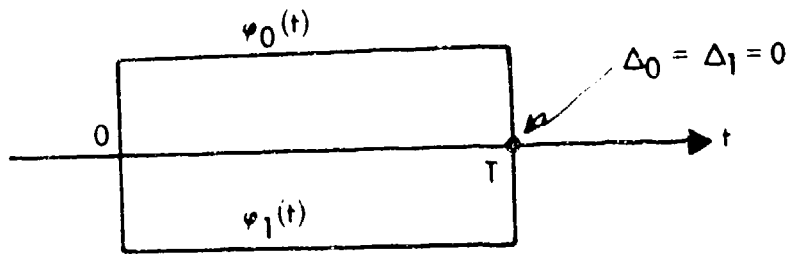
Figure A-2. Binary PSK Phase Trajectories
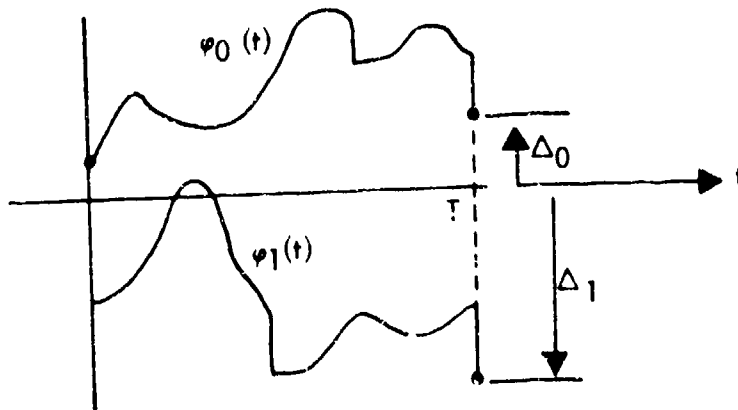
Figure A-3. Arbitrary Binary Angle Modulation

segment of the low-pass equivalent complex signal of Equation (A-2). We shall call this segment $z_N(t)$. It is given by

$$z_N(t) = A \sum_{i=0}^{N-1} e^{i\left[\varphi_{a_i}(t-iT) + \theta_i\right]} p(t-iT) \qquad (A-4)$$

where

$$p(t) = \begin{cases} 1, & 0 < t < T \\ 0, & \text{elsewhere} \end{cases}$$

We employ the segmented Fourier transform approach to derive the spectrum of $z(t)$. With this approach the spectrum is given by

$$S(w) = \lim_{N \to \infty} \frac{\overline{|F_N(w)|^2}}{NT} \qquad (A-5)$$

where $F_N(w)$ is the Fourier transform of $z_N(t)$. The bar in Equation (A-5) denotes taking the expected value over all random variables. From Equation (A-4) it is evident that

$$F_N(w) = A \sum_{i=0}^{N-1} e^{-iiwT} e^{i\theta_i} \int_0^T e^{i\varphi_{a_i}(t)} e^{-iwt} dt \qquad (A-6)$$

and

$$\left|F_N(w)\right|^2 = A^2 \sum_{i=0}^{N-1} \sum_{l=0}^{N-1} e^{-i(i-l)wT} e^{i(\theta_i - \theta_l)} \int_\infty^T e^{i\varphi_{a_i}(x)} e^{-iwx} dx$$

$$\int_0^T e^{-j\varphi_{al}(y)} e^{+jwy} \, dy \qquad\qquad (A\text{-}7)$$

The expected value of Equation (A-5) must be taken over all possible values of θ_i, θ_l, φ_{ai} and φ_{kl}. Taking the expecte values is facilitated by splitting the double summation of Equation (A-7) into two parts thus

$$\left| F_N(w) \right|^2 = A^2 \sum_{i=0}^{N-1} \int_0^T \int_0^T e^{j\left[\varphi_{ai}(x) - \varphi_{ai}(y) \right]} e^{-jw(x-y)} \, dx \, dy \qquad (A\text{-}8)$$

$$+ A^2 \sum_{\substack{i=0 \\ i \neq l}}^{N-1} \sum_{l=0}^{N-1} e^{-j(i-l)wT} e^{j(\theta_i - \theta_l)} \int_0^T e^{j\varphi_{ai}(x)} e^{-j\frac{wx}{dx}} \int_0^T e^{-j\varphi_{al}(y)} e^{+jwy} \, dy$$

The first term in Equation (A-8) is for $i = l$ and the second term is for $i \neq l$.

In the second term of Equation (A-8), ($i \neq l$), it should be evident that the terms for which $i < l$ are complex conjugates of corresponding terms for $i > l$. Equation (A-8) can therefore be rewritten as

$$\left| F_N(w) \right|^2 = A^2 \sum_{i=0}^{N-1} \int_0^T \int_0^T e^{j\left[\varphi_{ai}(x) - \varphi_{ai}(y) \right]} e^{-jw(x-y)} \, dx \, dy \qquad (A\text{-}9)$$

$$+ 2A^2 \, \mathrm{Re} \sum_{l=0}^{N-1} \sum_{i=l+1}^{N-1} e^{-jwT(i-l)} e^{j(\theta_i - \theta)} \int_0^T e^{j\varphi_{ai}(x)} e^{-jwX} \, dx$$

$$\int_0^T e^{-j\varphi_{al}(y)} \, e^{+jwy} \, dy$$

The first of Equation (A-9) is commonly referred to as the "self-spectrum", since it involves products of Fourier transforms in the same time slot; the second term is referred to as the "cross-spectrum", since it involves cross-products of Fourier transforms from two different time slots.

We require the expected value of Equation (A-9) for computing spectrum as in Equation (   ). It is written as

$$\left|F_N(w)\right|^2 = A^2 N \int_0^T \int_0^T \overline{e^{i\left[\varphi_{a_i}(x) - \varphi_{a_i}(y)\right]}} \, e^{-iw(x-y)} \, dx \, dy \qquad (A-10)$$

$$+ 2A^2 \, \mathrm{Re} \sum_{\ell=0}^{N-1} \sum_{i=\ell+1}^{N-1} e^{-iwT(i-\ell)} \overline{e^{i(\theta_i - \theta_\ell)} \int_0^T e^{i\varphi_{a_i}(x)} e^{-iwx} \, dx}$$

$$\overline{\int_0^T e^{-i\varphi_{a_\ell}(y)} e^{+iwy} \, dy}$$

We note that in terms of Δ_{a_i} (net phase increment relative to carrier caused by symbol a_i) we can write

$$\theta_i - \theta_\ell = \Delta_{a_\ell} + \sum_{n=1}^{i-\ell-1} \Delta_{a_{\ell+n}}$$

i.e., the net phase change from beginning of the ℓth symbol to beginning of the ith symbol ($i > \ell$) is the sum of the phase increments of the intervening symbols. The reason for the contribution, Δ_{a_ℓ} being split from the sum will be clear momentarily. With this notation, the expected value required in the cross-spectral term of Equation (A-10) becomes

$$\overline{e^{i(\theta_i - \theta_\ell)}} \int_0^T e^{i\varphi_{a_i}(x)} e^{-jwx}\, dx \int_0^T e^{-i\varphi_{a_\ell}(y)} e^{+jwy}\, dy$$

(A-11)

$$\overline{e^{i\sum_{n=1}^{i-\ell-1}\Delta_{a_{\ell+n}}}} \int_0^T \overline{e^{i\varphi_{a_i}(x)}} e^{-jwx}\, dx \int_0^T \overline{e^{-i\left[\varphi_{a_\ell}(y) - \Delta_{a_\ell}\right]}} e^{+jwy}\, dy$$

We note that the overall expected value has been split into the product of three independent terms' expected values. We shall now define the following functions:

$$C_\varphi(x) \triangleq \overline{e^{i\varphi_{a_i}(x)}} = \frac{1}{M}\sum_{m=1}^{M} e^{i\varphi_m(x)}$$

(A-12)

$$D_\varphi(x) \triangleq \overline{e^{i\left[\varphi_{a_i}(x) - \Delta_{a_i}\right]}} = \frac{1}{M}\sum_{m=1}^{M} e^{i\left[\varphi_m(x) - \Delta_m\right]}$$

for equally likely M-ary symbols.

Further, we note that

$$\overline{e^{i\sum_{n=1}^{i-\ell-1}\Delta_{a_{\ell+n}}}} = \prod_{n=1}^{i-\ell-1}\overline{e^{i\Delta_{a_{\ell+n}}}}$$

(A-13)

$$= C_\varphi^{i-\ell-1}(T)$$

where we have used the fact that $\Delta_{a_{\ell+n}} = \varphi_{a_{\ell+n}}(T)$ using Equations (A-11), (A-12), and (A-13) in Equation (A-16), we obtain

A-7

$$|F_N(w)|^2 \sim A^2 N \int_0^T \int_0^T \overline{e^{i\left[\psi_{ai}(x) - \psi_{ai}(y)\right]}} \, e^{-jw(x-y)} \, dx \, dy \qquad (A-14)$$

$$+2A^2 \, \mathrm{Re} \sum_{\ell=0}^{N-1} \sum_{i=\ell+1}^{N-1} e^{-jwT(i-\ell)} C_\varphi^{i-\ell-1}(T) \int_0^T C_\varphi(x) e^{-jwx} \, dx \left(\int_0^T D_\varphi(y) e^{-jwy} dy\right)^*$$

or

$$|F_N(w)|^2 = A^2 N \, \frac{1}{M} \sum_{m=1}^{M} \left| \int_0^T e^{i\varphi_m(x)} e^{-jwx} \, dx \right|^2 \qquad (A-15)$$

$$+2A^2 \, \mathrm{Re} \left[\int_0^T C_\varphi(x) e^{-jwx} dx\right]\left[\int_0^T D_\varphi(y) e^{-jwy} dy\right]^* \sum_{\ell=0}^{N-1} \sum_{i=\ell+1}^{N-1} e^{-jwT}\left(e^{-jwT} C_\varphi(T)\right)^{i-\ell-1}$$

For the double summation on i and ℓ in the cross-spectrum we can group those terms for which i – ℓ equals a constant, k, and rewrite the double sum as a single summation thus:

$$\sum_{\ell=0}^{N-1} \sum_{i=\ell+1}^{N-1} e^{-jwT} \left(e^{-jwT} C_\varphi(T)\right)^{i-\ell-1} = e^{-jwT} \sum_{k=1}^{N-1} (N-k)\left(e^{-jwT} C_\varphi(T)\right)^{k-1}$$

Thus Equation (A-15) becomes:

$$|F_N(w)|^2 = A^2 N \, \frac{1}{M} \sum_{m=1}^{M} \left| \int_0^T e^{i\varphi_m(x)} e^{-jwx} \, dx \right|^2$$

$$+2A^2 \, \mathrm{Re} \left[\int_0^T C_\varphi(x) e^{-jwx} dx\right]\left[\int_0^T D_\varphi(y) e^{-jwy} dy\right]^* e^{-jwT} \sum_{k=1}^{N-1} (N-k)\left(e^{-jwT} C_\varphi(T)\right)^{k-1} \qquad (A-16)$$

A-8

substituting Equation (A-16) into (A-5), we arrive at an expression for the spectral density, $S(w)$:

$$S(w) = \frac{A^2}{T} \; \frac{1}{M} \sum_{m=1}^{M} \left| \int_{0}^{T} e^{j\varphi m(x)} \, e^{-jwx} \, dx \right|^2 \tag{A-17}$$

$$\frac{+2A^2}{T}\left[\mathrm{Re} \int_{0}^{T} C_\varphi(x) \, e^{-jwx} \, dx \right]\left[\int_{0}^{T} D_\varphi(y) \, e^{-jwy} \, dy \right]^{*} e^{-jwT} \lim_{N \to \infty} \sum_{k=1}^{N-1} \left(1 - \frac{k}{N}\right)\left(e^{-jwT} C_\varphi(T)\right)^{k-1}$$

To complete the derivation of spectral density now we must evaluate the limit of the sum in the cross-spectral term:

$$\lim_{N \to \infty} \sum_{k=1}^{N-1} \left(1 - \frac{k}{N}\right)\left(e^{-jwT} C_\varphi(T)\right)^{k-1} \tag{A-19}$$

We must distinguish two cases to evaluate this limit: $\left| C_\varphi(T) \right| < 1$ and $\left| C_\varphi(T) \right| = 1$

<u>Case 1:</u> $\quad \left| C_\varphi(T) \right| < 1$

When $\left| C_\varphi(T) \right| < 1$, the limit obviously exists and is given by

$$\lim_{N \to \infty} \sum_{k=1}^{N-1} \left(1 - \frac{k}{N}\right)\left(e^{-jwT} C_\varphi(T)\right)^{k-1}$$

$$= \sum_{k=0}^{\infty} \left(e^{-jwT} C_\varphi(T)\right)^{k} \tag{A-19a}$$

$$= 1/(1 - e^{-jwT} C_\varphi(T)) \tag{A-19b}$$

Substituting Equation (A-19b) into Equation (A-17) yields the Case 1 $S(w)$:

$$\underline{S(w) - \text{Case 1, } \left| C_\varphi(T) \right| < 1}$$

$$S(w) = \frac{A^2}{T} \frac{1}{M} \sum_{m=1}^{M} \left| \int_0^T e^{i\varphi m(x)} e^{-iwx} dx \right|^2 \tag{A-20}$$

$$+ \frac{2A^2}{T} \text{Re} \left[\int_c^T C_\varphi(x) e^{-iwx} dx \right] \left[\int_0^T D_\varphi(y) e^{-iwy} dy \right]^* \frac{e^{-iwT}}{1 - e^{-iwT} C_\varphi(T)}$$

We note that the condition $\left| C_\varphi(T) \right| < 1$ has resulted in an entirely continuous spectrum. There are no spectral lines indicated in Equation (A-20). We shall see in the following that $\left| C_\varphi(T) \right| = 1$ will introduce delta functions in the spectrum.

<u>Case 2:</u> $\left| C_\varphi(T) \right| = 1$

Just as in Case 1, we wish to evaluate the limit given in Equation (A-18). However, since $\left| C_\varphi(T) \right| = 1$, the infinite sum does not converge for the frequencies such that

$$e^{-iwT} C_\varphi(T) = e^{-i2\pi n}, \text{ n an arbitrary integer} \tag{A-21}$$

and it will turn out that these will, in fact, be the frequencies at which there are delta functions in the spectrum.

Let us initially look at Equation (A-21) more carefully. In this case

$$C_\varphi(T) = e^{i\theta_c} \tag{A-22}$$

since the magnitude is unity. Equation (A-21) is therefore

$$e^{-jwT} \, e^{j\theta_c} \quad = \, e^{-j2\pi n}$$

$$e^{-j \, (w - \frac{\theta_c}{T}) \, T} \; = \, e^{-j2\pi n}$$

or $\qquad W = \dfrac{2\pi n}{T} + \dfrac{\theta_c}{T} \, , \; n = \Big[\ldots -1, \, 0, \, +1, \ldots \Big]$ $\qquad\qquad$ (A-23)

The frequencies indicated by Equation (A-23) are the locations of spectral lines about the assumed center frequency. They will be offset from the carrier by $\dfrac{\theta_c}{T}$ and spaced at the symbol rate, $\dfrac{1}{T}$.

APPENDIX B

COMPUTER PROGRAM FOR SPECTRAL OCCUPANCY

In this Appendix we shall show the techniq᠎ used in a Fortran computer program generated during the study to find spectral occupancy for arbitrary angle modulation signals. In Appendix A the spectral density for M-ary digital angle modulation is given by:

$$S(w) = \frac{A^2}{MT} \sum_{i=1}^{M} \int_0^T \int_0^T e^{i\left[\varphi_i(x) - \varphi_i(y)\right]} e^{-iw(x-y)} dx\, dy \tag{B-1}$$

$$+ \frac{2A^2}{T} \operatorname{Re} e^{-iwT} \int_0^T C_\varphi(x)\, e^{-iwx} dx \int_0^T D_\varphi{}^*(y)\, e^{+iwy} dy \sum_{\ell=0}^{\infty} C_\varphi(T)\, e^{-i\ell nT}$$

$$\left| C_\varphi(T) \right| < 1$$

The reader is referred to Appendix A for definition of terms. The condition that $|C_\varphi(T)| < 1$ means there are no spectral lines in the spectrum. The first term in Equation (B-1) is the self spectrum and the second term is the cross spectrum.

We have calculated $P(w_a)$ with the computer program by approximating each of the $\varphi_i(t)$ by a series of N steps, as shown in Figure B-1. Each of the steps has a duration $r = \frac{T}{N}$, as shown in Figure B-1. The value of the phase in the nth step interval for the ith φ_i is given by θ_{in}. We shall restrict ourselves in what follows to the stepwise approximation to continuous phase angle modulation wherein the initial phase of the carrier at the mth symbol time is $\theta_{(m-1)N}$, i.e., the ending phase of the preceding symbol.

Examining the first term (self spectrum) of Equation (B-1), we find that it is given by

$$S_s(w) = \frac{A^2}{MT} \sum_{i=1}^{M} \sum_{m=1}^{N} \sum_{n=1}^{N} e^{i\theta_{im}} e^{-i\theta_{in}} \int_{(m-1)r}^{mr} e^{-iwx} dx \int_{(n-1)}^{nr} e^{+iwy} dy \tag{B-2}$$

Now since

$$\int_{(m-1)r}^{mr} e^{-iwx} dx = r e^{-iw(m-1/2)r} \operatorname{Sinc} \frac{wr}{2} \tag{B-2A}$$
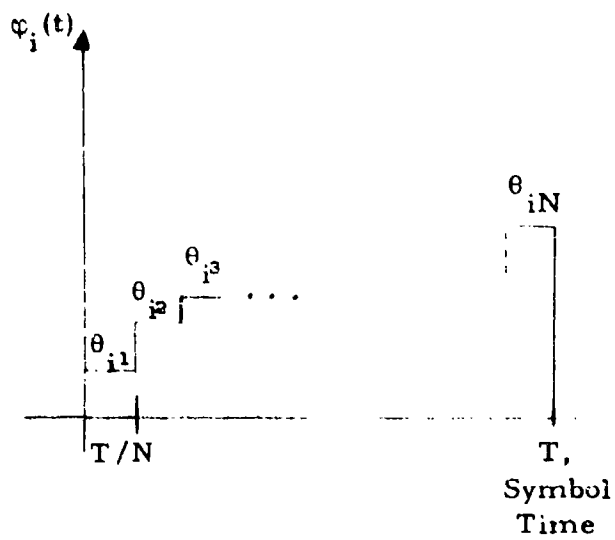
Figure B-1. Stepwise Approximation to $\varphi_1(t)$

where

$$\text{Sinc } x \triangleq \frac{\text{Sin } x}{x}$$

Equation (B·2) can be written as

$$S_s(w) = \frac{A^2 \tau^2}{MT} \sum_{i=1}^{M} \sum_{m=1}^{N} \sum_{n=1}^{N} e^{j\theta_{im}} e^{-j\theta_{in}} e^{jw(n-m)\tau} \text{sinc}^2 \frac{w\tau}{2} \qquad (B-3)$$

The power within bandwidth w_a about the carrier, due to $S_s(w)$, is given by

$$P_s(w_a) = \int_{-\frac{w_a}{2}}^{+\frac{w_a}{2}} S_s(w) \, dw$$

$$P_s(w_a) = \frac{A^2 \tau}{MN} \sum_{i=1}^{M} \sum_{m=1}^{N} \sum_{n=1}^{N} e^{j\theta_{im}} e^{-j\theta_{in}} \int_{-\frac{w_a}{2}}^{+\frac{w_a}{2}} e^{jw(n-m)} \text{sinc}^2 \frac{w\tau}{2} dw \quad (B-4)$$

If we make the definition

$$J_{wa}(n,m) = J_{wa}(n-m) \triangleq \int_{-w_a/2}^{+w_a/2} e^{jw(n-m)\tau} \text{sinc}^2 \frac{w\tau}{2} \, dw \qquad (B-5)$$

and

$$C_{im} \triangleq e^{j\theta_{im}}$$

we have

$$P_s(w_a) = \frac{A^2 \tau}{MN} \sum_{i=1}^{M} \left| \sum_{m=1}^{N} \sum_{n=1}^{N} C_{im} C_{in}^* J_{w_a}(n,m) \right| \qquad (B-6)$$

Defining a vector $\overline{C_i}$

$$\overline{C}_i = \left[C_{i1}, C_{i2}, \ldots, C_{iN} \right]$$

B-3

and a matrix J whose (n,m) entry is $J_{w_o}(n,m)$, we can rewrite Equation (B-6) as

$$P_s(w_o) = \frac{A^2 \tau}{MN} \sum_{i=1}^{M} \bar{C}_i J \bar{C}_i^* T \tag{B-7}$$

Equation (B-7) gives the contribution of the self spectrum to in-band power. We now require the contribution of the cross-spectrum to in-band power, the spectral density being the second term of Equation (B-1). If we define a term $G(w)$ such that

$$G(w) = \left[\int_0^T C_\varphi(x) e^{-iwx} dx \right] \left[\int_0^T D_\varphi^*(y) e^{+iwy} dy \right] \tag{B-8}$$

then we can write the cross-spectrum from Equation (B-1) as

$$S_c(w) = \frac{2A^2}{T} \text{ Re} \sum_{\ell=0}^{\infty} C_\varphi^\ell (T) e^{-i(\ell+1)wT} G(w) \tag{B-9}$$

We now examine $G(w)$ of Equation (B-8) to see what results when the phase functions consist of discrete steps. $C_\varphi(x)$ and $D_\varphi(x)$ in the nth step interval are given by

$$C_n = \frac{1}{M} \sum_{i=1}^{M} e^{i\theta_{in}} \tag{B-10}$$

$$D_n = \frac{1}{M} \sum_{i=1}^{M} e^{i(\theta_{in} - \theta_{iN})} \tag{B-11}$$

and consequently

$$\int_0^T C_\varphi(x) e^{-iwx} dx = \sum_{n=1}^{N} C_n \int_{(n-1)\tau}^{n\tau} e^{-iwx} dx$$

$$= \tau \sum_{n=1}^{N} C_n e^{-iw\tau(n-1/2)} \text{sinc} \frac{w\tau}{2} \tag{B-12}$$

Similarly,

$$\int_0^T D_\varphi^*(y) e^{+jwy} dy = \tau \sum_{m=1}^N D_m^* e^{+jw\tau(m-1/2)} \text{sinc} \frac{w\tau}{2} \tag{B-13}$$

From Equations (B-12), B-13), and (B-8) we thus arrive at

$$G(w) = \tau^2 \sum_{m=1}^N \sum_{n=1}^N C_n D_m^* e^{jw\tau(m-n)} \text{sinc}^2 \frac{w\tau}{2} \tag{B-14}$$

From Equation (B) and (B-14) we thus arrive at

$$S_c(w) = \frac{2A^2\tau^2}{T} \text{Re} \sum_{\ell=0}^\infty C_N^\ell \sum_{m=1}^N \sum_{n=1}^N C_n D_m^* e^{jw\tau(m-n-(\ell+1)N)} \text{sinc}^2 \frac{w\tau}{2} \tag{B-15}$$

The power within bandwidth w_a contributed by the cross term is thus

$$P_c(w_a) \wedge \int_{-w_a/2}^{+w_a/2} w) dw \tag{B-16}$$

$$= \frac{2A^2}{N} \text{Re} \sum_{\ell=0}^\infty C_N^\ell \sum_m^N \sum_n^N D_m^* \int_{-w_a/2}^{+w_a/2} e^{w\tau(m-n-(\ell+1)N)} \text{sinc}^2 \frac{w\tau}{2} dw$$

From the definition of $J_{wa}(n,m)$ in Equation (B-5), we note that Equation (B-16) can be written as

$$P_c(w_a) = \frac{2A^2}{N} \text{Re} \sum_{\ell=0}^\infty C_N^\ell \left[\sum_{m=1}^N \sum_{n=1}^N C_n D_m^* J_{w_a}(m-n-(\ell+1)N) \right] \tag{B-17}$$

If we let

$$A_\ell = \sum_{m=1}^N \sum_{n=1}^N C_n D_m^* J_{w_a}(m-n-(\ell+1)N) \tag{B-18}$$

If we further let $\overline{C}$ and $\overline{D}$ be vectors whose n^{th} components are given by Equations (B-10) and (B-11), and J_ℓ be a matrix whose (m,n) entry is given by

$$J_\ell(m,n) = J_{w_a}(m-n-(\ell+1)N) \qquad \text{(B-19)}$$

Equation (B-18) can be written as

$$A_\ell = \overline{C} \, J \, \overline{D}^{*T} \qquad \text{(B-20)}$$

and the contribution of the cross-spectrum to power in band w_a is given by

$$P_c(w_a) = \frac{2A^2\tau}{N} \, \text{Re} \, \sum_{\ell=0}^{\infty} \, C_N^\ell \, A_\ell \qquad \text{(B-21)}$$

The total power in band w_a, $P(w_a)$, from Equation (B-7) and (B-21), can now be written as

$$P(w_a) = \frac{A^2\tau}{N} \left[\frac{1}{M} \sum_{i=1}^{M} \overline{C}_i \, J \, \overline{C}_i^{*T} + 2\text{Re} \sum_{\ell=0}^{\infty} C_N^\ell \, A_\ell \right] \qquad \text{(B-22)}$$

The computer program we produced during the study computes $P(w_a)$ by Equation (B-22). Obviously, the infinite sum involved in the cross-spectrum is not computed exactly but is truncated at large enough ℓ that little inaccuracy is introduced. Since $|C_N| < 1$, the infinite series converges.

We reproduce below the Fortran program for evaluating $P(w_a)$ by Equation (B-22).

The preceding expressions for spectral occupancy were for the case that

$$|C_\varphi(T)| \triangleq \left| \frac{1}{M} \sum_{i=1}^{M} e^{i\varphi_i(T)} \right| < 1$$

and this condition corresponds to there being no spectral lines in the resulting signal. We also considered the case

$$|C_\varphi(T)| = 1$$

which corresponds to spectral lines for which Appendix A gives the spectral density as

$$S(w) \quad \frac{A^2}{MT} \sum_{i=1}^{M} \int_0^T \int_0^T e^{i\left[\varphi_i(x) - \varphi_i(y)\right]} e^{-iw(x-y)} \, dx \, dy$$

$$= \frac{A^2}{T} \left[\frac{1}{T} \sum_{\ell=-\infty}^{+\infty} \partial\left(w - \ell\frac{2\pi}{T}\right) - 1 \right] \left| \int_0^T C_\varphi(x) \, e^{-iwx} \, dx \right|^2$$

APPENDIX C

PERFORMANCE OF FILTERED MFSK-LIMITER
DISCRIMINATOR DETECTION

For the multilevel FSK signals of great interest in a 2 bits/Hz 99-percent spectral occupancy modem, an obvious demodulator is the limiter/discriminator. The limiter/discriminator enjoys the distinction of simplicity, expecially in comparison to the coherent demods discussed in Section III. In particular, the demod of interest here simply samples the output of the discriminator once per M-ary symbol time and a/d's the sample to yield $\log_2 M$ bits for the output decision. The discriminator is modeled as a device which outputs a signal proportional to the instantaneous frequency of the input signal. A Fortran computer program has been developed here capable of determining the error rate for M-ary FSK signals embedded in white Gaussian noise passed through a filter specified by its poles and zeros and detected by such a demodulator. The analytical basis for the computer program is discussed below and some of the results obtained are presented.

Analytical Basis for Discriminator Demodulation of FSK Signals

The computer program computes the probability of symbol error for a limiter/discriminator based on the probability distribution of instantaneous frequency for the signal plus noise. The distribution is derived in Chapter 8 of Schwartz, Bennett, and Stein.[1] If ν is the instantaneous frequency relative to the carrier frequency, then it is shown that

$$\text{Prob} (\nu < \eta) = \frac{1}{2} [1 - Q(\sqrt{b},\sqrt{a}) + Q(\sqrt{a},\sqrt{b})] - \frac{A}{2} \exp -\left(\frac{a+b}{2}\right) I_0 (\sqrt{ab}) \qquad \text{(C-1)}$$

where $Q(a, b)$ is the Marcum-Q function:

$$Q(a, b) = \int_b^\infty \exp\left(-\frac{a^2 + x^2}{2}\right) I_0 (ax) \, x dx$$

and

$$I_0 (z) = \frac{1}{2\pi} \int_0^{2\pi} \exp (z \cos \theta) \, d\theta$$

_____

[1] Communication Systems and Techniques, Mischa Schwartz, William R. Bennett, and Seymour Stein, McGraw-Hill Book Co., 1966, Chapter 8, Section 8-4, p. 329.

This program has been used to determine the average error rate for various M-ary FSK signals and various input bandpass filters. Some of our results are in the following section.

Results Obtained with Computer Program

The computer program discussed briefly previously is sufficiently complex that a check on the accuracy of its predictions is desirable. Some experimental results were found for binary FM in a report[2] by EMR, and their measured results were compared against the computer prediction. The particular case considered involved a bandpass filter of the four-pole Bessel type ahead of the limiter/discriminator. The ratio of 3-dB filter bandwidth to bit rate was set at 1. The binary modulating waveform was alternating one-zeros and the mod-index was 0.75. The only difference between the EMR setup and that for which the computer was run is EMR's inclusion of a low-pass filter at the discriminator output. This LPF had a 3-dB bandwidth = 1 x bit rate. The effect of this filter is probably small in this case.

The results are plotted in Figure C-1. The solid curve is from Figure 5-1 of the referenced EMR report and the two points are from the computer program. The close agreement between the two results was encouraging and helped establish faith in the computer program's predictions.

Figure C-2 provides some additional curves obtained with the computer program. These curves are for an eight-pole Bessel bandpass filter ahead of the limiter/discriminator. The signal into the bandpass filter is 8-ary FSK with mod index = 1/8 (the frequency spacing between adjacent frequencies is 1/8 the symbol rate). Average symbol error rate is plotted against the bandpass filter 3-dB bandwidth/bit rate ratio for various E_b/N_o at the input to the filter. Note that the error rate deteriorates as the bandwidth increases, because of more noise allowed into the discriminator. As the bandwidth is decreased the

---

[2] "Experimental Determination of Signal-to-Noise Relationships in PCM/FM and PCM/PM Transmission," Interim Report, for NASA/Goddard Space Flight Center, Contract NAS5-505, October 20, 1961, Electro-Mechanical Research, Inc., Sarasota, Fla.
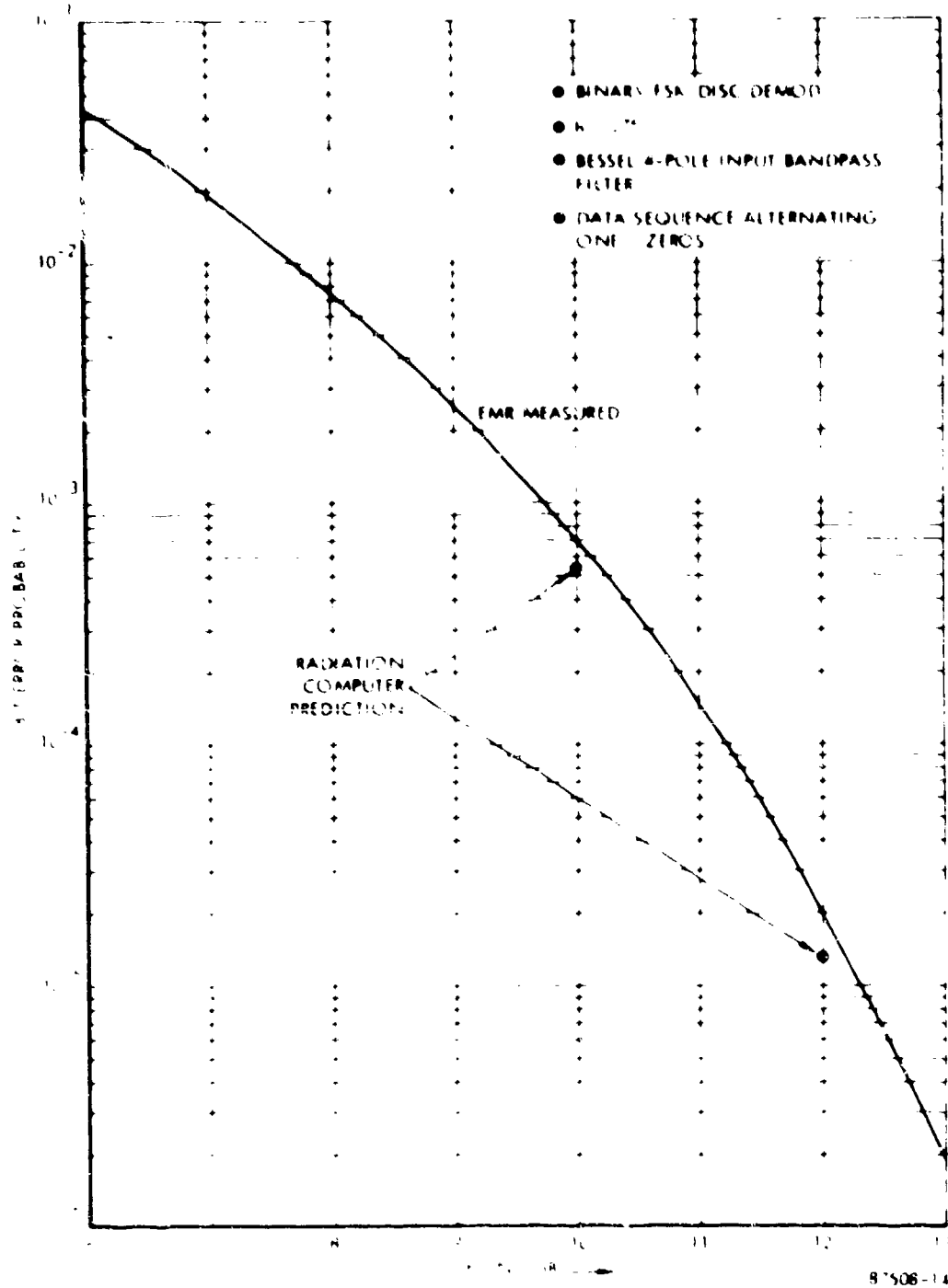
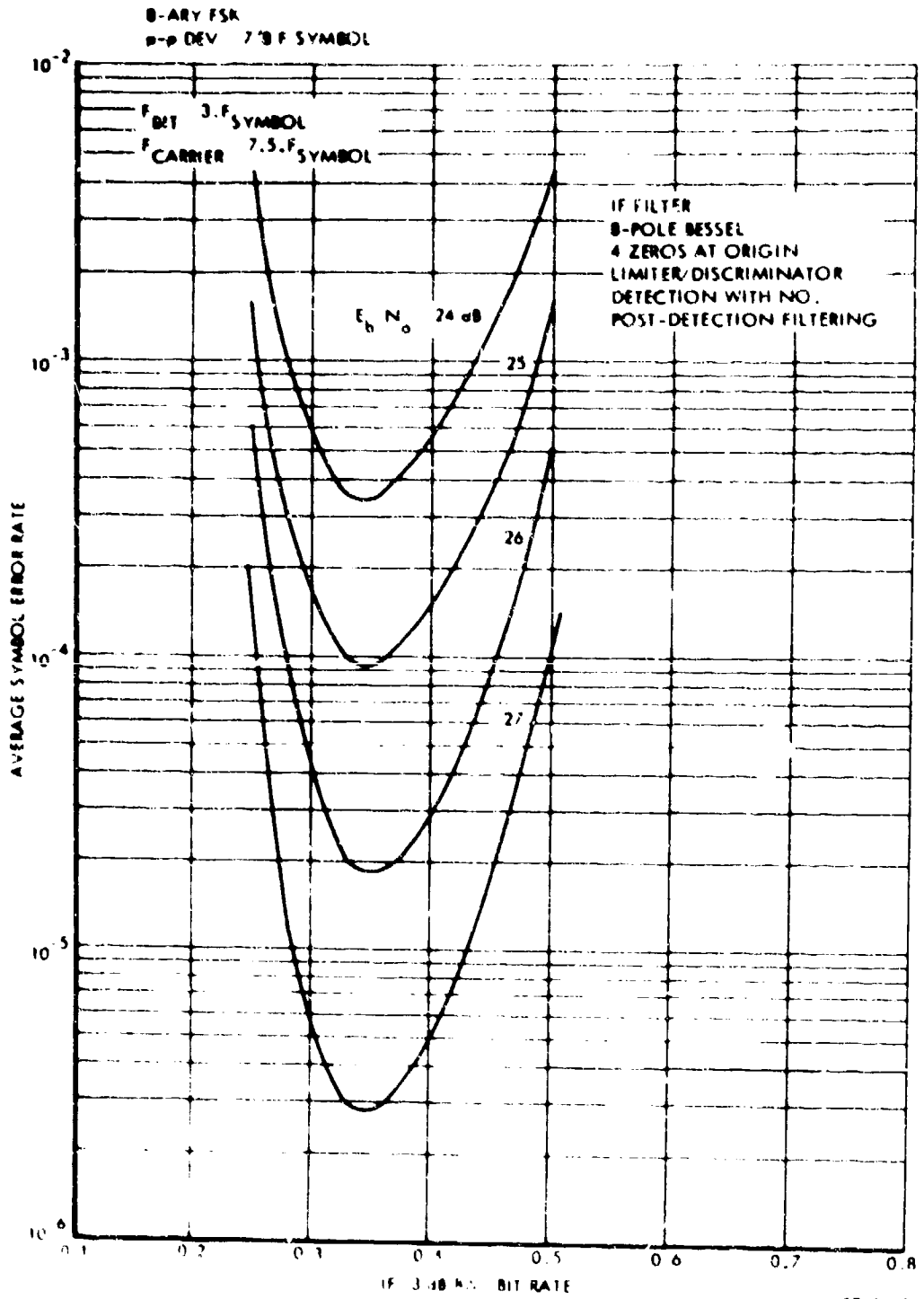Figure C-1. Comparison Between Measured Results and Computer Program Prediction

C-3

Figure C-2. 8-Ary FSK Performance through 8-Pole Bessel Filter
and Limiter Discriminator Detection

C-4

The computer program developed here contains routines for both these functions. The parameters for Equation (C-1) are defined below.

$$A = \frac{2\pi f_1 - \eta}{\sqrt{\eta^2 + (2\pi f_2)^2 - 4\pi \eta f_1}} \tag{C-2}$$

$$\begin{vmatrix} a \\ b \end{vmatrix} = \frac{R^2}{4N} \left\{ \frac{(\dot{R}/R)^2}{\eta^2 + (2\pi f_2)^2 - 4\pi \eta f_1} + \left[1 \mp \frac{\dot{\psi} - \eta}{\sqrt{\eta^2 + (2\pi f_2)^2 - 4\pi \eta f_1}} \right]^2 \right\} \tag{C-3}$$

The (−) sign in Equation (C-3) gives a and (+) gives b. R in Equation (C-3) is the envelope of the noise-free input signal and $\dot{R}$ is its derivative. ψ is the noise-free instantaneous frequency relative to the carrier frequency of the input signal. N is the mean input noise power f_1 and f_2 are essentially functions of the input filter. If G (f) is the normalized power density spectrum of the low-pass equivalent of the filtered noise, then f_1 and f_2 are given by

$$f_1 = \int_{-\infty}^{+\infty} f \, G \, (f) \, df$$

$$f_2 = \left[\int_{-\infty}^{+\infty} f^2 \, G \, (f) \, df \right]^{1/2} \tag{C-4}$$

f_1 and f_2 are therefore interpretable as the mean and rms frequencies in G (f).

The computer program computes the parameters f_1 and f_2 and N, given a particular bandpass filter and additive white Gaussian noise density. Then for a particular M-ary FSK input symbol sequence, the parameters R, $\dot{R}$, and $\dot{\psi}$ are evaluated at the selected symbol sampling times. These quantities are used in evaluating the distribution in Equation (C-1) to determine the probability that the instantaneous frequency for each symbol lies outside the appropriate range to decide the symbol correctly (i.e., the probability of symbol error is determined). If the probability of deciding the symbols in error is averaged over a sufficiently long representative sequence of M-ary symbols, the average error rate for M-ary FSK when demodulated by the limiter/discriminator is obtained.

C-5

FM signal begins to be distorted severely, also leading to performance degradation
There is an optimum bandpass filter bandwidth in this case around 1/3 the bit rate, which
is the symbol rate for the eight-level FSK signal, as one might expect. Such curves are
useful in determining the optimum bandpass filter bandwidth.

As another example of the results obtained with the computer program, Figure C-3
is included. Here, the performance of 8-ary FSK with mod index = 1/8 with discriminator
detection is plotted. The solid curves are for an eight-pole Bessel input bandpass filter.
The dashed curve is for a four-pole Bessel filter. The dashed curve is for a 3-dB band-
width/bit rate ratio of 1/3 and represents the best performance found to date for the
limiter/discriminator detector for 8-ary FSK mod index = 1/8. Also included for refer-
ence in Figure C-3 is the performance for one-symbol coherent and noncoherent receivers
for this signal. Note that the limiter/discriminator performance is only about 1 dB worse
than the optimum one-symbol observation noncoherent receiver. This performance is
approximately 7 dB away from the design goal of 20 dB E_b/N_o at $P_e = 10^{-7}$ (the design
goal is essentially one-symbol coherent performance). The simplicity of the limiter/
discriminator demod is attractive relative to the coherent receiver structures, however.

The curves of Figure C-3 point out the fact that the IF bandpass filter must be
chosen carefully for optimum performance with the limiter/discriminator demod. The
Bessel filters have particularly linear phase response across the band. Other filters such
as Tchebycheff filters with poor phase linearity, can severely cripple the performance.
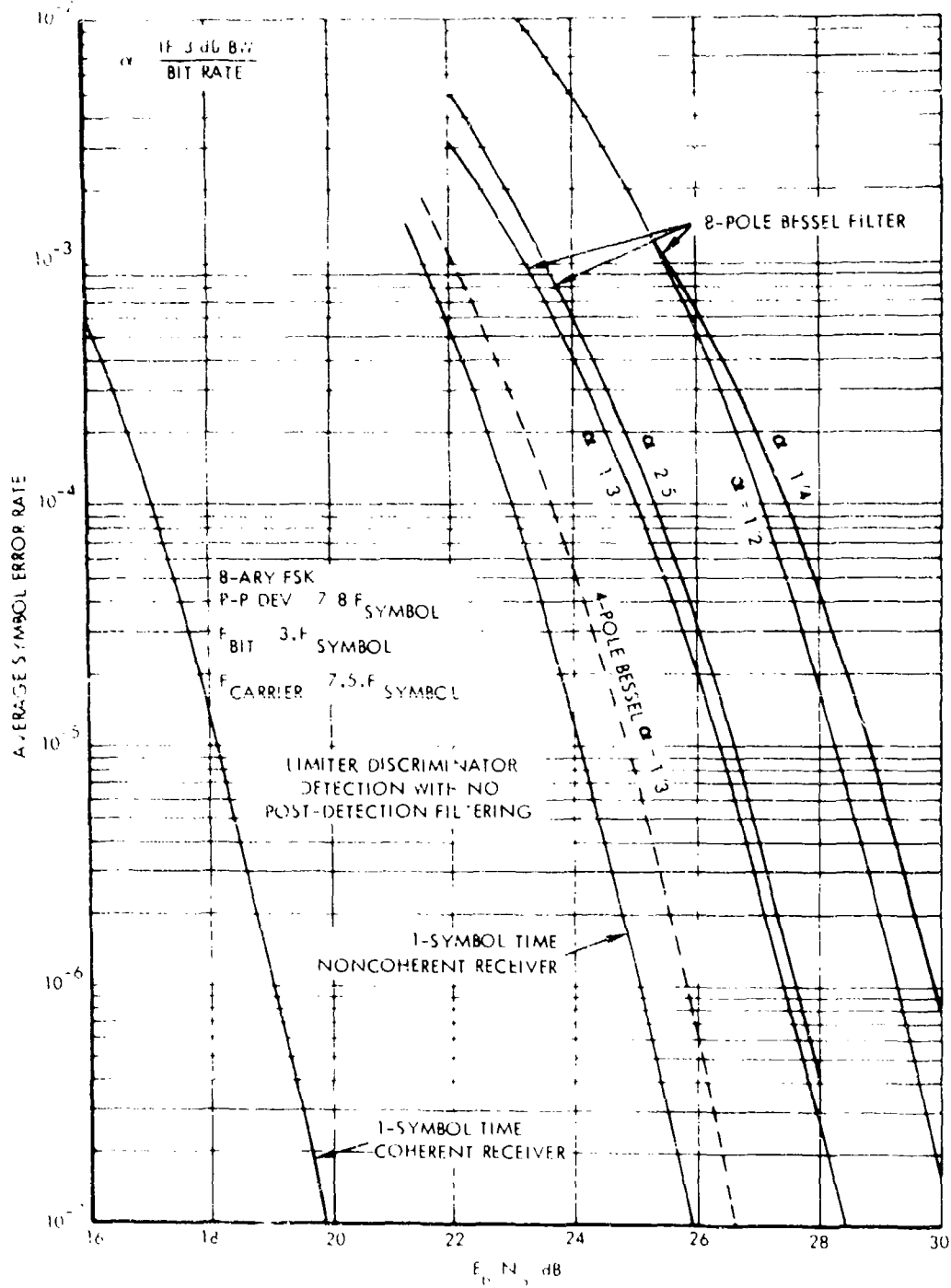
Figure C-3. 8-Ary Filtered FSK Performance with Limiter-Discriminator Detection

8/508-16

C-7

APPENDIX D

TEST PLAN

1.0   SCOPE

This plan describes a test program for the Broadband Digital Modem. The tests will be conducted at RADC and at Harris ESD in Melbourne, Florida.

2.0   OBJECTIVE

The overall objective is to characterize the critical performance parameters of the modem. Specific tests include the following:

a.   BER vs E_b/N_o vs IF filtering;

b.   BER vs E_b/N_o vs interference; and,

c.   Transmit spectrum with filtering and limiting.

3.0   MODEM DESCRIPTION

The Broadband Digital Modem was developed to improve the available bandwidth efficiency in digital line-of-sight microwave systems. The primary performance objective is a 10^{-7} BER at an E/N_o of 20 dB at a data rate of 27.?75 Mb/s. The unit provides a bandwidth efficiency of 2 bits per hertz of RF bandwidth, and interfaces at 70 MHz with hard-limiting radio systems.

3.1   Technique Description

The modulation technique is continuous-phase, 4-ary FSK with a modulation index of 1/8 (i.e., the four tones are spaced at 1/8th the symbol rate frequency intervals). The modulator is shown conceptually in Figure D-1. The demodulator employs coherent detection and multisymbol observation techniques to achieve the required performance. The demodulator is shown in Figure D-2.
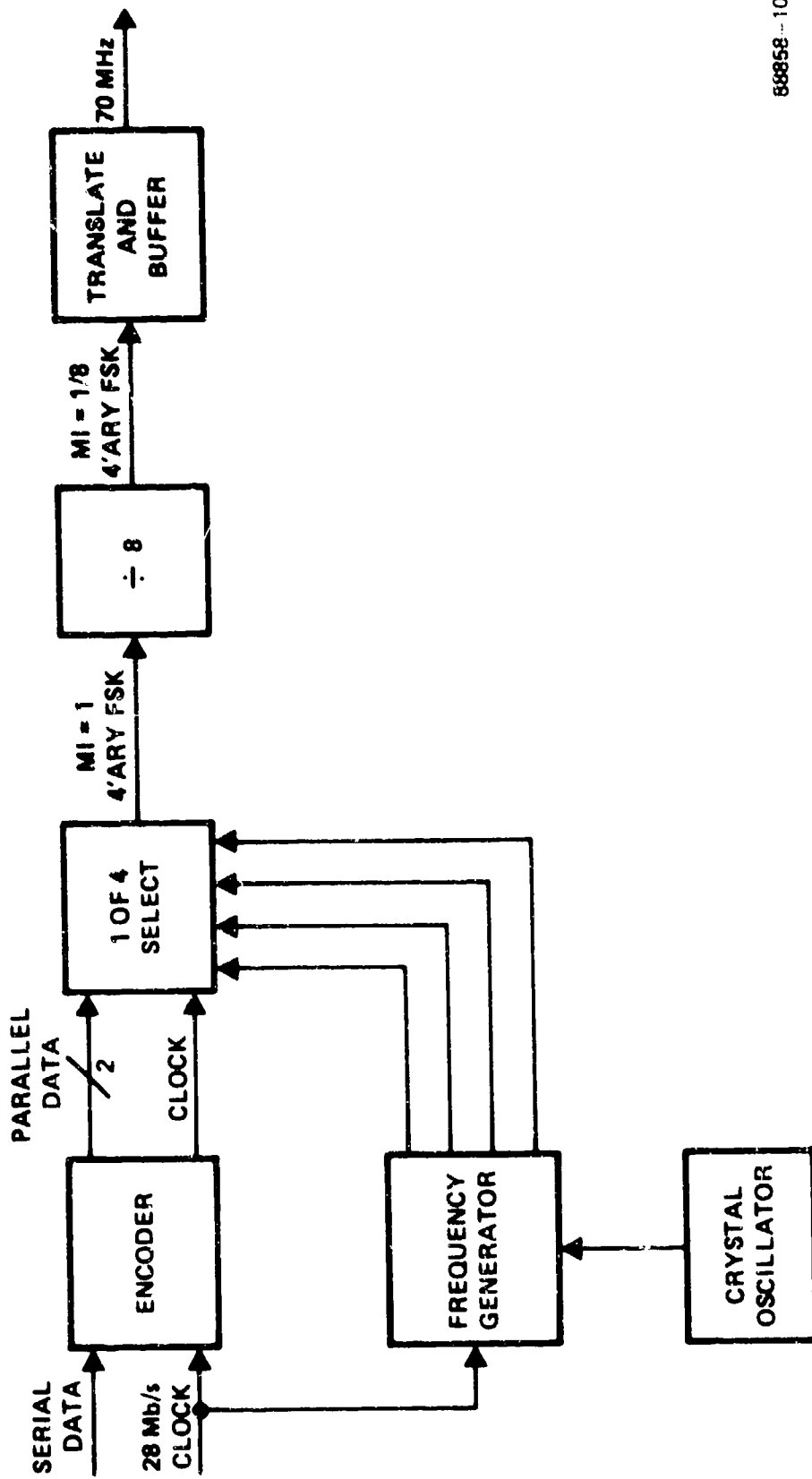
Figure D-1. Modulation Index 1/8, Continuous Phase, 4-ary FSK

68858-10
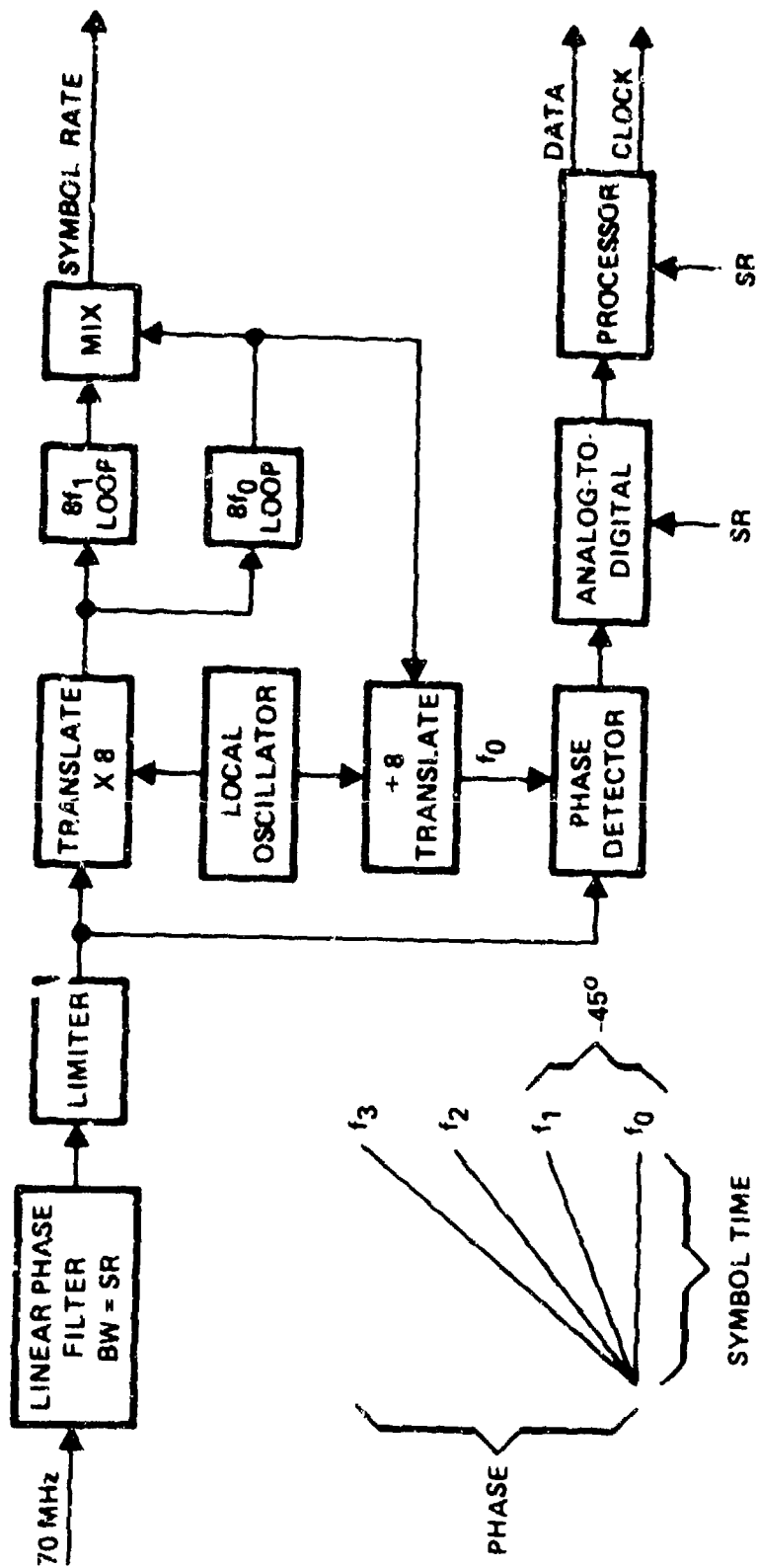
D-2

Figure D-2. Coherent Detection, Multisymbol Observation

88858-12

3.2 Hardware Description

The modulator and demodulator are individually packaged in 19-inch chassis with integral power supplies. On the transmit side, the modulator provides a bit rate clock and accepts data and associated timing through 75-ohm, unbalanced, bipolar interfaces. The modulated 70-MHz carrier is outputted at a +1 dBm level to the radio. The demodulator accepts a +1 dBm, 70-MHz signal from the radio and outputs data and synchronous timing.

4.0 TEST PROGRAM

The test program includes tests at Harris ESD in Melbourne, Florida, and at RADC. The in-plant tests are designed to provide a performance baseline from which to interpret results from the later radio and link tests and to verify the characteristics of various internal parameters. These tests are performed with the modem looped back at 70 MHz with additive thermal noise. The RADC tests include both back-to-back tests with the radio and simulator and link tests utilizing the Stockbridge radio.

4.1 In-Plant Tests

The test configuration for in-plant tests is shown in Figure D-3.

4.1.1 E/N_o Calibration

The calibration of E/N_o is accomplished directly at the demodulator input. The signal attenuator is set at 120 dB and the noise power is measured using a filter with a known noise bandwidth. The noise bandwidth is established by graphical integration techniques. The signal attenuator setting is then decreased until the total power increases by 3 dB. At this point, the signal and noise powers are equal and the SNR is 0 dB in the filter bandwidth. The noise bandwidth of the filter is 33.33 MHz, or 0.9 dB greater than a bit rate bandwidth. The E/N_o is then +0.9 dB at this attenuator setting. The desired E/N_o is obtained by adjusting the attenuator setting.
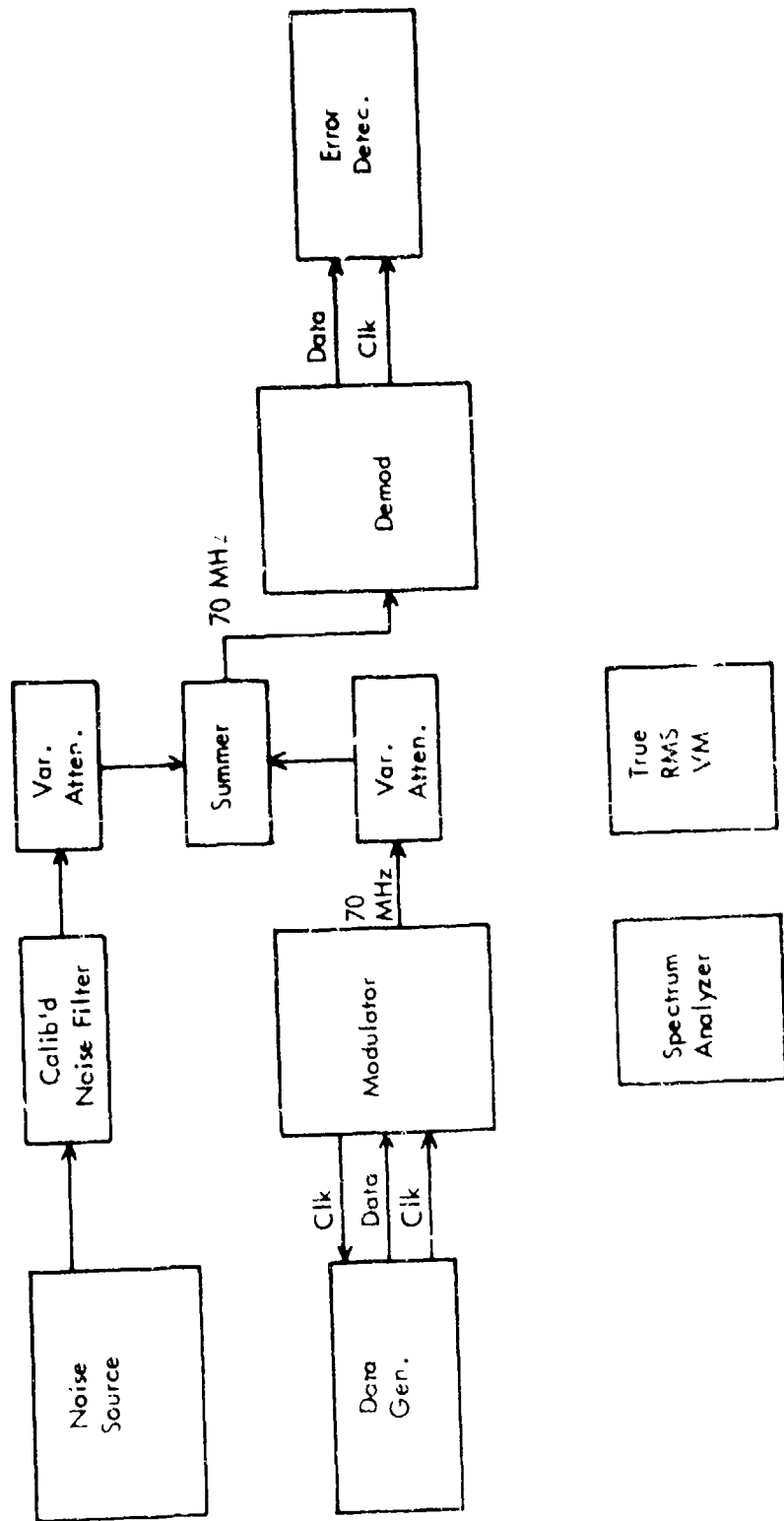
Figure D-3. In-Plant Test Configuration

4.1.2 Spectral Occupancy

The objective of this test is to demonstrate that 99 percent of the transmitted energy is contained within an RF bandwidth of one-half the bit rate. A computer-generated spectral mask, plotting energy in a 4-kHz bandwidth versus offset frequency from center, is available. The actual transmit spectrum is plotted using a spectrum analyzer set for a 3-kHz IF bandwidth. The absolute level is calibrated by observing the difference in spectral height at center frequency between an unmodulated tone and a randomly modulated signal. Since the computer mask meets the 99-percent requirement, the actual transmitter also does if the transmitted spectrum falls on or below the mask.

4.1.3 Bit Error Rate vs E/N₀

The objective of this test is to characterize the BER performance of the modem over the range from 10^{-2} to 10^{-9} as a function of E/N_0. The test setup is calibrated as in Para. 4.1.1, above. The attenuator is adjusted to provide an E/N_0 of 10 dB. The error detector is adjusted to provide an error sample of at least 100 events. The indicated error rate is recorded on 7-cycle semi-log paper. The attenuator is adjusted to provide an E/N_0 of 11 dB and the indicated error rate is recorded. This process is repeated until an E/N_0 of 22 dB is reached.

4.1.4 Residual Error Rate

The objective of this test is to demonstrate that the residual or noise-free error rate of the modem exceeds 10^{-10}. The noise attenuator is set to 120 dB. The error detector is set to count errors per 10^{11} clock counts. (Note: Approximately 1 hour is required per reading, and two or more samples may be required.)

4.2 RADC Tests

The test configuration for the RADC tests is shown in Figure D-4. The overall objective of these tests is to characterize the modem performance when interfaced
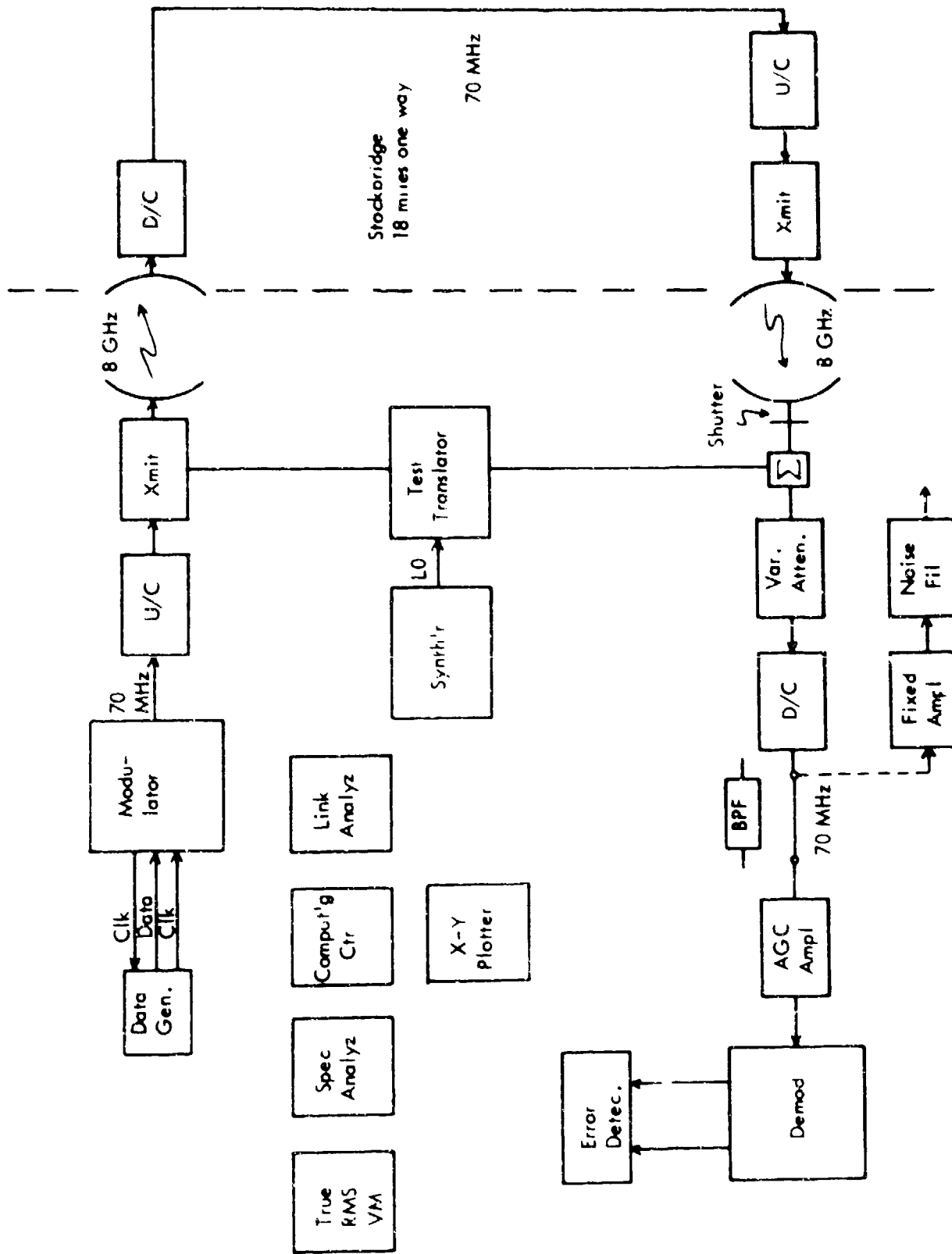
Figure D-4.   RADC Test Configuration

with the LC8D radio. The link analyzer is used to document the amplitude and delay characteristics of the test configuration.

4.2.1   E/N$_0$ Calibration

The calibration of E/N$_0$ is accomplished directly at the demodulator input. A fixed-gain amplifier is required outboard to the radio to provide the power level necessary for the HP 431C meter. With the waveguide shutter closed and the simulator configured for loop back at 8 GHz, the downconverter (D/C) noise is read through the calibrated filter with the receive attenuator set at 90 dB. The attenuator setting is then decreased until the meter reading increases by 3 dB, which indicates the SNR in the calibrated filter is 0 dB. As described in Para. 4.1.1, above, E/N$_0$ is + 0.9 dB at this point. The desired E/N$_0$ is obtained by adjusting the attenuator setting.

4.2.2   Spectral Occupancy

The objective of this test is to determine the degree to which the transmitted spectrum conforms to the requirements of FCC 19311. A second objective is to determine the effects of hard limiting on the filtered spectrum.

4.2.2.1   Unfiltered Output Spectrum

The objective of this test is to determine the effects of hard limiting on the nominal, unfiltered, modulator output spectrum as related to the FCC 19311 requirements. The modulator output spectrum is plotted with the spectrum analyzer and x-y plotter. The modulator output is then applied to the U/C and the 8-GHz spectrum recorded in a similar manner. The two curves are then compared to determine the spectral effects of the hard-limiting transmitter.

4.2.2.2   Filtered Output Spectrum

The objective of this test is to determine the net filtering gain available when the modulator output is filtered and then passed through a hard limiter. It is

anticipated that some spectrum restoration will occur in the limiter. The 14-MHz, 4-pole filter in the demodulator is used as a transmit filter directly on the modulator output. The 70-MHz and 8-GHz spectra are recorded and compared as in Para. 4.2.2.1, above.

4.2.3   Bit Error Rate vs E/N_o

The objective of this test is to characterize the BER and the recovered clock jitter performance of the modem as a function of E/N_o. Tests are run with the simulator looped at 8 GHz and over the link to Stockbridge and back. The test setup is calibrated as described in Para. 4.2.1. The receive attenuator is used to adjust E/N_o in 1-dB steps. The BER is recorded at each step to produce a complete 7-cycle graph of performance as a function of E/N_o. The computing counter is used to measure recovered clock jitter, as appropriate.

4.2.4   Bit Error Rate vs E/N_o and IF Filtering

The objective of this test is to determine the effects of IF filtering on the performance of the modem. With the simulator looped at 8 GHz, the performance tests of Para. 4.2.3, above, are repeated with 25-MHz and 33-MHz IF filters.

4.2.5   Residual Error Rate

The objective of this test is to demonstrate that the residual or noise-free error rate of the modem operating over the link exceeds 10^{-10}. The receive attenuator is adjusted to provide an E/N_o of 30 dB. Errors are accumulated for approximately 3 hours.

4.2.6   Cochannel and Adjacent-Channel Interference

The objective of this test is to determine the effects of co- and adjacent-channel interference on BER performance. The Stockbridge loop-around is used as the desired signal. The interfering signal is generated by power-dividing the modulator

D-9

output to obtain a second 70-MHz signal and driving the second simulator transmitter. The translator oscillator is adjusted to provide co- or adjacent-channel interference. The transmitter output is summed with the desired signal at the receiver front end. The calibration procedure described in Para. 4.2.1, above, is repeated for the individual signals. The absolute interference level is calibrated with the waveguide shutter closed. Attenuators are added to provide the appropriate level. The desired signal is recalibrated by opening the shutter and disconnecting the interference at 8 GHz, leaving the attenuators on the summer. With the desired signal at an E/N_0 yielding an error rate of approximately 10^{-8}, the interference level is varied and the change in error rate noted. The loss in effective E/N_0 is calculated by finding the two error rates on the measured curve and reading the E/N_0 difference. The experiment is repeated for interference translated one channel above and one channel below the desired goal.

5.0 TEST DATA EVALUATION

The test results are analyzed and provided in Section V of this report.

ERRATA

June 1976

RADC-TR-76-117 dated May 1976
Title: Broadband Digital Modem

Please change title on subject report to read: BROADBAND DIGITAL MODEM

cover

Corrections made 6/24/76 prc

C u — c c c c

MISSION
of
Rome Air Development Center

RADC is the principal AFSC organization charged with
planning and executing the USAF exploratory and advanced
development programs for information sciences, intelli-
gence, command, control and communications technology,
products and services oriented to the needs of the USAF.
Primary RADC mission areas are communications, electro-
magnetic guidance and control, surveillance of ground
and aerospace objects, intelligence data collection and
handling, information system technology, and electronic
reliability, maintainability and compatibility. RADC
has mission responsibility as assigned by AFSC for de-
monstration and acquisition of selected subsystems and
systems in the intelligence, mapping, charting, command,
control and communications areas.

D-1